THERMAL EFFECTS ON FORMATION AND REMOVAL OF THIN POLYMER FILMS

BY

YUAN-CHANG LIN

A DISSERATION PRESENTED TO THE GRADUATE SCHOOL
OF THE UNIVERSITY OF FLORIDA IN PARTIAL
FULFILLMENT OF THE REQUIREMENTS
FOR THE DEGREE OF DOCTOR OF PHILOSOPHY

UNIVERSITY OF FLORIDA

1987

ACKNOWLEDGEMENTS

The author sincerely wishes to thank the chairman of his supervisory committee, Dr. Christopher D. Batich, for his guidance and advice throughout the research program.

The author is deeply appreciative to Dr. David E. Clark, Dr. Robert T. DeHoff, Dr. Kenneth B. Wagener, and Dr. Jerry W. Williams, members of the supervisory committee, for their keen interest, instructions, and prompt supervision in this work.

The author is obliged to Dr. Molley C. Dougherty of the College of Nursing for providing part of the financial support through the project of custom-made vaginal balloons for strengthening circumvaginal musculature, to Dr. Michael D. Sacks for financing purchase of the chemicals, and to Professor Fu-Main Li for his advice and encouragement.

Special thanks are due to Dr. Wen K. Shih and Mr. Gary W. Scheiffele for running the thermal gravimetric experiment, to Dr. S. Wanigatunga and Mr. Yun-Xiang Chang of the Department of Chemistry for running the nuclear magnetic resonance experiment, to Mr. Rudy Strohschein, Jr., of the glass shop in the Chemistry Department for his assistance, beyond the scope of duty in the fabrication of the reaction

vessel and vacuum apparatus, to Dr. Richard A. McCluskey and Mr. Alfred Schulz for reviewing the manuscript, and to Dr. Fang-Yin Lee for his assistance in word-processing the manuscript.

The author also wishes to express his deepest appreciation to his parents, Mr. and Mrs. Chun-Hsiung Lin, his beloved wife, Hsiau-Mei Tong, and his children, June and Andy, for their financial support, encouragement, and enduring patience throughout this study.

TABLE OF CONTENTS

LIST OF TABLES

LIST OF FIGURES

Abstract of Dissertation Presented to the Graduate School of the University of Florida in Partial Fulfillment of the Requirement for the Degree of Doctor of Philosophy

THERMAL EFFECTS ON FORMATION AND REMOVAL OF THIN POLYMER FILMS

By

Yuan-Chang Lin

December 1987

Chairman: Dr. Christopher D. Batich
Major Department: Materials Science and Engineering

Two areas are reported here. First, studies of the burn-out residue of polymers used in ceramic processing for electronic applications are discussed. This includes synthesis of a novel polymer. Second, a thermal, gas phase method of producing very thin polymer layers is examined.

In the manufacture of multilayer ceramics (MLC) for microelectronic packaging, polymers and small organic materials used as binders, plasticizers, and lubricants

frequently leave deleterious residues after burn-out. This residue has been studied for some currently used materials and also for an experimental polymer synthesized here.

A part of this work was to synthesize a functional polymer with hydroxyl and acetal functional groups on the side chain and ester linkage on the backbone chain. Nuclear magnetic resonance (NMR) and infrared (IR) spectrum indicated the formation of this novel functional polymer. X-ray photoelectron spectroscopy (XPS), was applied to study the binder residue after burn-out. A few monolayers of carbon were found, by angular-dependent XPS, on the Al_2O_3 substrate. This result was further confirmed by the alternative C_{1s} - C_{kvv} method. Linear and nonlinear least square methods were used to test the experimental data and model and demonstrated the consistency between them.

Dimethylaminoethylmethacrylate, a hydrophilic monomer, was successfully grafted on the polypropylene film through a peroxide initiation, gas-phase method. The grafting of the thin polymer film was characterized by infrared and x-ray photoelectron spectroscopy. The change of surface energetics of the polypropylene film was further confirmed by the contact angle measurement. Three different methods were used to estimate the thickness of grafted film: substrate attenuation, curve-resolved XPS, and overlayer-substrate angular-dependent XPS. The estimated thicknesses measured by these three different methods are similar.

CHAPTER 1
INTRODUCTION

Thermal energy (or temperature) plays a very important role in polymer reactions. On one hand it can cause polymer degradation and yield small molecules. On the other hand it can be used to graft thin polymer film on a substrate. Thermal energy therefore has very subtle uses in polymer reactions in which it can both remove and form films on a substrate.

Many polymers and organic materials are used in the ceramic industry for fabrication of ceramic products or for making polymeric-ceramic composites. For processing and fabrication purposes, polymers and organic materials are used as binders, plasticizers, lubricants, deflocculants, and wetting agents, while for making composites, polymers and organic materials are introduced into the ceramic substrates to give specific properties such as tensile strength, compression strength and elasticity for this initial period.

In the manufacture of ceramic materials for use in a microelectronic device such as multilayer ceramics (MLC), ceramic powders are mixed with polymeric binders and small organic additives resulting in a milk-like viscous solution

called the ceramic slurry. The ceramic slurry is then cast into a green sheet on a carrier moving at a constant speed. At this stage the green sheet should have the necessary strength, dimensional stability, and flexibility for subsequent processing. Thereafter, the green sheets are sprayed with metal with the desired pattern and laminated into a multilayer structure. The green multilayer structure is fired in a furnace to drive off the organic materials and a dense, strong multilayer ceramic product with the desired pattern of conduction paths is thus formed. A flow chart for manufacturing multilayer ceramics is shown in Fig. 1.1. The technique and method for making the multilayer ceramics has been discussed by several researchers (1-3).

Alumina (Al_2O_3) has high strength, good insulating properties, good thermal conductivity, and low cost, which makes it the preferred material for fabrication of the MLC substrate.

As mentioned previously, the green sheet needs to maintain its mechanical strength, dimensional stability, and flexibility during fabrication of MLC substrate. This can be achieved by careful selection of the polymeric binders. The ideal binder usually requires

. high green strength for handling,
. high stability during firing,
. that it be free of carbon residues in the burn-out process,

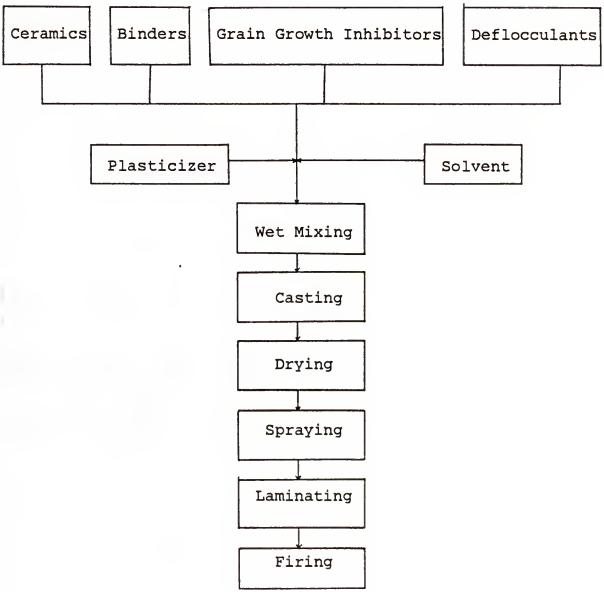

Figure 1.1 Simplified flow chart for manufacturing multilayer ceramics.

. ease in forming homogeneous mixture with ceramics,

. that it be nontoxic, and reasonably inexpensive.

Poly(vinyl butyral) (PVB) resin is the most commonly used binder for ceramic substrates. It contains acetal, hydroxyl, and acetate functional groups. The function of acetal groups is for internal plasticization (in this case, reducing the amount of hydrogen bonds) while the hydroxyl groups can form hydrogen bonding with the hydroxyl gorups on Al_2O_3 surface. This bonding between the ceramic surface and binders results in a high green strength of polymeric-ceramic composite.

Although PVB has been widely used as a binder in the ceramic industry, some drawbacks of PVB have been reported (4). Therefore, much work concerning binder properties has been carried out in the past few years. Chlorined polyolefin, polyurethane, poly(vinyl acetate), polyamide, and poly(vinyl alcohol) have been used as alternatives for binder application in both the electronic and ceramic industries (5-7). As part of this project, we attempted to synthesize a novel functional polymer by using a direct polycondensation method at room temperature (in contrast to conventional melt-polycondensation), followed by post reaction of the polymeric sites to introduce the specific functional groups onto the backbone chain for achieving the specific purpose. In addition, we have measured some properties of the residue remaining after burn-out. It was

desired to have a material with the processing advantages of PVB but better burn-out capabilities by introduction of main chain ester groups.

It is known that thermal gravimetric analysis (TGA), derivative thermogravimetry (DTG), differential thermal analysis (DTA), thermal volatilisation analysis (TVA), gas chromatography (GC), infrared (IR) spectroscopy , and mass spectrometry (MS) are useful techniques for analysis of the thermal degradation of pure polymer or polymer/ceramic composites. X-ray Photoelectron Spectroscopy (XPS) or Electron Spectroscopy for Chemical Analysis (ESCA) is a very useful tool for surface and interface analysis. It allows the investigation of elemental analysis, chemical bonding state, and specific functional groups residing on the surface. This is important because the physical, mechanical, chemical, and electrical properties of materials frequently depend on the several outermost angstroms of surface. In addition to the qualitative analysis, XPS can also give quantitative information such as an overlayer thickness measurement. Although XPS involves many advantages in surface/interface analysis it has not yet been applied in binder/ceramics burn-out study. Therefore, it was decided to do an extensive XPS examination both in qualitative and quantitative analysis of the binder/ceramic burn-out product in order to emphasize that a variety of information can be obtained from the XPS method.

Chapter 2 deals with novel polymer synthesis and describes a method for polycondensation at room temperature. A specific condensation reagent dicyclohexylcarbodiimide (DCC) and a catalyst 4-pyrrolidinopyridine were used in order that the reaction could proceed at room temperature. The product (OPE-1) was extensively characterized by nuclear magnetic resonance (NMR) and the infrared (IR) spectroscopy methods. Chapter 3 presents various methods and reagents for hydroxylation of the double bond of OPE-1. The phase transfer reagent benzyltriethylammonium chloride was added so that the water-soluble oxidant could be transferred to the organic phase, and subsequently allows hydroxylation of the double bond to occur. This product was denoted as OPE-2. The third step for synthesizing the novel polymer is acetalization. This is also detailed in Chapter 3. The final functional polymer is termed as OPE-3. It is worth noting that the experiments were done at room temperature or under mild condition which is different from the conventional method carried out at the high temperature. Although the reaction processes described in this work have been applied in organic molecules, they have not been widely used in polymeric materials.

Chapter 4 presents the results, mainly by XPS, of binder burn-out experiments. It should be noted that the study of burn-out of binder/ceramics by XPS analysis has not been reported. Chemical derivatization techniques with XPS

were used to characterize the surface functional groups of the carbon residues. The thickness of this overlayer was measured by two independent methods and their results were compared. The angular-resolved XPS is introduced to study the distribution of the surface functional groups. A mathematical model was obtained by a linear and nonlinear least square fit of the experimental data. The effect of surface roughness, x-ray flux, non-uniform overlayer, and change of solid angle on the model is discussed. Chapter 5 demonstrates the grafting of a hydrophilic monomer onto the hydrophobic polypropylene film by a gas-phase method. Modification of the polymer surface has been studied by various methods such as chemical, physical, plasma and ionizing-radiation modification. However, no report exists, as far as we know, concerning the use of peroxide compound as a free radical initiator for grafting copolymerization by gas-phase method. The result is characterizaed by XPS, IR, and contact angle measurement. The grafting of the overlayer is further studied by quantitative XPS measurement. Other information obtained by XPS are also illustrated. Finally, Chapter 6 summarizes the results of the entire study.

CHAPTER 2
POLYESTERIFICATION

2.1 Background

2.1.1 Methods for Polyesterification

Polyesters are macromolecules with repeating carboxylate groups in the main chain. Several methods have been applied to synthesize various kinds of polyesters. In general, they can be divided into five methods as described below:

1. Polycondensation of diols with dicarboxylic acids:

   $nHO\text{-}R\text{-}OH + nHO_2C\text{-}R_1\text{-}CO_2H \rightarrow HO(R\text{-}OCO\text{-}R_1\text{-}COO)_nH + (2n-1)H_2O$

2. Polycondensation of hydroxycarboxylic acids:

   $nHO\text{-}R\text{-}CO_2H \rightarrow H(O\text{-}R\text{-}CO)_nOH + (n-1)H_2O$

3. Polycondensation of diols with esters or anhydrides:

   $nHO\text{-}R\text{-}OH + nR_2O_2C\text{-}R_1\text{-}CO_2R_2 \rightarrow H\ (O\text{-}R\text{-}OCO\text{-}R_1\text{-}CO)_n\text{-}OH + (2n-1)R_2OH$

4. Polycondensation of diols with acid chlorides (Schotten-Baumann reaction):

   $nHO\text{-}R\text{-}OH + nClOC\text{-}R_1\text{-}COCl \rightarrow H(O\text{-}R\text{-}OOC\text{-}R_1\text{-}CO)_nCl + (2n-1)HCl$

5. Ring-opening polymerization of Lactone:

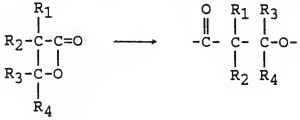

It should be noted that most of the reactions, except the Schotten-Baumann reaction, are carried out at high temperatures in a molten state or in a solution form. Polyesterification under such conditions, high temperature and long reaction time, need to be carefully controlled so as to prevent dehydration of the diol (yielding an unsaturated double bond), decarboxylation of the acid, and ester pyrolysis.

2.1.2 Reagents for Enhancement of the Polyesterification

Ogata et al. have published a series of papers describing polycondensation of dicarboxylic acids and diesters under mild conditions by introducing hetero atoms such as O, S, N, or P into the backbone chain to increase the reactivity of the functional groups (8). On the other hand, researchers have tried to use different kinds of dehydrating agents to enhance the esterification process under mild conditions or room temperature. Kadaba (9) found that boron trifluoride etherate-alcohol ($BF_3 \cdot C_2H_5OC_2H_5$ / R-OH) was a good reagent for the esterification of

heterocyclic carboxylic acids. Boron trifluoride is a Lewis acid and can form a complex with the carbonyl oxygen of the carboxyl group and thus increase its ability for nucleophilic attack by the alcohol. This behavior is the same as that of the acid catalyst in the acid -catalyzed esterification. In addition, boron trifluoride can form stable hydrates with water so as to drive the reaction to product formation. Liu, Chan, and Lee (10) also found that N, N-dimethylphosphoramidic dichloride ($(CH_3)_2$ $NPOCl_2$) and phenyl dichlorophosphate ($C_6H_5OPOCl_2$) were efficient agents for a variety of aromatic and aliphatic compounds for esterification at room temperature.

Higashi et al. (11) reported that hexachlorocyclotriphosphatriazene can promote esterification of aromatic compounds with a high yield. Trimethylchlorosilane was used by Nakao et al. as a coupling reagent in the esterification of carboxylic acid and alcohol (12). However, this reagent is only good for primary and secondary alcohol and not for t-butyl alcohol for esterification. Hashimoto, and Furukawa prepared the dehydrating agent by combination of triphenylphosphine and carbon tetrachloride in the presence of triethylamine (13). They demonstrated that this specific reagent is good for phenyl alcohol and not good for alkyl alcohol for esterification. Takimoto et al. (14) utilized 2-chloro-1,3,5,-trinitrobenzene as the condensing agent for converting aromatic and aliphatic carboxylic acid into

esters. The rate of the ester formation dependes on the types of the acids and the alcohols used. Phenyl dichlorophosphate-dimethylformamide complex was also used as a condensing agent for esterification by Garcia, Arrieta, and Palomo (15). They concluded that this reagent is suitable for unsaturated acids and malonic acid for esterification.

Recently, various versatile and facile methods for esterification have been developed. Mohacsi (16) reported that o-methyl-caprolactim is a unique reagent for the preparation of methyl esters from carboxylic acids. Chlorosulfony isocyanate in the presence of triethylamine was also studied by Keshavamurthy et al. (17) as a dehydrating agent for esterification. They compared their data with other data reported for other reagents or methods and suggested that chlorosulfonyl isocyanate is a more effective and milder condensing reagent. As mentioned previously, some of the condensation reagents are not good for esterification of tertiary alcohol; however, Takimoto, Abe, Kodera, and Ohta examined the reaction of 2-chloro-3,5-dinitropyridine with carboxylic acids and alcohols and found that ester could be formed by reaction of carboxylic acids with tertiary alcohol in the presence of pyridine and 2-chloro-3,5-dinitropyridine (18).

The above mentioned condensation agents and methods for esterification were all conducted under mild conditions or

at room temperature. However, these reactions concerned the small organic molecules and not the macromolecules.

It is worth noting that very few reports discussed the conditions using dicarboxylic acid and diol to synthesize the polycondensation esters. This may be due to the weak nucleophilicity of the hydroxyl groups which are not strong enough to attack the carbonyl group of the acid at room temperature or under mild conditions even with an acid catalyst. Yasuda et al. (19) performed the direct polycondensation reactions of dicarboxylic acids and diols using triphenylphosphine as a condensation reagent at room temperature. They concluded that a good result could be obtained by a combination of triphenylphosphine and hexachloroethane for polyesterification. Modification of backbone structure is important. For instance, it has been shown by Vogl (20) that functional polymers play a very important role in the development of polymer science. Polymers with some specific functional groups either in their backbone chain or side chain can affect very significantly the properites of macromolecules, such as chemical reactivity, biological properties as well as photo, thermal, and catalytic reactivity.

It is also worth noting that most of the synthetic functional polymers originate from the free radical or ionic polymerization of the monomers. This is attributed to the high possibility of thermal degradation of functional groups

or crosslinking of the reactive sites during the course of conventional melt-polycondensation. Thus, it is decided to synthesize a polymer by direct condensation at room temperature, followed by post reaction under mild conditions to obtain a polyfunctional polymer.

2.2 Materials and Methods

2.2.1 Materials

Polybutadiene-diol (no. mol. wt. 2800) was purchased from Scientific Polymer Products, Inc. Methylmalonic acid, 4-pyrrolidinopyridine were obtained from Aldrich Chemical Company. Dicyclohexylcarbodiimide (DCC), dry tetrahydrofuran (THF), high purity methanol and methylene chloride were purchased from Fisher Scientific Company and stored over 3Å molecular sieves (Fisher) before use.

2.2.2 Methods

Methylmalonic acid was predried in a vacuum oven at 50°C for 16 hours. The reagent, polybutadiene-diol (0.011 mole), dissolved in a small amount of THF, was stirred in a 250 ml round bottom flask with a ground joint size 24/40. A mechanical stirring system composed of a glass-rod shaft and a half-moon shaped Teflon blade was used for agitation. Methylmalonic acid (0.010 mole) dissolved in THF was then added. The resulting solution was stirred for 15 min before addition of 4-pyrrolidinopyridine (0.001 mole) and

dicyclohexylcarbodiimide (0.012 mole). The solution was continuously mechanically stirred for 48 hours at room temperature.

The resulting viscous product was repeatedly washed with methanol and water until no residue was found after the methanol evaporated. The product OPE-1 was dried in a vacuum oven for several days at 50°C. This OPE-1 was then kept in a vacuum desiccator for further use.

2.2.3 IR Analysis

Fourier Transform Infrared (FTIR) spectra were recorded on a NICOLET 60SX spectrometer equipped with a liquid nitrogen cooled mercury cadmium telluride (MCT) detector. Spectra were collected at 4 cm^{-1} resolution.

2.3 Results and Discussions

2.3.1 The Use of Dicyclohexylcarbodiimide as a Condensation Reagent and 4-Pyrrolidinopyridine as a Catalyst in this Study

A schematic diagram of the chemical structure and reaction path is shown in Fig. 2.1.

DCC was used as a condensation reagent to enhance the reaction in this study. DCC has been used by researchers to synthesize esters from a variety of acids. In addition to using DCC as a condensation reagent, some catalytic amounts of pyridine or tertiary amines were also added by researchers in acyl transfer reaction. Höfle and Steglich

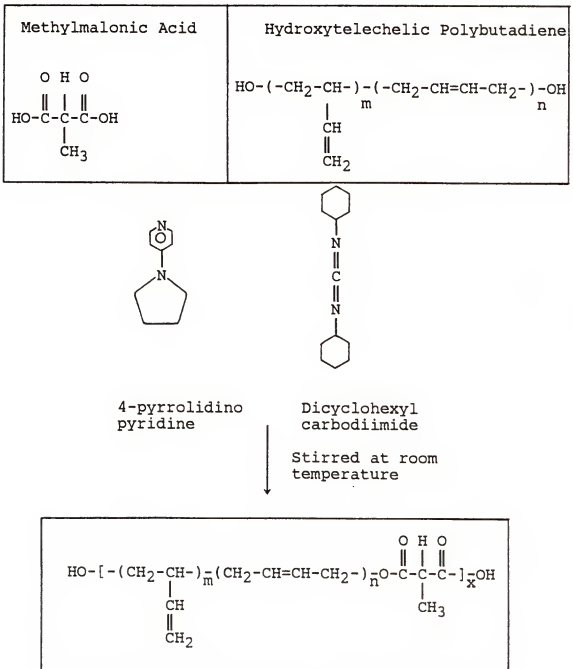

Figure 2.1 Schematic diagram of polyesterification.

(21) found that 4-dialkylaminopyridine and 4-pyrrolidinopyridine are more powerful catalysts in acylation reaction and superior to pyridine and tertiary amines. They demonstrated that sterically hindered alcohols, which were not reacted by acylation, could be reacted successfully using these two catalysts. Kim and Yang (22) showed 4-dimethylaminopyridine is a good reagent for esterification of carboxylic acids and alcohols under mild conditions. The condensation reagent they used was 2-fluoro-1,3,5-trinitrobenzene. Hassner et al. (23) investigated the catalytic effects of various pyridine derivatives on acylation and found 4-pyrrolidinopyridine was the most effective one, even better than 4 dimethylamino- pyridine. The combination of dicyclohexylcarbodiimide and 4-pyrrolidinopyridine as catalytic reagents in esterification was first demonstrated by Hassner and Alexanian (24). Various organic aromatic and aliphatic acids and alcohols were used as examples to show the merit of this esterification method. The acid was converted by DCC to an anhydride. This anhydride was then reacted with 4-pyrrolidinopyridine to form an intermediate acylpyridinium species followed by the nucleophilic attack by alcohol on the carbonyl group of the acid and produced the ester. We attempted to apply this method to synthesize an unsaturated polyester by direct polycondensation under mild conditions

and then modify the resulting product by a suitable reaction to produce the functional polymer.

2.3.2 Microstructure of Hydroxytelechelic Polybutadiene from NMR Analysis

Polybutadiene oligomer with hydroxyl groups at the ends was used as the starting material for synthesis of the functional polymer. Oligomers with reactive groups at the ends of the chains are also called telechelic polymers. The polybutadiene oligomer used in this study can be called the prepolymer which is polymerized from the 1,3-butadiene monomer. There are two possible products from the polymerization process; 1,2-polymerization and 1,4-polymerization as shown in Fig. 2.2. Both of them have unsaturated double bonds either in the side chains or in the main chains resulting in the structure and steric isomerism.

NMR spectra were obtained by using an NT 300 spectrometer which has an electromagnetic radiation of 75 MHz for ^{13}C and 300 MHz for ^{1}H. In general, samples of 0.1 g - 0.2 g were dissolved in deuterated solvents $CDCl_3$ with tetramethylsilane (TMS) as an internal reference. This solution was then pipetted into 5 mm tubes (PP - 507) and examined at room temperature. Spectra of the hydroxy telechelic polybutadiene are shown in Fig. 2.3 and Fig. 2.4 for ^{1}H-NMR and ^{13}C-NMR respectively. In the ^{1}H-NMR spectrum, the peak at 0 ppm is assigned to the tetramethylsilane which has a low electronegativity of the silicon atom resulting in

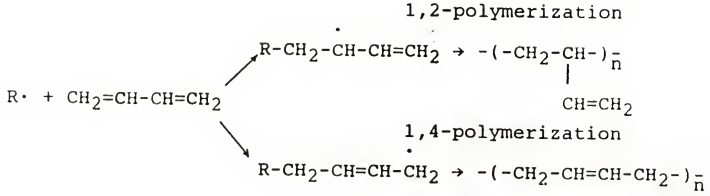

Figure 2.2 Polymerization of 1,3-butadiene.

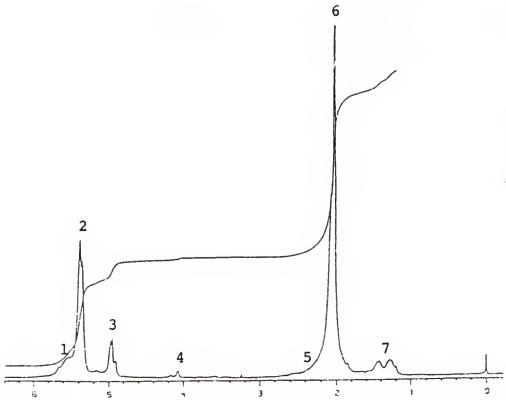

Figure 2.3 ^{1}H-NMR spectrum of hydroxytelechelic polybutadiene.

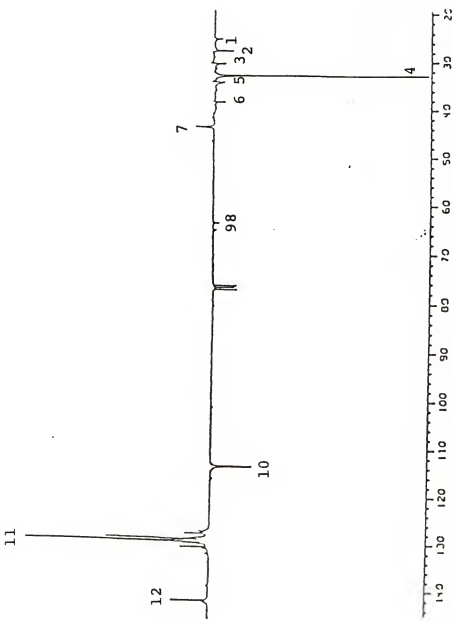

Figure 2.4 ^{13}C-NMR spectrum of hydroxytelechelic polybutadiene.

the downfield shift of the protons of other molecules. The bands at the position of 1.2 - 1.6 ppm and 4.9 - 5.1 ppm are assigned to the methylene groups of the vinyl units while the bands at the position of 2.2 - 2.4 ppm and 5.5 - 5.9 ppm represent the methine group of the vinyl units. The strong bands at 1.9 - 2.2 ppm and 5.3 - 5.5 ppm are assigned to the 1,4-polybutadiene units. The former bands arise from the methylene groups while the latter bands represent the methine proton. The small peak in the chemical shift range from 4.0 - 4.2 ppm is attributed to the methylene group which is adjacent to the hydroxyl group. These peak assignments are summarized in Table 2.1. In addition to using NT 300 spectrometer, we also used the Varian XL-200 spectrometer to measure the ^{1}H-NMR spectrum (200 MHz). The result is shown in Fig. 2.5. The two results shown in Fig. 2.3 and Fig. 2.5 are very similar except Fig. 2.3 demonstrates a better resolution. The percentage of vinyl units in this oligomer can be obtained using the ratio of peak area 3 and 2. A value of 12 percent is obtained. This value may be lower since the peak area of 2 is overlapped with the peak area of 1, which can result in a higher value of 2 in the denominator for calculation.

Several papers (25, 26) were published concerning the sequence distribution of cis-1,4, trans-1,4 and 1, 2 units of polybutadiene by ^{1}H-NMR spectroscopy. Santee and his colleagues (25) found that the methine proton in n-

TABLE 2.1

Peak Assignments of ^{1}H-NMR Spectrum for Hydroxytelechelic Polybutadiene

Hydrogen type	Shift (ppm vs. TMS)	Chemical Structure
1	5.5 - 5.9	$-\overset{*}{C}H=CH_2$
2	5.3 - 5.5	$-\overset{*}{C}H=CH-$
3	4.9 - 5.1	$-CH=\overset{*}{C}H_2$
4	4.0 - 4.2	$-CH_2CH=CH-\overset{*}{C}H_2-OH$
5	2.2 - 2.4	$-CH_2-\overset{*}{C}H-$ $\vert$ CH $\Vert$ CH_2
6	1.9 - 2.2	$-CH=CH-\overset{*}{C}H_2-$
7	1.2 - 1.6	$-\overset{*}{C}H_2-CH-$ $\vert$ CH $\Vert$ CH_2

* : denotes the proton type shifted.

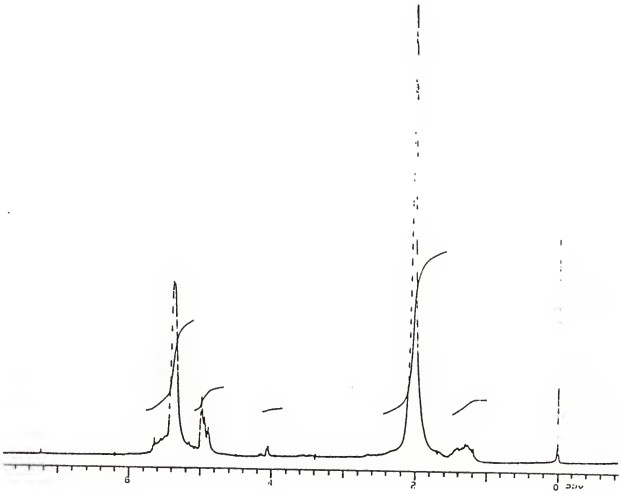

Figure 2.5 ^{1}H-NMR spectrum of hydroxytelechelic polybutadiene.

butyllithium-catalyzed polybutadiene splits into six peaks which are attributed to the triad sequences of cis and trans units with the use of high resolution ^{1}H-NMR. Tanaka (26) also concluded that polybutadiene with high contents of cis and trans units is randomly distributed between cis and trans units.

In addition to the cis and trans units, the polybutadiene we used contains a high percentage of vinyl units. Taking this into account, the distribution of the microstructure becomes more complicated. However, the number of possible triads can be calculated by probability statisics. As mentioned previously, the polymerization of 1,3-butadiene can result in 1,4 and 1,2 polymerization. Furthermore, the 1,4 units can have cis and trans configurations and 1,2 units can also yield structurally regular sequences (structures (a) and (b), respectively) as shown in Fig. 2.6. Therefore, the number of possible triads is 64.

Peak assignments are based on published work (27-29). Pham (29) studied the ^{1}H-NMR and ^{13}C-NMR spectrum of commercial polybutadiene, Arco R45M, using a high resolution (350MHz) spectrometer. He was able to determine the types of hydroxylated chain ends and the distribution of microstructure of the polybutadiene.

Figure 2.4 depicts the 75 MHz ^{13}C-NMR spectrum of the hydroxytelechelic polybutadiene. This spectrum was obtained

(a)

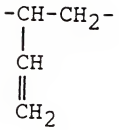

(b)

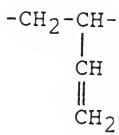

Figure 2.6 Structurally regular sequences of 1,2-polybutadiene.

by the spin-echo technique, which describes carbons with an odd number of attached hydrogens pointing upwards and those with an even number of attached hydrogens pointing downwards. In this Figure CH groups are upwards and CH_2 groups are downwards. This technique is designed for simplifying of peak assignment. For example, if this spectrum is substracted from the normal spectrum, it will result in the appearence of CH_2 peaks only.

The bands in the chemical shift range from 20 - 50 ppm are attributed to the aliphatic-carbon signals while the bands between 110 and 145 ppm are due to the olefinic-carbon signals. The peaks at 24.9, 27.4, 30.1, 32.7, 34.0, and 38.1 ppm are assigned to the methylene carbons on the cis unit of the cis-vinyl linkage, cis unit of the cis-cis linkage, trans unit of the trans-vinyl linkage, trans unit of the trans-trans linkage, vinyl unit of the trans-vinyl linkage, and trans unit of the vinyl-trans linkage, respectively. An expanded diagram of this region is shown in Fig. 2.7. Figure 2.8 shows the chemical structures of these assignments. Clague et al. (30) studied the microstructure of polybutadiene with various amounts of 1,2 structure while the ratio of cis-1, 4 to trans -1, 4 units was kept constant. They concluded that the three structures were randomly distributed and the 1, 2 units were incorporated head to tail. Recently, Bywater (31) investigated the microstructure of commercial polybutadiene (Phillips

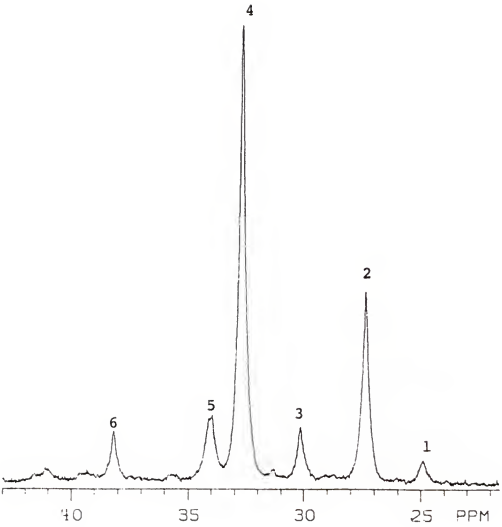

Figure 2.7 ^{13}C-NMR spectrum of aliphatic carbons for hydroxytelechelic polybutadiene.

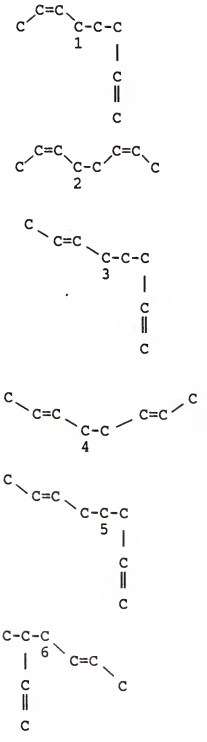

Figure 2.8 Peak assignments of methylene carbons and the corresponding microstructure for hydroxytelechelic polybutadiene.

Petroleum Co.) in the aliphatic region using high resolution ^{13}C-NMR spectrometer. The complicated methylene carbons originating from various combinations of 1, 4 and 1, 2 units were determined. On the basis of these data reported and with chemical shift information, the assignments can be made as shown in Fig. 2.4. However, small shifts may be expected due to different amounts of components present in the polymer and reaction conditions applied.

The upfield peak centered at 43.5 ppm represents vinyl CH; methine carbon on the vinyl unit of the trans-vinyl-trans linkage. The small bands around 41 ppm probably represents the methine carbon on the vinyl unit of the trans-vinyl-vinyl linkage while the very weak peak appearing at 46.5 ppm is attributed to the methine carbon on the vinyl unit which is adjacent to the terminal hydroxyl group. The relative chemical shift of these methine carbons is expected as can be seen from the chemical structures as shown in Fig. 2.9. It is noted that the chemical shift between 32.7 and 27.4 ppm is 5.3 ppm which is the characteristic value for the trans and cis oriented methylene carbons (31-33). A comparison of this value is shown in Table 2.2. It indicates the validity of the assignment in this work. Table 2.3 summarizes the peak assignments of methylene and methine carbons in the aliphatic region.

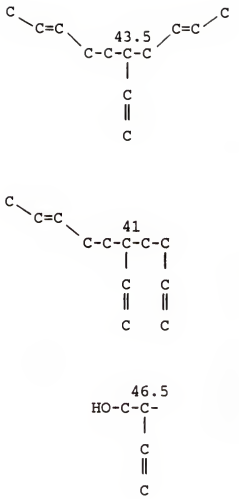

Figure 2.9 Peak assignments of methine carbons and the corresponding microstructure for hydroxytelechelic polybutadiene.

TABLE 2.2

Chemical Shift for Methylene Carbons between Cis and Trans Units

	Mochel[a]	Furukawa[b]	Tanaka[c]	Bywater[d]	This work
trans-trans	33.2	33.8	33.6	32.6	32.7
cis-cis	27.9	28.6	28.4	27.3	27.4
difference of chemical shift	5.3	5.2	5.2	5.3	5.3

[a]Mochel : See reference (32)

[b]Furukawa : See reference (33)

[c]Tanaka : See reference (26)

[d]Bywater : See reference (31)

TABLE 2.3

Peak Assignments of Methylene and Methine Carbons for Hydroxytelechelic Polybutadiene in the Aliphatic Region

Carbon type	Shift (ppm vs.TMS)	Chemical structure
1	24.9	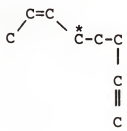
2	27.4	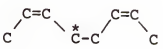
3	30.1	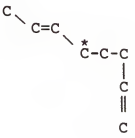
4	32.7	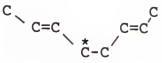

TABLE 2.3--continued

5	34.0	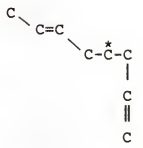
6	38.1	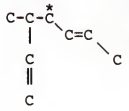
7	43.5	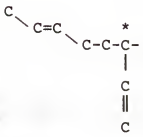

An attempt was made to estimate the relative amount of trans, cis, and vinyl units from the ^{13}C-NMR spectrum. This was done using peak areas.

The value thus obtained is 16 percent of the vinyl units which has a higher value than that reported using ^{1}H-NMR method. This is expected; the reason for getting a lower content of vinyl units using ^{1}H-NMR method has been mentioned previously. On the other hand, cis unit was found to be 26 percent.

The two very weak peaks at 63.2 and 64.3 ppm are attributed to the methylene carbons adjacent to the terminal hydroxyl groups. Their chemical structures are depicted in Fig. 2.10. The terminal hydroxyl groups exist in a very small concentration as can be seen from the peak intensity. Sometimes their resonance is not observed. This result is consistent with the data shown in Fig. 2.3, which also demonstrates a very small peak for terminal hydroxyl protons at 4.0 - 4.2 ppm. A small peak intensity of terminal hydroxyl protons was observed in other polymers, such as polyethyleneglycol, polyethyleneglycol monostearate (28).

The three peaks around 77 ppm are the solvent, $CDCl_3$. The peaks at lower field (110 - 145 ppm) are assigned to the olefinic carbon. The downwards peak at 114.2 ppm is due to the terminal methylene unit, $=CH_2$, while the upwards peak at 142.5 ppm represents the methine carbon, - CH=. The doublet peaks centered at 130.0 ppm are assigned to the olefinic

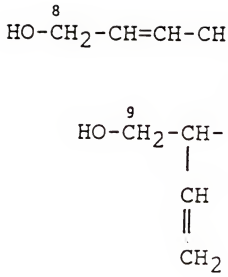

Figure 2.10 Peak assignments of the terminal methylene carbons and the corresponding microstructure for hydroxytelechelic polybutadiene.

carbons of cis-cis and trans-trans linkage. An expanded region is shown in Fig. 2.11. It can be seen clearly that two doublets are present in this region. Their peak assignments are at 130.14, 130.01, 129.62, and 129.43 ppm. Furukawa et al. (33) investigated the microstructure of equibinary polybutadiene prepared by 2,6,10-dodecatriene-1,12-diyl nickel ($C_{12}H_{18}Ni$), trifluoroacetic acid (CF_3COOH) as catalysts. They assigned the peak shifts for trans-trans linkage and cis-cis lingkage to 131.2 and 130.6 ppm, respectively. Tanaka et al. (34) also studied the equibinary polybutadiene with the same catalysts. The peaks they assigned were 130.30, 130.19, 129.77, and 129.59 ppm. Conti et al. (35) reported the structure of equibinary polybutadiene initiated with π-allyl nickel trifluoroacetate (π-C_3H_5-Ni-$OCOCF_3$), 2,6,10-dodecatriene-12-yl nickel trifluoroacetate (π-$C_{12}H_{19}$-Ni-$OCOCF_3$). They found the peaks were located at 130.85, 130.75, 130.25, and 130.10 ppm. However, the polybutadiene we used is more complicated due to the higher content of vinyl units. A few minor peaks are present in this olefinic carbon region. This is due to the vinyl units combined with the cis and trans unit resulting in additional resonance peaks. Elgert et al. (36) studied the microstructure of polybutadienes with different composition of cis, trans, and 1, 2 units. They assumed the additivity of the chemical shift resulting from different environments of a carbon atom can be applied to the polymer

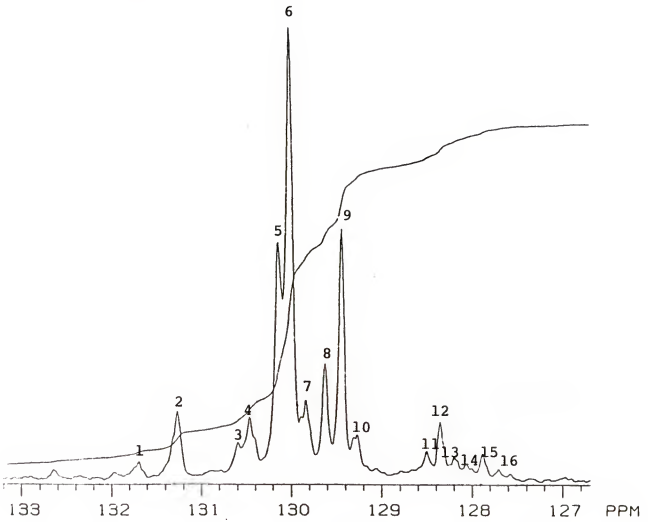

Figure 2.11 ^{13}C-NMR spectrum of hydroxytelechelic polybutadiene at the lower field.

molecules. Thus, by using the empirical set of shift parameters, one can calculate the chemical shift due to the neighboring 1, 2 unit on the cis or trans-1, 4 unit. Therefore, with these parameters, we can calculate the chemical shift due to a neighboring 1, 2 unit on the carbons of trans and cis-1, 4 double bond centered at 130.01 and 129.62 ppm, respectively. For example, assuming the triad vinyl-trans-vinyl is present, then the chemical shifts of the carbons of the trans double bond due to the two vinyl units are 131.72 and 128.16 ppm as can be seen from the chemical structure shown in Fig. 2.12. The observed values of these two carbon atoms are 131.70 and 128.20 ppm, respectively which are in good agreement with the calculatd values. Table 2.4 depicts the chemical shifts of the methylene and methine carbon present at the lower field of Fig. 2.4. Detailed assignments of the cis and trans double bonds in the olefinic region are listed in Table 2.5. It is noted that the chemical shift of the calculated value agrees well with the observed value. This indicates that the method used in the peak assignment is valid.

According to the data from the manufacturer, the molecular weight ($\bar{M}_n$) of the hydroxytelechelic polybutadiene is 2800. Therefore, we can calculate the approximate number of repeated units. A value of 52 was obtained.

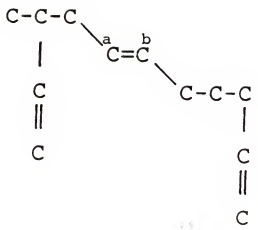

Chemical shift ^{a}C = 130.01 - 1.66 - 0.19 = 128.16

Chemical shift ^{b}C = 130.01 + 1.25 + 0.46 = 131.72

Figure 2.12 Microstructure of vinyl-trans-vinyl triad and the corresponding chemical shift for hydroxy-telechelic polybutadiene.

TABLE 2.4

Peak Assignments of Methylene and Methine Carbons for Hydroxytelechelic Polybutadiene at the Lower Field

Carbon type	Shift (ppm vs. TMS)	Chemical Structure
8	63.2	$HO-\overset{*}{C}H_2-CH=CH-CH_2$
9	64.3	$HO-\overset{*}{C}H_2-CH(-CH=CH_2)-$
10	114.2	$-CH=\overset{*}{C}H_2$
11	130.0	$-\overset{*}{C}H=CH-$
12	142.5	$-CH=\overset{*}{C}H_2$

TABLE 2.5

Comparison of the Chemical Shift of the Observed and the Calculated Value of Olefinic Carbons

Peak	Type[a]	Chemical shift (ppm) Observed value	Calculated value
1	vtv	131.70	131.72
2	ttv	131.26	131.26
3	vcv	130.60	130.58
4	vtt	130.46	130.47
5	ctc	130.14	130.12
6	ttt	130.01	130.01
7	ttv	129.83	129.82
8	ccc	129.62	129.62
9	tct	129.43	129.44
10	tcv	129.26	129.13
11	vtc	128.48	128.46
12	vtt	128.35	128.35
13	vtv	128.20	128.16
14	vcc	128.05	128.02
15	vct	127.84	127.84
16	vcv	127.71	127.71

a : v = vinyl
t = trans
c = cis

2.3.3 NMR Analysis of the Oligomeric Polyester (OPE-1)

The ^{1}H-NMR spectrum of the OPE-1 is shown in Fig. 2.13. It is noted that some new peaks appeared. The methylene groups adjacent to the terminal hydroxyl groups have been shifted to the lower field upon formation of the ester linkage with the diacid, i. e.,

$$- CH_2 - OH + HOOC - C - \rightarrow - CH_2 - O - CO -$$

As expected, these deshielded methylene groups resonate at lower field 4.55 ppm compared with the terminal methylene group adjacent to the hydroxyl group. However, there are some terminal hydroxyl groups still left after the esterification process as indicated from the weak peak at 4.06 ppm. The degree of conversion can be calculated by the following equation:

$$\text{conversion } \% = \frac{A_4}{A_4 + A_5} \cdot 10^2$$

where,

A_4 = peak area of $-CH_2-O-CO$

A_5 = peak area of $-CH_2-OH$

A 69 percent conversion was observed in this case. The formation of an ester linkage can be further confirmed by the appearance of the new peak at 3.45 ppm which originated from the methine proton of the methylmalonic acid. An expansion of this region is shown in Fig. 2.14. The increased intensity of the bond in the chemical shift range from 1.2 - 1.6 ppm is attributed to the formation of a new

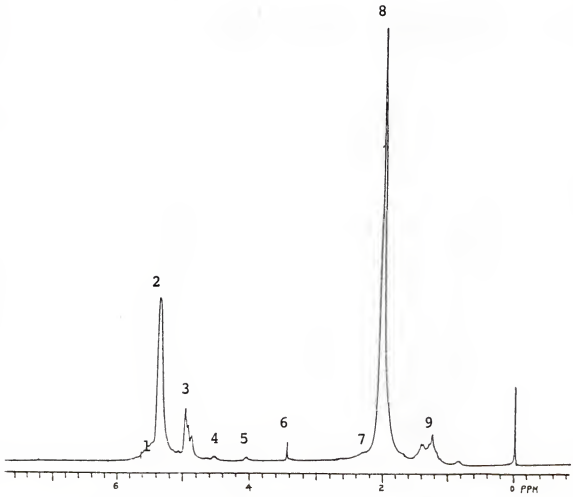

Figure 2.13 ^{1}H-NMR spectrum of OPE-1.

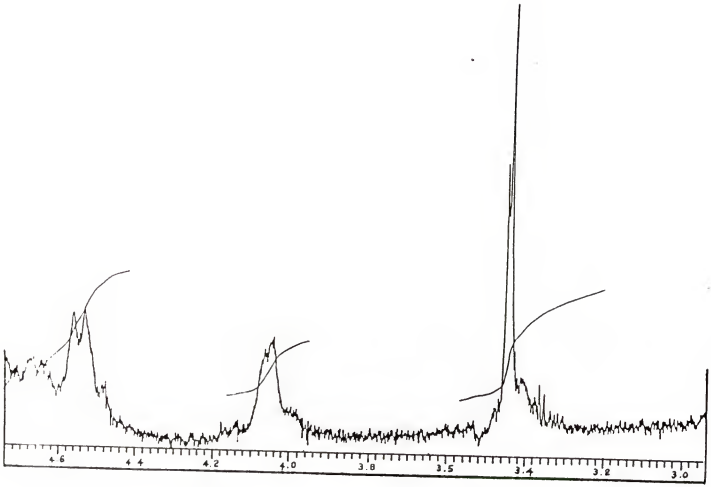

Figure 2.14 ^{1}H-NMR spectrum of OPE-1 (expanded spectrum).

peak which comes from the methyl group of the methylmalonic acid. An assignment of these peaks is listed in Table 2.6.

The ^{13}C-NMR spectrum of OPE-1 is shown in Fg. 2.15. The spin-echo technique was also applied here for easy identification of the peaks. In comparison with the spectrum of hydroxytelechelic polybutadiene, some additional peaks are observed at 13.8, 46.3, 65.6, 67.4 and 169.9 ppm, though they all appear as very weak peaks. The peak at 13.8 ppm arises from the methyl carbon of the methylmalonic acid, while the peak at 46.3 ppm is attributed to the methine carbon bonded to the ester carbon. The peaks at 65.6 and 67.4 ppm are attributed to the methylene carbons bonded to the ester oxygen atoms. It is noted that the formation of an ester linkage results in the downfield shift of some methylene carbons which are originally bonded to terminal hydroxyl groups. The formation of ester linkages can be further suggested by the appearance of the new peak at 169.9 ppm as shown in Fig. 2.16. This ester group contains a nonprotonated carbon atom and may give a lower intensity. Table 2.7 shows the assignment of these new peaks and their corresponding chemical structure.

It is useful to know some physical properties of the hydroxytelechelic polybutadiene and OPE-1 polymers. The number-average molecular weight ($\bar{M}n$) and weight-average molecular weight ($\bar{M}w$) of the hydroxytelechelic polybutadiene reported from the manufacturer are 2800 and 6000,

TABLE 2.6

Peak Assignments of ^{1}H-NMR Spectrum for OPE-1

Hydrogen type	Shift (ppm vs. TMS)	Chemical Structure
1	5.5 - 5.9	$-\overset{*}{C}H=CH_2$
2	5.3 - 5.5	$-\overset{*}{C}H=CH-$
3	4.9 - 5.1	$-CH=\overset{*}{C}H_2$
4	4.55	$-\overset{*}{C}H_2-O-CO-$
5	4.06	$-\overset{*}{C}H_2-OH$
6	3.45	$OOC-\overset{*}{C}H(CH_3)-COO$
7	2.2 - 2.4	$-CH_2-\overset{*}{C}H(-CH=CH_2)-$
8	1.9 - 2.2	$-CH=CH-\overset{*}{C}H_2-$
9	1.2 - 1.6	$-\overset{*}{C}H_2-CH(-CH=CH_2)$ and $OOC-CH(\overset{*}{C}H_3)-COO$

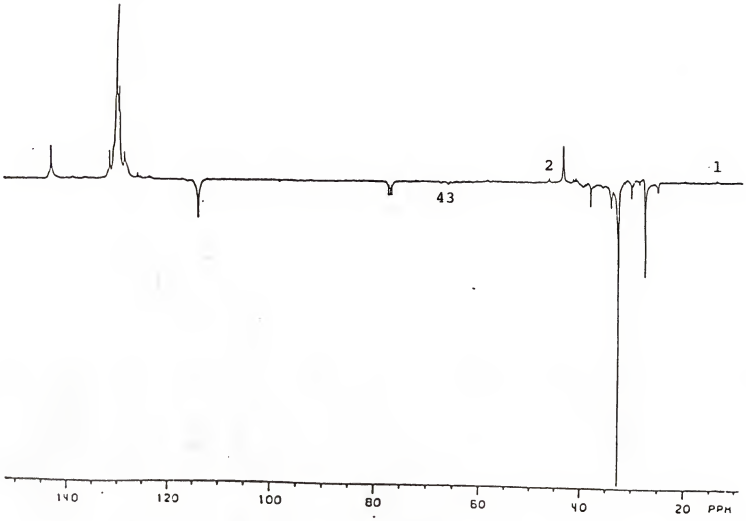

Figure 2.15 ^{13}C-NMR spectrum of OPE-1.

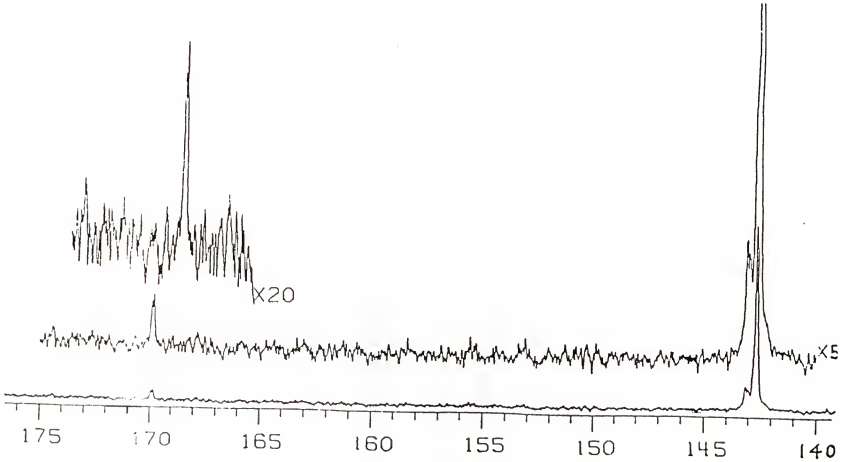

Figure 2.15--continued

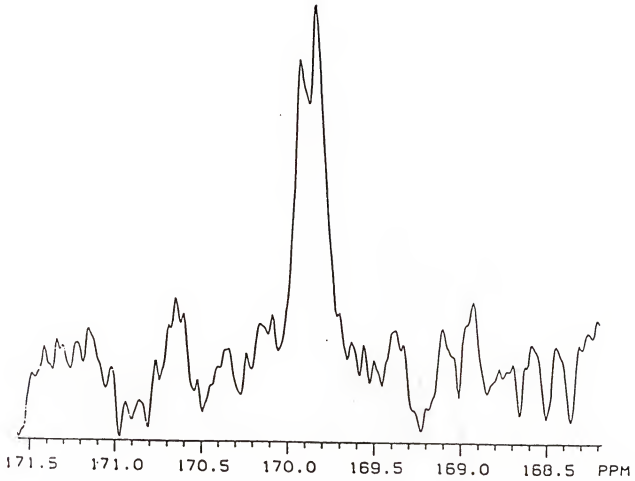

Figure 2.16 ^{13}C-NMR spectrum of OPE-1 at ester peak.

TABLE 2.7

Peak Assignments of ^{13}C-NMR Spectrum for OPE-1

Carbon type	Shift (ppm vs. TMS)	Chemical Structure
1	13.8	
2	46.3	
3	65.6	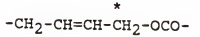
4	67.4	
5	169.9	

respectively. The value of Mn from ^{1}H-NMR end-group analysis for hydroxytelechelic polybutadiene has a approximate value of 2900 which is close to the data reported from the manufacturer. The average degree of condensation polymerization can also be estimated by measuring the peak area of $-CH_2OH$ and $-COO-CH_2-$. A value of 3.0 is obtained. The values of Mn and Mw for OPE-1 are 8000 and 18000, respectively using gel permeation chromatography.

Both ^{1}H-NMR and ^{13}C-NMR spectra show very weak peaks of the functional ester groups. This is due to the low nucleophilicity of the hydroxyl groups. The low intensity of the terminal hydroxyl groups shown in Fig. 2.3 and 2.4 may be another possible reason for the very weak peaks of the functional ester groups.

The influence of solvent on the polycondensation reaction was reviewed by Berlin and Matvejeva (37). Lipatova investigated the reaction of oligopropylene glycol with diisocyanate in the absence of solvent at a temperature of 100°C. He found the reactivity of NCO groups decreased when the molecular weight of oligopropylene glycol increased from 500 to 2000. However, when the low molecular weight materials were diluted with a solvent the reactivity for the high and low molecular weight of oligopropylene glycol were essentially the same. He attributed this to the solvation effect on the reactive sites. Ogata (38) also studied the effect of solvent on the reactivity of functional groups in

polycondensation reactions. He suggested that the reaction between the solvent and functional groups may result in the polarization or solvation between the functional groups and solvent, which may enhance or retard the overall reaction. The dependence of the reactivity of oligomers on their molecular weight was reported (37). The reactivity of oligoethylene glycol with phenyl isocyanate in chlorobenzene was found to decrease with an increasing of the molecular weight of the oligomer. The results were attributed to the formation of associates due to intermolecular and intramolecular hydrogen bonds which result in the reduction of the reactivity of the end hydroxyl groups.

2.3.4 IR Results

Figure 2.17 shows the spectrum of the OPE-1 polymer. The small peak at 3076 cm^{-1} is attributed to the CH asymmetric stretching of the terminal methylene groups. The peak at 3006 cm^{-1} is attributed to the stretching of the methine group adjacent to the double bonds. The appearance of 3076 cm^{-1} and 3006 cm^{-1} bands indicates the presence of unsaturated double bonds such as $-CH=CH_2$. The peaks at 2917 cm^{-1} and 2844 cm^{-1} are assigned to the asymmetric and symmetric stretching of aliphatic methylene groups, respectively. The peaks at 1735 cm^{-1} and 1752 cm^{-1} are the characteristic peaks for the unsaturated esters, i.e.,

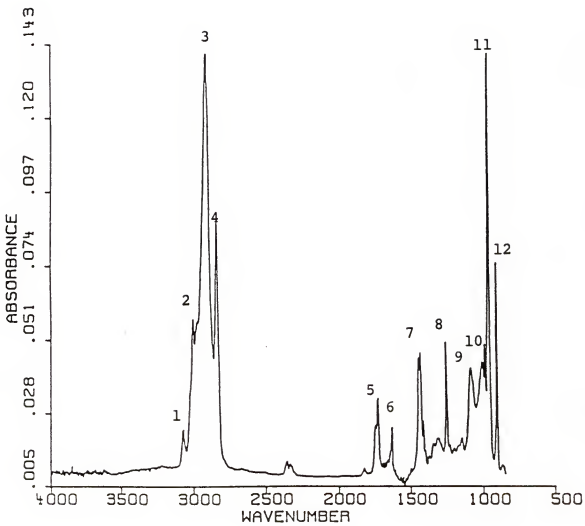

Figure 2.17 IR spectrum of OPE-1.

-CH=CH-CH_2-O-CO-. The peak at 1640cm^{-1} is due to the stretching of olefinic double bonds.

The absorption band at 1445 cm^{-1} is attributed to CH bending of the methylene group adjacent to the double bonds, i.e., -CH_2-C=C-. The peaks at 1259 cm^{-1} and 1093 cm^{-1} are attributed to the stretching of C-O-C group. There are usually two peaks between 1300 cm^{-1} and 1050 cm^{-1} for C-O-C stretching. One is responsible for asymmetric stretching, while the other is responsible for symmetric stretching. The asymmetric stretching peak (1259 cm^{-1}) is usually stronger than the ester peak -O-CO- (1735 cm^{-1}). This is indeed the case as shown in Fig. 2.17. The two stretching peaks of the C-O-C group further indicates the formation of the ester peaks. The peak at 994 cm^{-1} represents the CH bending (out of plane) of the terminal vinyl groups. The strong peak at 967 cm^{-1} is assigned to the CH bending (out of plane) of the trans olefinic double bonds. The peak at 912 cm^{-1} is attributed to the CH bending (out of plane) of the terminal vinyl groups -CH=CH_2.

The assignments of the above bands were obtained from the references (39-40). The chemical structure of OPE-1 is thus characterized by the specific absorption bands and the formation of ester linkage as suggested by the peaks at 1735 cm^{-1}, 1259 cm^{-1}, and 1093 cm^{-1}. Table 2.8 summarizes these peak assignments and the corresponding chemical structures.

TABLE 2.8

Peak Assignments of IR Spectrum for OPE-1

Peak	Frequency (cm^{-1})	Chemical Structure
1	3076	Asymmetric stretching of $=CH_2$
2	3006	Stretching of -CH=
3	2917	Asymmetric stretching of $-CH_2-$
4	2844	Symmetric stretching of $-CH_2-$
5	1735	Stretching of -O-CO-
6	1640	Stretching of -C=C-
7	1445	CH bending of $-CH_2-C=C-$
8	1259	Asymmetric stretching of C-O-C
9	1093	Symmetric stretching of C-O-C
10	994	CH bending of $-CH=CH_2$
11	967	CH bending of trans -CH=CH-
12	912	CH bending of $-CH=CH_2$

The spectrum of the polybutadiene is shown in Fig. 2.18. When Fig. 2.17 is compared with Fig. 2.18, three additional peaks are shown in Fig. 2.17 at 1735 cm^{-1}, 1259 cm^{-1}, and 1093 cm^{-1}. From NMR and IR analysis, it is concluded that the polycondensation of diol and diacid at room temperature results in a polyester (OPE-1). Notice that the peak position around 2350 cm^{-1} is the CO_2 which is common in the IR spectrum.

The spectrum of methylmalonic acid is shown in Fig. 2.19. The assignments of the peak position are as follows: the most characteristic band for acid identification in IR is the strong and broad band in 2500 cm^{-1} to 3500 cm^{-1}. This is due to the formation of hydrogen bonding between COOH groups. Several bands appear between 2800 cm^{-1} and 2500 cm^{-1} which are due to the combination tones of the fundamental vibrations around 1400 cm^{-1} and 1300 cm^{-1} - 1200 cm^{-1}, and indicates the formation of carboxylic acid dimer. The sharp peaks in the region (2980 cm^{-1} - 2850 cm^{-1}) are attributed to the stretching of CH_3 and CH groups.

Another diagnostic peak for acid dimer formation is the peak at 1700 cm^{-1} which is assigned to the stretching of C = O groups. The bands around 1400 cm^{-1} and 1300 cm^{-1} to 1200cm^{-1} are due to coupling between OH bending and CO stretching of dimer as indicated in Fig. 2.20. The peak at 915 cm^{-1} is due to the out of plane bending of OH groups.

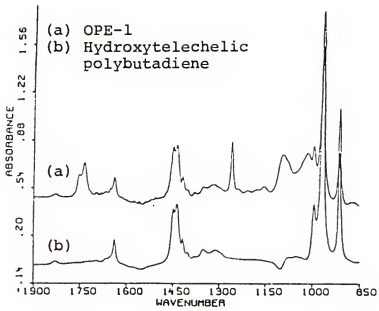

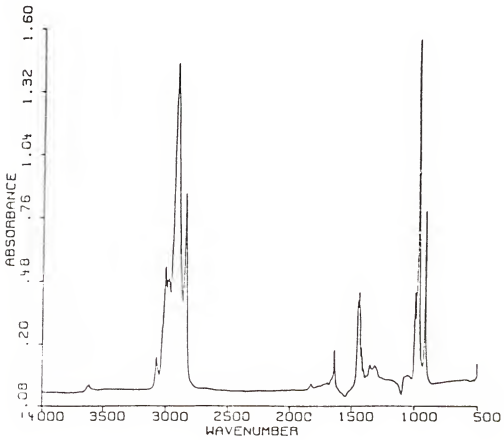

Figure 2.18 IR spectrum of hydroxytelechelic polybutadiene.

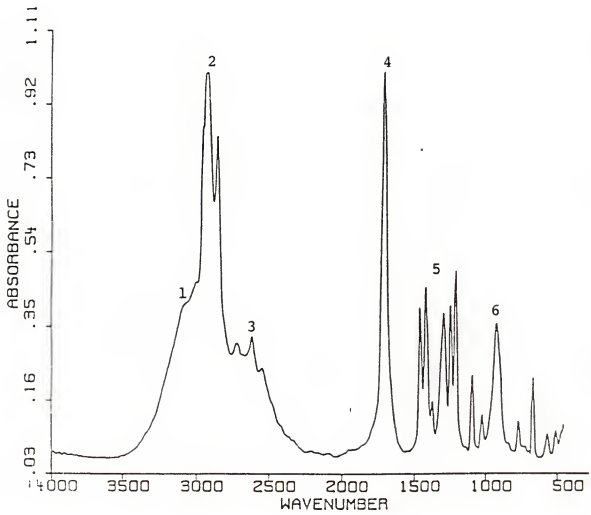

Figure 2.19 IR spectrum of methylmalonic acid.

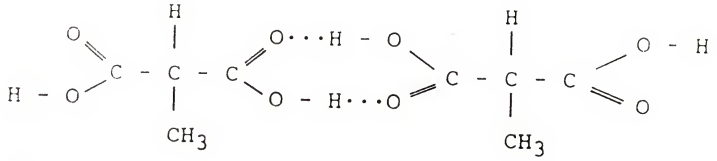

Figure 2.20 Schematic diagram of coupling between OH bending and stretching of acid dimer.

Table 2.9 lists the diagnostic peaks for methylmalonic acid and the corresponding assignment.

The spectrum of the dicyclohexylurea, a side product during the reaction, is also shown in Fig. 2.21. Some major bands are assigned as following: the band around 3320 cm^{-1} is due to stretching of N-H groups, the band in the region of 2850 cm^{-1} - 3000 cm^{-1} is due to the CH_2 stretching, the peak at 1625 cm^{-1} is due to the stretching of the amide group. The bands around 1550 cm^{-1} and 1300 cm^{-1} are assigned to the bending of N-H and stretching of C-N groups. Figure 2.22 shows the spectrum of dicyclohexylurea listed in the Aldrich library. Comparing Fig. 2.21 with 2.22, they are similar.

TABLE 2.9

Diagnostic Peak Assignments of IR Spectrum for Methylmalonic Acid

Peak	Frequency (cm^{-1})	Chemical structure and assignments
1	3500 - 3000	OH stretching
2	2980 - 2850	CH and CH_3 stretching
3	2800 - 2500	Combination tones of vibrations at 1400 cm^{-1} and 1300-1200 cm^{-1}
4	1700	Stretching of C=O
5	1400, 1300-1200	Coupling between OH bending and CO stretching of dimer
6	915	OH bending

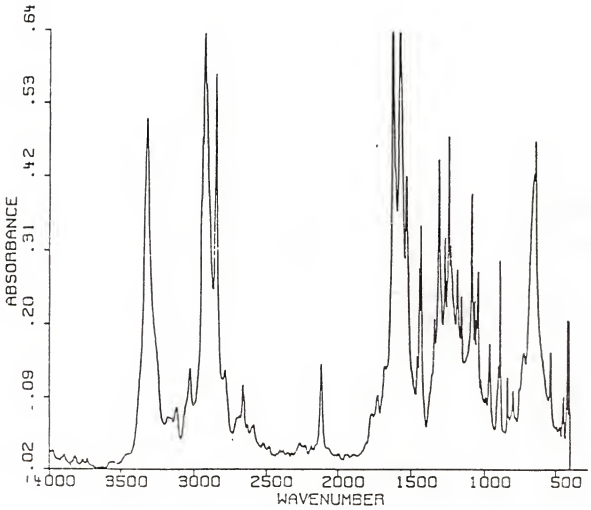

Figure 2.21 IR spectrum of dicyclohexylurea.

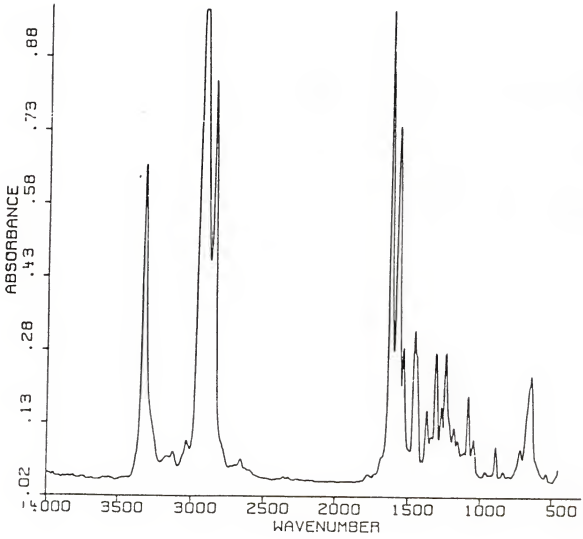

Figure 2.22 IR spectrum of dicyclohexylurea (Aldrich).

CHAPTER 3
HYDROXYLATION AND ACETALIZATION

3.1 Background

3.1.1 Methods for Hydroxylation

Several methods have been applied to the hydroxylation of organic olefin compounds, including the use of hydrogen peroxide (41), aromatic and aliphatic peracids (42), halogens and silver carboxylates (43), osmium tetroxide (44), and potassium permanganate (45). The choice of the method depends on the structure of the product needed and the toxicity and cost of the reactants.

Hydroxylation of olefins with permanganate has long been used in the organic laboratory. Because this reagent can oxidize olefin in several ways, it is necessary to control the reaction conditions very carefully in order to get a good yield of the desired product.In alkaline solution, glycol is the main product while in a neutral or acidic condition, a ketol is formed (46). Coleman et al. (47) showed that the oxidation of oleic acid with potassium permanganate results in a mixture of diol and ketol. A high yield of ketol will be obtained when the reaction mixture is kept neutral while obtaining the diol in basic solution. Wolfe et al. (48) studied the oxidation mechanism of olefins

using potassium permanganate. They reported that glycol and ketol are formed from a common intermediate. The formation of the final products depends largely on the reaction conditions. A reaction mechanism was proposed.

3.1.2 Phase Transfer Catalyst

Conventionally, aqueous permanganate solution is used in the hydroxylation of the olefins. However, the organic compounds should be at least partially soluble in water in order to react with the oxidant. Eastman and Quinn (49) attempted to oxidize 2,2,4-trimethylpentane in permanganate solution, but the reaction did not proceed at the tertiary hydrogen even after several months in the aqueous permanganate solution. They showed, however, that the oxidation of 2,4-dimethylpentane-2-ol could proceed because of the solubility of the reactant in the aqueous phase. This was attributed to the formation of hydrogen bonding between water and alcohol groups. To overcome this solubility problem, an attempt was made to use polar organic solvents such as ethanol, acetone, and t-butyl alcohol to increase the solubility of both reactants (50). On the other hand, Starks (51) reported that terminal olefins can be oxidized to carboxylic acid by potassium permanganate solution containing some phase transfer catalysts. Sam and Simmons (52) found that potassium permanganate can be solubilized in

benzene by complexing with dicyclohexyl-18-crown-6 and can act as an efficient oxidant.

Tetrabutylphosphonium chloride and tetrabutylammonium bromide were used by Okimoto and Swern (53) as phase transfer catalysts for hydroxylation of oleyl and elaidyl alcohol in cold, dilute alkaline potassium permanganate solution. They found the hydroxylation would not take place if phase transfer catalysts were not used. Lee and Chang (54) did a series of experiments in comparison the use of a quaternary ammonium ion, a crown ether, and acyclic polyethers as phase transfer catalysts for the oxidation of alkenes by potassium permanganate. Ogino and Mochizuki (55) reported the use of triethylbenzyl ammonium chloride as a phase transfer catalyst in a non-aqueous organic system. They found the precipitation of manganese dioxide would not occur when the reaction was carried out in the anhydrous condition. Recently, Taylor et al. (56) reported that vigorous stirring and dilution will increase the yield of diol due to the reduction of localized permanganate ions.

3.1.3 The Phase Transfer Process

A phase transfer catalyst can accelerate the reaction between ionic compounds and organic, water-insoluble compounds in organic solvent. As the name implies, it can transfer the ionic molecules which are not soluble in

organic solvent into the organic medium in the form of ion pairs.

The solubility of the ion pair in the solution depends on the Coulombic force, the hydrogen bonding force, the dipole force within the pair and solvent molecules. Swern and Okimoto (57) did a series of experiments to evaluate the efficiency of extracting permanganate ion from water into benzene or methylene chloride with six different phase transfer agents. They found methylene chloride is in general better than benzene as a phase transfer solvent. Brandstrom (58) tested the extractability of tetra-n-butylammonium bromide from water into various solvents. He also demonstrated that chlorinated hydrocarbons were superior to other solvents. He attributed this to the donorability of the electron from the solvent resulting in a solvent-separated ion pair. Gibson and Weatherburn (59) reported that permanganate anion is easier to extract from aqueous solution into organic solvents than other anions (ClO_4^-, BrO_3^- et al.) This is probably because the permanganate anion is less hydrated due to the lower charge to volume ratio. For this reason, less energy is required for transformation of the anion from aqueous solution into the organic solvent (60). The size of the quaternary ion is also important in the extraction process. The larger the alkyl groups surrounding the central nitrogen atom of the ammonium cations, the more lipophilic the cations are. This special

structure of the quaternary ion would enhance the extraction process.

We may conclude from the above that methylene chloride and quaternary ammonium salt with large alkyl groups would be suitable for extraction of permanganate ion from the aqueous phase into the organic phase. If the ion pairs formed in the organic phase are thermodynamically stable and no interaction between the ion pairs and solvent molecules occurs, the ion pairs can react with the organic substrate easily. From the above literature methylene chloride and benzyltriethylammonium chloride have been chosen as the reagents for this study.

3.1.4 Methods for Acetalization

It is well known that acetals can be formed by the reaction of alcohols with aldehydes in the presence of small amounts of acid such as sulfuric acid or hydrochloric acid. The reaction can be described by the following equations:

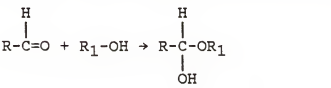

(3.1)

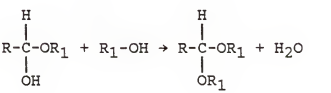

(3.2)

The hemiacetal is usually not stable and reacts immediately with another alcohol molecule to form an acetal with the aid of an acid catalyst. The resulting acetals are purified by dissolving them in a good solvent and reprecipitating them in a nonsolvent. For 1,2-glycol or 1,3-glycol, the reaction of diols with aldehydes results in the formation of cyclic acetals as can be seen from the following equations:

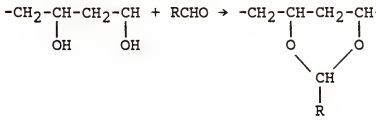

(3.3)

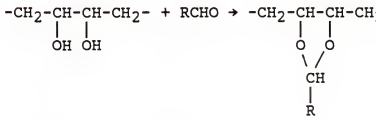

(3.4)

Overall there are five methods in making poly(vinyl acetals):

1. Dissolution method: Poly(vinyl alcohol) is suspended in a nonsolvent which can dissolve the final product, i.e., the reaction occurs heterogeneously and ends homogeneously.
2. Precipitation method: Poly(vinyl alcohol) is dissolved in a suitable solvent with the aldehyde. The homogeneous phase gradually changes into a heterogeneous phase when the acetal precipitates.

3. Heterogeneous method: Poly(vinyl alcohol) in the film or fiber form which can not dissolve in any solvent is reacted with aldehyde to form acetal.
4. Direct method: Poly(vinyl acetate) is dissoved in a good solvent and is converted to poly(vinyl alcohol) in acid solution followed by acetalization.
5. Homogeneous method: The poly(vinyl alcohol) is homogeneously reacted with aldehyde in a water solution. A solvent for the acetal which is miscible with water is continuously added into the mixture to prevent precipitation of the final acetal.

Herrmann and Haehnel prepared the poly(vinyl acetals) by reaction of poly(vinyl alcohol) with benzaldehyde (61). Rombach (62) in E. I du pont de Nemours & Co, Inc, developed a water solution process for making poly(vinyl butyrals). A reactor was charged with a 10% solution of poly(vinyl alcohol), sulfuric acid, and butyraldehyde. The whole solution was maintained at 90°C for 1.5 hours. Poly(vinyl butyral) formed by precipitation, was washed after neutralization with basic solution and dried. Koshita et al. (63) also prepared poly(vinyl butyral) by heating solution mixtures containing poly(vinyl alcohol), water, methanol, butyraldehyde, and a small amount of sulfuric acid, at 60°C - 70°C for several hours. Flowers and Winter (64) synthesized poly(vinyl formal) by reaction of poly(vinyl acetate), glacial acetic acid, formalin, and concentrated

sulfuric acid together at 70°C. Ammonium hydroxide was then added to adjust the PH value in the range of 9 to 10. The final mixture was poured into water to precipitate the poly(vinyl formal). Other methods and reactants for conducting poly(vinyl acetal) are listed in references (65, 66).

3.2 Materials and Methods

3.2.1 Materials

Polyesters were derived from products (OPE-1) of previous experiments. Methylene chloride, sodium bisulfite, potassium permanganate, dioxane, concentrated sulfuric acid, and ethanol were obtained from Fisher Scientic Company. Benzyltriethylammonium chloride was obtained from Kodak, and butyraldehyde was obtained from the Aldrich Company.

3.2.2 Methods

3.2.2.1 Hydroxylation

Due to the possibility of decomposition of the permanganate solution from thermal heat, the solution was prepared fresh from solid permanganate powders before conducting the experiments. OPE-1 (4.82g) in 30 c.c. of CH_2Cl_2 was placed in a three-necked round bottom flask with a capacity of 500 ml and ground joint size of 24/40. This round bottom flask was equipped with a mechanical stirring system composed of a glass-rod shaft and a half-moon shaped

Teflon blade. A schematic diagram of the reaction system is shown in Fig. 3.1. After being stirred 30 minutes, the OPE-1 was completely dissloved in CH_2Cl_2, and a 100 ml solution containing benzyltriethylammonium chloride and potassium permanganate was added drop by drop into the flask. Sodium hydroxide solution (50 ml) was then added into the mixture. Temperature was kept constant at 0°C by using an ice salt bath. The reaction was continued for 48 hours with vigorous stirring so that the oxidant would be well-dispersed in the whole bulk solution. The reaction mixture was then decolorized by the addition of an aqueous sodium bisulfite solution. The white precipitate was filtered out, and washed several times by stirring with a hydrochloric acid solution and distilled water. Finally, the solvent was removed by evaporation in a vacuum oven at 50°C for 24 hours. This product is defined as OPE-2.

3.2.2.2 Acetalization

The products from the hydroxylation were dissolved in a mixture of dioxane and ethanol in a three-necked round bottom flask with a reflux condenser. A mechanical stirring system with a glass-rod shaft and a half-moon shaped Teflon blade were used for vigorous agitation. The whole system was then immersed in a constant temperature-controlled circulation bath. A small amount of concentrated sulfuric acid was added drop by drop into the mixture when the

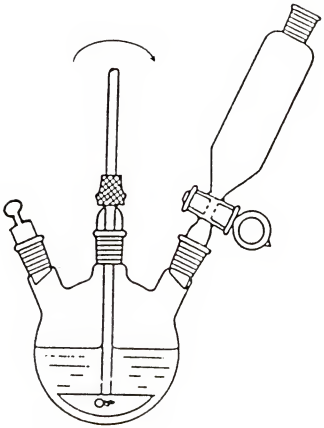

Figure 3.1 Reaction system for the oxidation of unsaturated OPE-1.

resulting solution became homogeneous. Butyraldehyde (1 g) was then added into the above solution. The reaction temperature was kept at 75°C for 12 hours. The solvents (dioxane, ethanol and unreacted butyraldehyde) were evaporated by the suction pump with the aid of a capillary tube. The precipitated polymers were redissolved in the mixture of dioxane and ethanol and reprecipitated in a large volume of methanol several times. The resulting polymers were then dried in a vacuum oven at 50°C for 24 hours. This product is denoted as OPE-3.

3.3 Results and Discussions

3.3.1 Hydroxylation of the Double Bonds

Figure 3.2 shows the hydroxylation result of the unsaturated polyester. It is noted that a broad and strong band appears at 3430 cm^{-1}. This is due to the formation of OH groups. Another result is the reduction of the intensity of -CH groups associated with -CH=CH- located at 967 cm^{-1} and 912 cm^{-1}. This implies that some of the unsaturated double bonds have been converted to single bonds with hydroxyl groups attached to the carbon atom. The stretching of the C-O-C groups shown in Figure 2.17 at 1259 cm^{-1} and 1093 cm^{-1} is shifted to the lower frequencies at 1200 cm^{-1} and 1075 cm^{-1}, respectively. This may be attributed to the formation of hydrogen bonding and state of measurement. Moller and Rothschild (67) have discussed the shift of

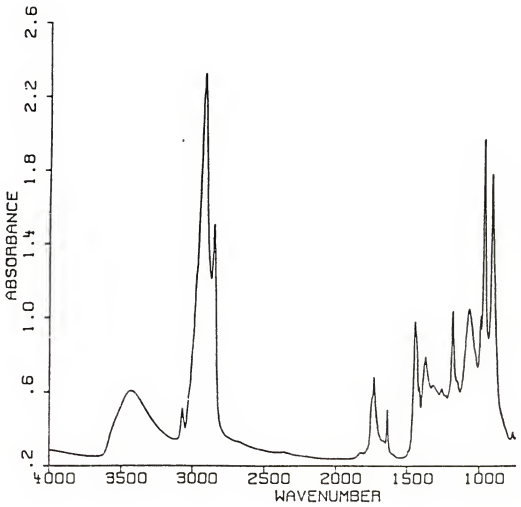

Figure 3.2 IR spectrum of OPE-2.

frequency under various conditions as being due to the formation of hydrogen bonding. The electron clouds of a functional group will rearrange themselves when another atom with strong electronegativity such as an oxygen atom approaches. This results in the deformation of the electron structure and changes the bond angles and bond distances. Consequently, less energy is required for causing the vibration. The state of measurement also affects the frequency. Koenig (68) obtained the infrared spectra of hemoglobin, bovine serum albumin, ribonuclease, β-lactoglobulin, and α-casein in aqueous solution as well as in cast film. The spectra measured by film form showed lower frequencies than the corresponding liquid-phase frequencies. This was attributed to the hydrogen-bonding effect. Nakanishi and Solomon (39) gave an example of how the band shifts are due to the formation of hydrogen bonding. Dimedone forms the intermolecular hydrogen bonding in solid state resulting in a shift of C=O functional group from 1675 cm^{-1} to 1616 cm^{-1}. In our case, the intermolecular hydrogen bonding may also be formed resulting in a shift of the frequency. This band may overlap with the band C-OH stretching vibration. The presence of hydroxyl groups can be further confirmed by the reaction of the dihydroxyl groups with the aldehyde and the formation of cyclic acetal which will be discussed later.

Numerous researchers have reported that the presence of an unstable cyclic intermediate will further advance the ring opening reaction and form ketols, glycols, or acids, depending on the basicity of the reaction conditions (69). The reactions they used were for small organic molecules. We attempted to use this method for macromolecular reactions as the reaction mechanism may be similar. This is shown in Fig. 3.3. The efficiency of the reaction clearly depends on the interaction between the reactive site of the unsaturated polyester and the formed quarternary ammonium permanganate, followed by the nucleophilic attack of the hydroxyl group and hydrolysis of the unstable intermediate.

3.3.2 Results of the Acetalization

3.3.2.1 Acetalization of the Poly(vinyl Alcohol)

Since most of the acetalization methods originated from the patents, we attempted to assemble experiences and get optimum condition parameters for the experiments. Therefore, a preliminary experiment was carried out by reacting poly(vinyl alcohol) with butyraldehyde. Figure 3.4 shows the IR spectrum of poly(vinyl alcohol). The peak assignments are shown in Table 3.1. From these assignments, it is apparent that the poly(vinyl alcohol) contains some vinyl acetates and some hydroyzed groups which can be denoted by the following structure:

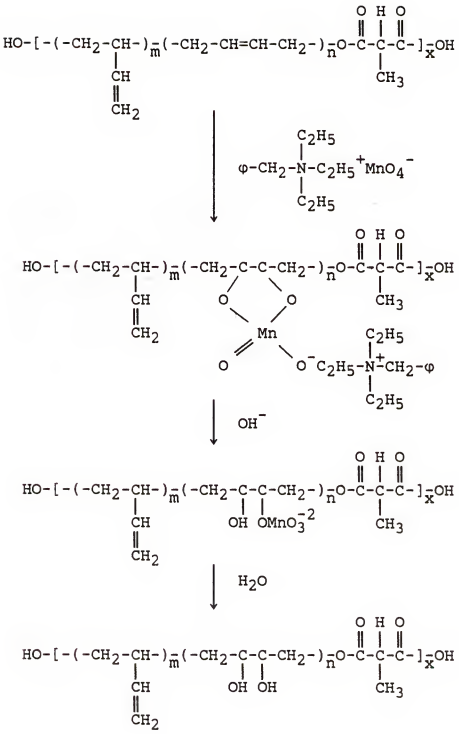

Figure 3.3 Hydroxylation mechanism.

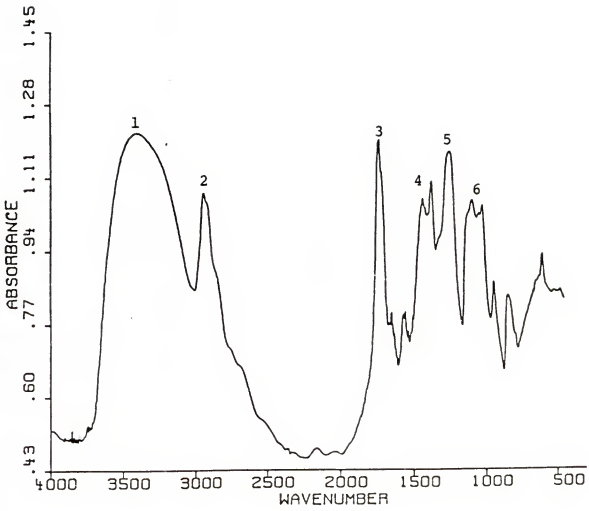

Figure 3.4 IR spectrum of poly(vinyl alcohol).

TABLE 3.1

Peak Assignments of IR Spectrum
for Poly(vinyl alcohol)

Peak	Frequency (cm^{-1})	Functional Groups
1	3340	OH stretching
2	2940	CH stretching of $-CH_2-$ and $-CH_3-$
3	1733	-O-CO- stretching
4	1433	CH bending of $-CH_2-$ and CH_3-
5	1250	-C-O-C- stretching
6	1050	C-O-C stretching and C-OH stretching

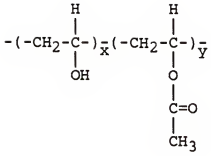

Figure 3.5 shows the acetalization result of poly(vinyl alcohol), i.e., poly(vinyl butyral). The peak assignments are listed in Table 3.2. From these assignments, we can conclude that the compound has the following structure:

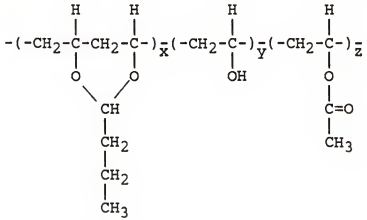

The intensity of the OH peak decreases significantly when the cyclic acetal peaks appear at 1120 cm^{-1} and 990 cm^{-1}. It is also worth noting that the intensity of the acetate peak at 1733 cm^{-1} decreases very much. This is due to the hydrolysis of the acetate group. It can be seen that some acetate groups are still left in the backbone after the reaction. For comparison, the poly(vinyl butyral) spectrum list in the Aldrich library is shown in Fig. 3.6. Comparing

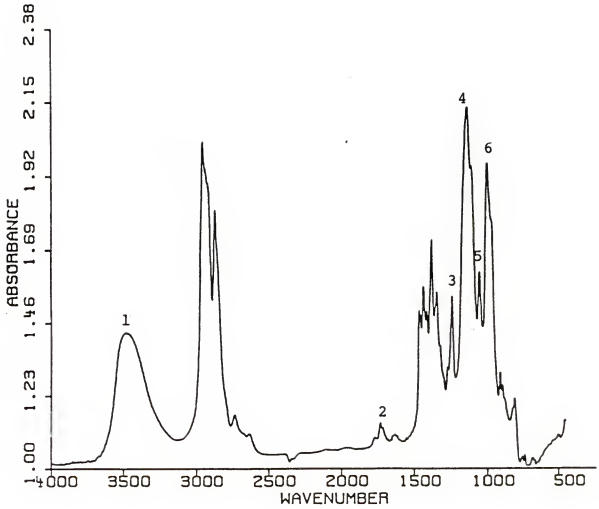

Figure 3.5 IR spectrum of the acetalization of poly(vinyl alcohol).

TABLE 3.2

Peak Assignments of IR Spectrum for Poly(vinyl Alcohol) Reacted with Butyraldehyde

Peak	Frequency (cm^{-1})	Functional Groups
1	3480	OH stretching
2	1733	-O-CO- stretching
3	1240	-C-O-C- stretching
4	1120	Cyclic acetal C-O-C-O-C
5	1047	-C-O-C- stretchinng
6	990	Cylic acetal C-O-C-O-C

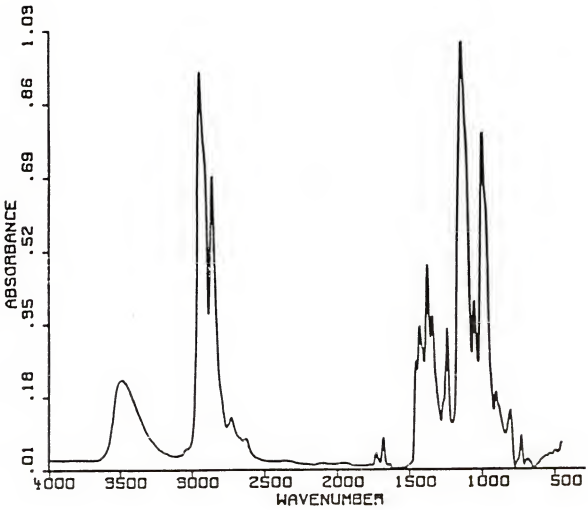

Figure 3.6 IR spectrum of poly(vinyl butyral).

Fig. 3.5 with Fig. 3.6, we see that the spectrum lists are very similar.

3.3.2.2 IR Analysis

Figure 3.7 shows the acetalization spectrum of the OPE-3. The intensity of the hydroxyl groups greatly decreases. This is due to some of the hydroxyl groups having been converted to acetal groups. A new peak appearing at 2870 cm^{-1} is assigned to the CH_2 and CH_3 stretching from the acetal groups. C and E peaks are assigned to the asymmetric and symmetric stretching of CH_2 groups in the main chain. The peak at 3072 cm^{-1} is due to stretching of the methylene group $=CH_2$. The peak F is assigned to the ester peak. The peak at 1715 cm^{-1} is assigned to the carbonyl group. This may indicate that some of the unsaturated double bonds had been oxidized to C=O groups in the hydroxylation stage. The peak I is due to CH bending of $-CH_2-C=C-$ groups. Some residues of double bonds are observed at 1639 cm^{-1}. J and K peaks are due to the asymmetric and symmetric stretching of C-O-C groups. However, it is worth noting that peak K is sharp and broad. This is due to the overlap of C-O-C stretching and cyclic acetal C-O-C-O-C at 1120 cm^{-1}. The formation of cyclic acetal will be further confirmed by the ^{13}C-NMR spectra. L and M peaks are assigned to the CH bending of trans -CH=CH- and $-CH=CH_2$, respectively. Table 3.3 lists the assignment of these peaks.

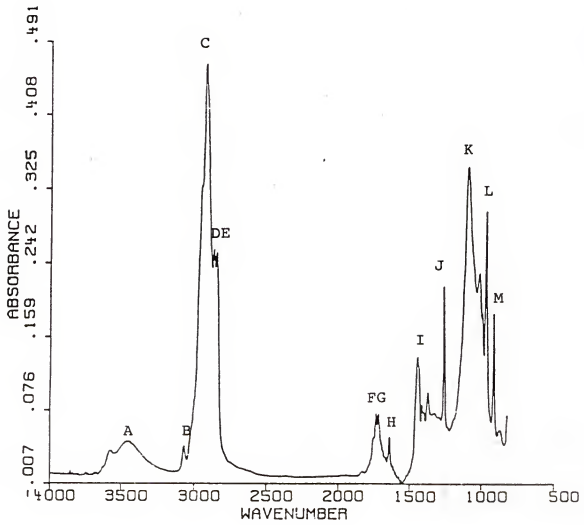

Figure 3.7 IR spectrum of OPE-3.

TABLE 3.3

Peak Assignments of IR Spectrum for OPE-3

Peak	Frequency (cm^{-1})	Chemical structure
A	3460	OH stretching
B	3072	Asymmetric stretching of $=CH_2$
C	2917	Asymmetric stretching of $-CH_2-$
D	2870	CH stretching of $CH_2-CH_2-CH_3$
E	2849	Symmetric stretchinng of $-CH_2-$
F	1735	Stretching of -O-CO-
G	1715	Stretching of C=O
H	1639	Stretching of -C=C-
I	1447	CH bending of $-CH_2-C=C-$
J	1259	Asymmetric stretching of C-O-C
K	1200 - 1030	Cyclic C-O-C-O-C and symmetric stretching of C-O-C
L	967	CH bending of trans -CH=CH-
M	912	CH bending of $-CH=CH_2$

3.3.2.3 NMR Analysis

Figure 3.8 depicts the 200 MHz ^{1}H-NMR spectrum of the OPE-3. The spectrum was recorded at room temperature and tetramethylsilane was used as the internal standard. The solvent used was $CDCl_3$. The strong bands at 2.12 ppm and 5.40 ppm represent the 1,4-butadiene units (cis and trans) while the bands in the range from 4.8 ppm - 5.2 ppm arose from the 1,2-butadiene units. It is observed that the reaction of butyraldehyde with OPE-2 results in the formation of a cyclic acetal (OPE-3) which resonated in the chemical shift range from 3.0 ppm to 4.6 ppm as a complex series of multiples. The assignment of peaks is as follows: the weak bands around 4.6 ppm are due to the cyclic methine proton; the chemical shifts in the range from 3.8 ppm to 4.4 ppm are assigned to the main chain methylene group linked with the ester oxygen and to the main chain methine proton. The broad bands in the region from 3.0 ppm to 3.8 ppm are probably from the methine proton adjacent to the OH group, the hydroxyl proton, and the methine proton adjacent to the ester group. The formation of cyclic acetal will be further confirmed by ^{13}C-NMR spectrum later. The butyl methylene groups overlap with the methylene groups in the 1,2 olefinic, α-methylene in the cyclic acetal, and form an unresolved band from 1.2 ppm to 1.8 ppm while the butyl terminal methyl groups appeared as a distorted triplet centered at 0.9 ppm. The peak at 1.2 ppm is due to the

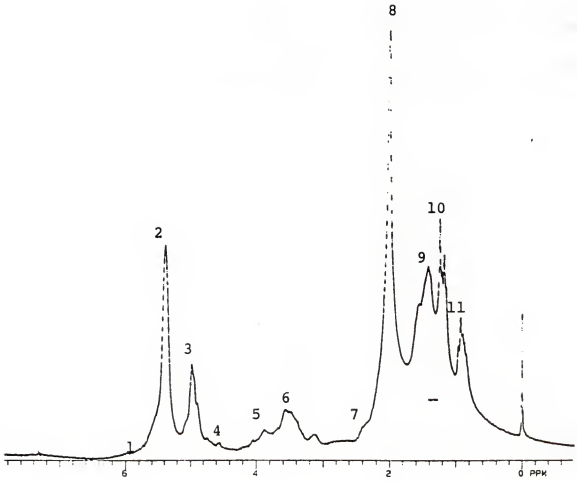

Figure 3.8 ^{1}H-NMR spectrum of OPE-3.

methyl proton arising from the methylmalonic acid. Table 3.4 shows the chemical shift vs. the corresponding proton type. To obtain the above peak assignments, some excellent references have been used (27, 28, 70).

The ^{13}C-NMR spectrum of the OPE-3 is shown in Fig. 3.9. In comparison with the spectrum shown in Fig. 2.4 in chapter 2, the chemical shift of the new bands or peaks can be assigned more conveniently. The most characteristic band of the OPE-3 is the appearance of the acetal carbon which is observed at 103.2 ppm. As expected, this methine carbon is shifted further downfield than other resonance in the cyclic structure because it directly attaches to oxygen atoms. The small peak at 96.1 ppm probably arose from the racemic cyclic structure of the methine carbon.

From the stereochemistry viewpoint, the meso cyclic structure is more stable than the racemic one because the former is less strained. The other characteristic bands are the methine carbon bonded to the cyclic oxygen at 72.1 ppm, and the carbon bonded to the hydroxyl group appears at 66 ppm. It is worth noting that the area ratio under peaks 72.1 ppm and 103.2 ppm is 2.2. This is expected from the cyclic acetal structure. The region in the chemical shift from 10 ppm to 45 ppm seems very complicated due to different kinds of methylene group resonance. However, if one ignores the "old methylene peaks" originating from the 1,4 and 1,2 polybutadiene, one can assign the methylene and methyl

TABLE 3.4

Peak Assignments of ^{1}H-NMR Spectrum for OPE-3

Proton type	Shift (ppm vs. TMS)	Chemical Structure
1	5.6	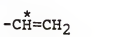
2	5.4	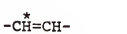
3	4.98	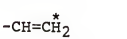
4	4.58	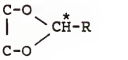
5	3.8 - 4.4	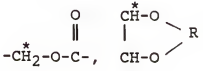
6	3.0 -3.8	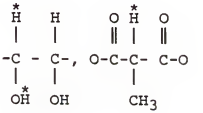
7	2.3	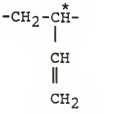

TABLE 3.4--continued

8	2.1	$-CH_2^*-CH=CH-CH_2-$
9	1.2 - 1.8	$-CH_2^*-CH_2^*-CH_3$, $-CH_2^*-CH(-CH=CH_2)-$
		$-CH_2^*-C(=O)-C(=O)-CH_2$ (C4), $-CH_2^*-C(-OH)-C(-OH)-CH_2$
10	1.2	$-O-C(=O)-C(=O)-C(-CH_3^*)-O$
11	0.9	$-CH_2-CH_2-CH_3^*$

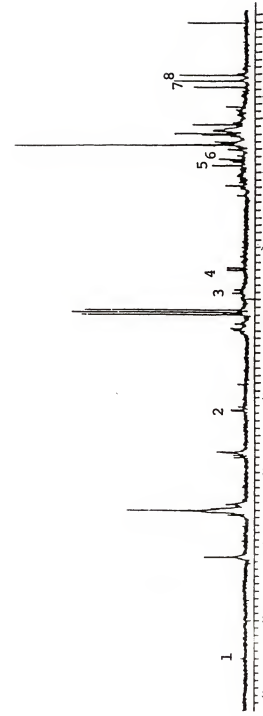

Figure 3.9 ^{13}C-NMR spectrum of OPE-3.

carbons from the acetalization process. The peak around 15.8 ppm is assigned to the methyl carbon of the cyclic acetal, while the peak of methylene groups of the cyclic acetal appeared at 17.5 ppm and 36.1 ppm. An assignment of the major peaks for this acetalization experiment is summarized in Table 3.5. The approximate degree of alkylation can be calculated by using the peak-area ratio of 2 to 4 in Fig. 3.9. A value of 45% was obtained. Other peaks which are not assigned here can be referred to Tables in chapter 2. Imai, Shiomi, et al. (71, 72) studied the alkylation of poly(vinyl alcohol) with alkyl halide. They dissolved the poly(vinyl alcohol) in dimethyl sulfoxide (DMSO) by heating. Alkyl halide and pyridine were then added to the solution and the mixture was heated in a sealed tube under nitrogen at 120°C. Their products were characterized by 67.8 MHz ^{13}C-NMR. The peak assignments shown in Fig. 3.10 are very similar to our results. Bruch and Bonesteel (73) used a more sophisticated two-dimensional NMR method to identify the complicated structure of poly(vinyl butyral). They used ^{13}C-DEPT (Distortionless Enhancement by Polarization Transfer) spectroscopy and two-dimensional ^{13}C-^{1}H correlated spectroscopy to do the proton line assignment. The coupling constants of each proton were further measured by the two dimensional J-resolved spectrum. The peaks shown in their spectra are again very similar to our spectra. By combining the IR and NMR data, we may conclude that the new synthetic

TABLE 3.5

Peak Assignments of ^{13}C-NMR Spectrum for OPE-3

Carbon type	Shift (ppm vs. TMS)	Chemical struture
1	170.1	
2	103.2	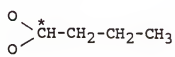
3	72.1	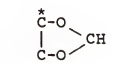
4	66	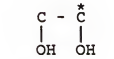
5	36.5-37.5	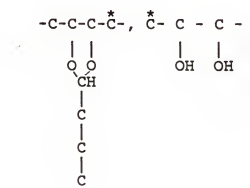
6	36.1	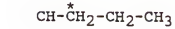
7	17.5	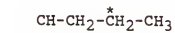
8	15.8	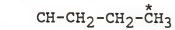

* : Denotes the carbon type shifted.

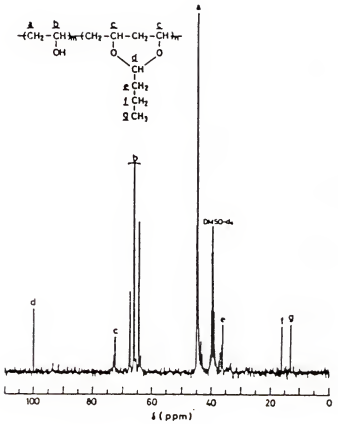

Figure 3.10 67.8 MHz ^{13}C-NMR spectrum of butyralized poly(vinyl alcohol) in DMSO-d_6 at 120°C (from reference 71).

polymer has the structure as shown in Fig. 3.11. The application of this novel functional polymer will be discussed in Chapter 4.

3.3.2.4 Solution Viscosity Measurement

The instrinsic viscosity was measured by using a Ubbelohde viscometer. The following equation is applied (74):

$$[\eta] = (\eta_{sp} / c)_{c=0} = [(Ln \eta_r)/c]_{c=0}$$

where,

$[\eta]$ = intrinsic viscosity,

η_{sp} = specific viscosity,

η_r = relative viscosity,

c = polymer concentration in g/dl.

The measurement was carried out in the tetrahydrofuran at 30°C. The values obtained are 0.18 dl/g and 0.34 dl/g for the hydroxytelechelic polybutadiene and OPE-3, respectively. This implies that the product (OPE-3) has a higher molecular weight than the reactant (hydroxytelechelic polybutadiene).

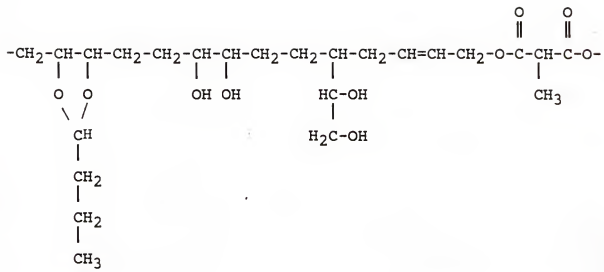

Figure 3.11 The structure of synthetic OPE-3 functional polymer.

CHAPTER 4
BINDER BURN-OUT AND XPS STUDIES

4.1 Background

4.1.1 Binder Burn-Out Process

The binder burn-out process involves simultaneous mass and heat transfer as well as chemical reaction resulting in a very complicated system. First, gaseous molecules diffuse through the film surrounding the particles of Al_2O_3. Second, gaseous molecules diffuse into the pores of the solid and react with binders. Third, gaseous products diffuse out through the pores and into the bulk flow of carrier gas. Ideally organic materials must be completely removed from the ceramic compact through the mass transfer process so that atomic diffusion occurs in the firing stage, permitting the particles to be bonded together and eventually causing the pores to shrink, forming a dense ceramic substrate. It is usually found, however, that some defects existing in the final products, which may originate from inhomogeneous dispersion of the ceramic slurry or be attributed to the entrapped carbon residues in the ceramic substrate.

In order to avoid oxidation of the metal in the green sheet, a nonoxidized atmosphere is usually applied which may lead to the incomplete removal of carbon residues remaining

in the ceramic substrate. These carbon residues can cause problems such as forming conduction paths, lowering insulation resistance, and increasing dielectric loss. Furthermore, the pathways where the gaseous molecules or volatile organic materials would pass through may be blocked during the transfer process, resulting in entrapment of carbonaceous materials and a high internal pressure build up. Cracks may be formed due to the above mentioned phenomena. As a consequence, it is important to use a binder which has the required properties for fabrication of the electronic substrates.

An understanding of factors such as dispersion behavior of binders in the powder system, pore size, pore size distribution of powder, absorption of binder onto powder surface, binder degradation and diffusion phenomena, processing variables, as well as polymer-ceramic interaction are the basis for producing nondefective ceramic substrate. Grachev et al. (75) studied the kinetics of thermal-oxidative degradation of poly(vinyl butyral) and poly(vinyl alcohol). They found the rate of formation of polyenes and carbonyls during heat treatment depended on the reaction temperature and amounts of butyral groups in the PVB and suggested that reaction involves two different rates. The thermal-oxidative degradation of poly(vinyl alcohol) was also carried out by Vasile et al. (76). They reported that

the decomposition mechanism and thermal stability of PVA depend largely on its degree of hydrolysis.

Thermal degradation of poly(methyl methacrylate) was studied by Martin et al. (77). They found degradation of poly(methyl methacrylate) would be initiated by random chain scission and proposed four possible sources of random chain scission initiation. Zulfiqar et al. (78) also examined the thermal degradation of poly(methyl methacrylate) and its copolymer with phenyl methacrylate. The products were chacterized by thermal volatilisation analysis (TVA), thermal gravimetric analysis (TGA) and infrared analysis. They found that the copolymer is more stable than the individual homopolymer. The degradation products involved monomers, small organic molecules, and anhydride ring structures. A degradation mechanism was suggested.

Thermal degradation of poly(vinyl butyral) in the presence of Al_2O_3 substrate was reported by Otsuka and his colleague (79-82). To minimize oxidation of metal an experiment was conducted in a reducing atmosphere. They found carbon residues would be trapped in the ceramic bulk if the sintering rate is faster than the burn-out rate and suggested that a low heating rate of 200°C/h should be used in the temperature range of 680°C to 1450°C in order to produce a dense substrate. The effect of mixing conditions on the final product was studied. If the wet-mixing time is long, the permeability of air through the ceramic body will

be retarded. Therefore, the burn-out prosess is incomplete and results in carbon residues being trapped in the bulk. Firing shrinkage of the final product as a function of the mixing condition, thickness of the green sheet, temperature, and air permeability was also presented. Furthermore, dispersion of firing shrinkage will be reduced if a low binder concentration and a sufficient amount of carrier gas were used.

4.1.2 Thermal Gravimetric Analysis

In the degradation of polymeric materials or polymer/ceramic composites thermal gravimetric analysis (TGA) is a very useful method in studying the kinetic parameters related to the burn-out process. The major advantages of this method are:

- Experiments can be operated either by isothermal or nonisothermal method.
- Continuous measurement of weight loss versus temperature or time as the sample is heated at a controlled rate.
- Experiments can be carried out in a static environment, in a vacuum or in a carrier gas with a known flow rate.
- A variety of heating rates can be employed.
- Only a small amount of sample is needed for experiments.

The usefulness of TGA can be expanded if DTG (derivative thermogravimetry) and DTA (differential thermal analysis) are incorporated with TGA. The slope of the TGA

curve, i.e., DTG curve can give information about reaction mechanisms, while DTA can indicate if the reaction is endothermic or exothermic.

In addition to the above basic thermal analysis instruments, thermal volatilisation analysis (TVA), gas chromatography (GC), infrared (IR), and mass spectroscopy (MS) methods are usually in combination with TGA in order to do a comprehensive study of binder burn-out phenomena.

4.1.3 Basic Principle of XPS

X-ray photoelectron spectroscopy has been widely applied in the field of solid state physics, polymer chemistry, organic chemistry, inorganic chemistry, and catalysis. The fundamental theory is based on the photoelectric effect. The kinetic energy of a photoelectron emitted from a sample exposed to x-ray (photon), usually $MgK_{\alpha 1,2}$ or $AlK_{\alpha 1,2}$, is measured by the energy analyzer. This photoelectric process follows the energy conservation law, i.e.,

$$E_B + E_k = h\nu \qquad (4.1)$$

where,

E_B = binding energy of an electron ejected by the photon.

E_k = kinetic energy of the emitted electron.

$h\nu$ = incident photon energy, 1253.6 ev.for $MgK_{\alpha 1,2}$ and 1486.6 ev. for $AlK_{\alpha 1,2}$.

Equation (4.1) is valid in a gas-phase XPS. For a solid XPS, however, the equation needs to be modified with a parameter φ_{sp}, work function of the spectrometer; the equation then becomes (83)

$$E_B + E_k + \varphi_{sp} = h\nu \qquad (4.2)$$

An energy level of a conducting solid in electrical equilibrium with the spectrometer is shown in Fig. 4.1. The Fermi level of the sample and the spectrometer is the same when the system is in the thermodynamic equilibrium state. However, a chemical potential difference exists between the vacuum level of the sample and the spectrometer, which is the work function difference between the sample and spectrometer. In spectrometry the kinetic energy of a photoelectron actually measured is the photoelectron kinetic energy with respect to the vacuum level of the spectrometer. This is due to the work function of the sample which is not easily measured and varies from one sample to another, while the work function for the specific spectrometer is constant. From Fig. 4.1. it is easy to see that the binding energy of a sample is the energy with respect to the Fermi level. From the information of the binding energy of a photoelectron the type of the atom as well as the chemical environment can be realized. A schematic diagram of the photoemission process is shown in Fig. 4.2. The photoemitted electron with energy E_i is retarded to E_f in order to increase the resolving power of the system by a factor of E_i/E_f before entering

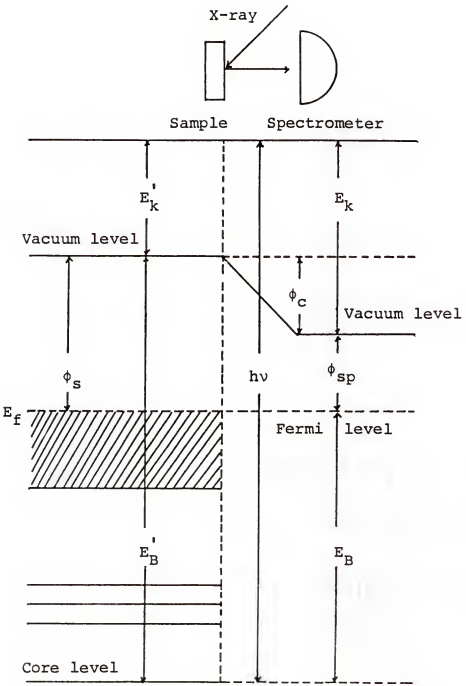

Figure 4.1 Schematic diagram of energy level of XPS experiment.

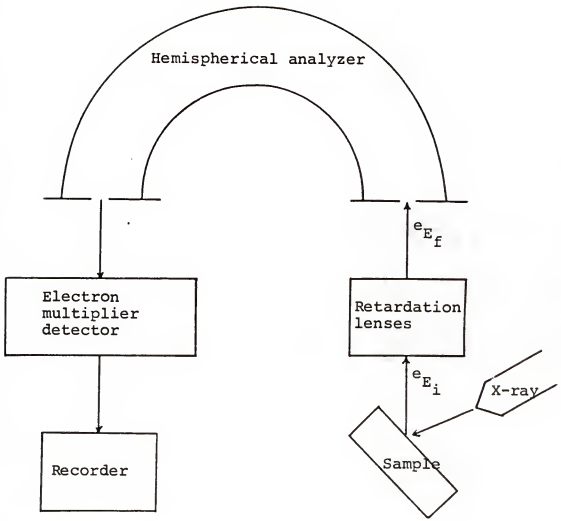

Figure 4.2 Schematic chart for the photoemission process.

into the 180° hemispherical analyzer. The photoelectron passing through the analyzer is then directed to the electron multiplier where a multiplication of 10^6 to 10^8 is operated in the pulse counting mode. The multiplied electron pulses are then directed into the recorder. A plot of electron count rate versus binding energy constitutes the x-ray photoelectron spectrum.

4.1.4 Qualitative Analysis and Atomic Analysis of XPS

The qualitative analysis in XPS is usually done by a survey scan in the energy range of 0 to 1150 ev. for MgK_α excitation. The binding energy of the core electrons emitted from all elements of the periodic table except H and He can be used for elemental analysis. However, overlap of the photoelectron lines sometimes occurs leading to the difficulty in identifying the elements. The problem may be solved by the inspection of other photoelectron lines or Auger lines. For example, the photoelectron line of O_{1s} and Sb_{3d} is nearly at the same position and can not be distinguished from each other. This problem can be solved by inspecting the line position of O_{2s} and O_{Auger} at 23 ev. and 745 ev., respectively. The photoelectron line at 531 ev. should be identified as O_{1s} if O_{2s} and O_{Auger} lines simultaneously appear. If the line position of the photoelectron overlaps with the Auger line, this problem can be overcome by using the twin-anode x-ray sources. Because

the kinetic energy of the Auger electron is independent of the energy source due to its intra-atom process, the photoelectron line, on the other hand, will change its position in kinetic energy according to the energy source used.

For determination of the atomic percents in a sample a narrow scan of each element is always used. By measuring the peak intensity after background subtraction, the normalized peak intensity can be obtained by dividing the measured peak intensity with (a) the photoionization cross section, for instance as calculated by Scofield (84) corresponding to each core level electron, (b) with instrument transmission function (for the fixed retarding ratio mode, this is $E^{1.0}$) (85), and (c) with the mean-free-path function, $E^{0.75}$. The cross section is introduced because the interaction probabilities between the core level electron of each element and a particular x-ray quantum is different. The following equations summarize the calculation procedures in this work:

- Determining the integrated peak intensity for each element.
- Calculating the sensitivity factor which is equal to (the cross section x (kinetic energy of the photoelectron)$^{1.75}$).
- Calculating the normalized peak intensity which is equal to (measured peak intensity / sensitivity factor)

. Calculating the atomic percent which is equal to

$$\frac{\text{normalized peak intensit}}{\sum_{1}^{n} (\text{normalized peak intensity})_n}$$

4.1.5 Chemical Effects of XPS

In addition to indicating the type of atom from the approximate binding energy of the photoelectron, additional information can be obtained from a shift of binding energy. In general, the shift in binding energy is affected by the different oxidation state or chemical bonding environment. Andrade (86) and others have reported that the chemical shift effect is the result of the difference in electronegativity of the adjacent atom. The outer-shell electron will be attracted to the high-electronegativity atom resulting in less electrostatic shielding of the inner-shell electron of the low-electronegativity atom with its nucleus. This implies that the inner-shell electron is more strongly bonded to the nucleus and a higher energy is required to eject the inner-shell electron. A charge potential model (87), based on electrostatic physics, was proposed to account for the chemical shift effect.

Chacin, Batich, and Williams (88) demonstrated the strength of the chemical shift effect in their study on the adhesion failure between copper and Teflon bonding. The fluorine containing carbon peak was clearly distinguished from the pure hydrocarbon peak due to the higher

electronegativity of the fluorine atom resulting in a shift of binding energy. The fracture path through a kidney stone was able to be determined by observation of the chemical shift of the oxidized carbon relative to the pure hydrocarbon (89). Batich et al. concluded that the fracture of the kidney stone was mainly through the organic matrix since a higher intensity of pure hydrocarbon originating from the protein was observed while a small oxidized carbon peak coming either from calcium oxalate or protein was found at the higher energy side of the pure hydrocarbon. The shift in binding energy also showed great value in determination of the composition and structure of a homopolymer and a copolymer (90). Clark et al. used simple, well-defined organic compounds as the model system to determine the binding-energy shift in various chemical environments. The structure and composition of a copolymer system was nicely defined.

Sometimes the chemical shift is too small to distinguish the peak position especially for those atoms which have several chemical binding states. This problem may be solved by curve-fitting analysis or a chemical derivatization technique. The curve-fitting analysis applies a computer iteration program which numerically fits the experimental envelope into component peaks. The experimental data and detailed procedures will be further presented in

chapter 5. The chemical derivatization technique will be discussed in section 4.1.6.

4.1.6 Chemical Derivatization Technique of XPS

Chemical derivatization or functional group labeling is a very useful technique in analysis of the specific functional groups on the surface. The objective of this technique is to use a specific derivatizing reagent containing XPS-sensitive "tag" elements which can easily be identified in subsequent XPS analysis. In general, the labeling reagent must react selectively with the desired functional group only and must be stable when exposed to x-rays.

The first example of chemical derivatization as applied to XPS was reported by Riggs and Dwight (91). They treated polytetrafluoroethylene (PTFE) with sodium in ammonia and then reacted that with bromine in order to detect the presence of unsaturated functional groups. The binding energy of unsaturated double bonds is almost the same as hydrocarbon and not distinguishable. However, XPS shows a higher intensity of bromine in the treated PTFE than in the untreated sample. This implies that unsaturated double bonds were introduced into the sample surface due to the chemical reaction. Briggs and Kendall used a derivatization reaction to study the surface functional groups on the polyethylene which was treated with corona

discharge (92). Several functional groups such as carbonyl, hydroxyl, carboxyl, and hydroperoxide functionality were found on the PE surface, which were responsible for the increasing adhesion between surfaces. Batich et al. (93) first applied XPS to the derivatization of carboxyl functional groups with thallium ethoxide (TlOEt). The films of methacrylic acid and ethylene copolymer were immersed in thallium ethoxide for 30 seconds in nitrogen, and then washed with ethanol. The unique tag of Tl has a good sensitivity for XPS measurement. A sensitive and quantitative result was obtained. The derivatization of surface hydroxyl groups on acrylic copolymers and glassy carbon was carried out respectively by Dickie et al. (94) and Collier et al. (95). The former did experiments on model copolymers by using gas-phase trifluoroacetic anhydride and found good agreement between surface concentrations of hydroxyl groups and bulk stoichiometry. The latter used titanium diisopropoxide bis(2,4-pentanedionate) as a labeling reagent containing titanium as the unique chemical tag. The analytical result was quantitative.

The determination of carboxylic acid anhydride by reaction with morpholine using the titrimetric method was reported by Johnson, (96) and Critchfield (97). Morpholine was dissolved in methanol solution and reacted with acid anhydride at room temperature for several minutes. The mixture was then titrated with a methyl yellow-methylene

blue mixed indicator. The difference in titration between the sample and the blank is the amount of anhydride. This method involves wet chemistry and some disadvantage might be expected. Batich (98) applied the labeling technique for derivatization of the acid anhydride groups on a well-defined polymer. A quantitative result was obtained in preliminary experiments. The derivatization of carbonyl groups with gaseous hydrazine to form the hydrazone was studied by Gerenser et al. (99). Samples of the polyethylene (PE) films were preactivated with a corona discharge treatment. To identify carbonyl groups residing on the surrface, PE film was exposed to hydrazine vapor pressure for 5 minutes. Result of the XPS showed the nitrogen peak at 399.7 ev. consistent with the formation of a hydrazone. Ohmichi et al. (100) also compared the difference between the functional groups on the surface of poly(ethylene terephthalate) (PET) film formed by the corona discharge treatment and the glow discharge treatment. The labeling reagent used for derivatization of surface carbonyl groups was p-chlorophenyl hydrazine. The elemental tag of Cl has a high photoelectric cross section for ESCA measurement. The reaction was carried out in a liquid phase for 30 minutes. Their results showed that the amount of carbonyl groups present on the PET surface was proportional to the treatment-level by corona discharge whereas the decreasing of carbonyl functional groups was found at high treatment-

level for glow discharge. Characterization of surface carbonyl groups by the XPS derivatization technique was also reported by Eriksson et al. (101). Polyethylene film pre-etched with potassium permanganate ($KMnO_4$) and concentrated sulfuric acid (H_2SO_4) mixture was reacted with pentafluorophenyl hydrazine (PFPH) in ethanol. Through the peak of the tag element the carbonyl functional groups on the PE film were positively identified.

Based on the above literature the derivatization technique has become a promising method for the complement of XPS analysis. The problems of overlap peaks, low-sensitivity functional groups, and low-resolution of the instrument can potentially be solved by this technique.

4.1.7 Angular-Resolved XPS

In addition to qualitative analysis of XPS, quantitative measurement such as surface-modified thin film or oxide overlayer thickness can be accomplished by using variable angle XPS. By changing the electron take-off angle between the sample surface and analyzer, different sampling depths can be obtained. As the electron take-off angle is decreased, the effective sampling depth is decreased resulting in enhancement of the surface features. This is due to the small mean free path of the electron, which is defined as the travel distance of an electron in a material before undergoing inelastic scattering. The enhancement of

the surface feature at low electron take-off angle can be seen more clearly in Fig. 4.3. Therefore, by using this valuable technique it is easy to distinguish the surface from the bulk concentration.

The enhanced surface sensitivity at low electron take-off angle can be used in a quantitative sense by applying the following equation known as the Beer-Lambert law (102):

$$d I = F C S N e^{-t/\lambda} d t \qquad (4.3)$$

where,

d I = photoelectron intensity,

F = x-ray flux,

C = photoelectric cross section of a subshell of an atom,

S = spectrometer function,

N = atomic density,

λ = electron mean-free-path,

dt = thickness of the volume element.

By integrating the above equation from 0 to t, i. e.,

$$\int d I = F C S N \int_0^t e^{-t/\lambda} d t$$

the following equation can be obtained,

$$I = F C S N \left(1 - e^{-t/\lambda} \right) \qquad (4.4)$$

If the integrating range changes form t to ∞, then the following equation is used,

$$I = F C S N e^{-t/\lambda} \qquad (4.5)$$

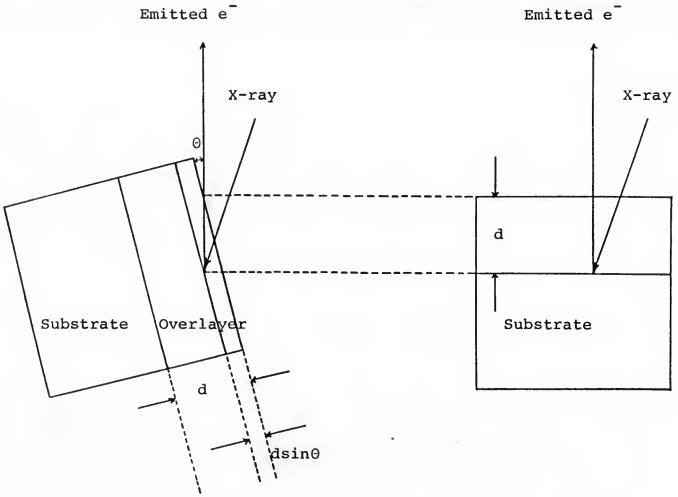

Figure 4.3 Angular-resolved XPS showing the enhancement of the surface feature at low electron take-off angle (θ) compared with the take-off angle normal to the surface.

Equation (4.4) represents the photoelectron intensity of a core level from the uniform overlayer while equation (4.5) gives the intensity of a core level from the substrate. It is worth noting that $1/\lambda$ is the attenuation coefficient. For a higher value of λ the attenuation of the signal of the substrate will be less pronounced. The total sampling depth is usually assumed to be 3λ (bulk). In this case 95% of the intensity of the signal comes from the upper 3λ layer.

It should be noted that the above mathematical model is valid only for an atomically-flat surface. Fadley (83) discussed extensively the various factors which could affect the angular-dependent model. He proposed an idealized spectrometer geometry as shown in Fig. 4.4. A uniform flux I_o of x-rays is incident on the atomically flat surface of the sample at an incident angle φ. The x-rays then penetrate into the bulk of the sample with a refraction angle φ' which is the same as φ for all of the work reported here. Photoelectrons of the core levels from the sample are emitted and propagated to the surface. Some of the emitted photoelectrons, when traveling to the surface, will be inelastically attenuated with an exponential function. Only those electrons with enough energy to overcome the surface potential can subsequently escape from the sample at a take-off angle Θ. The escaped photoelectrons within the aperture

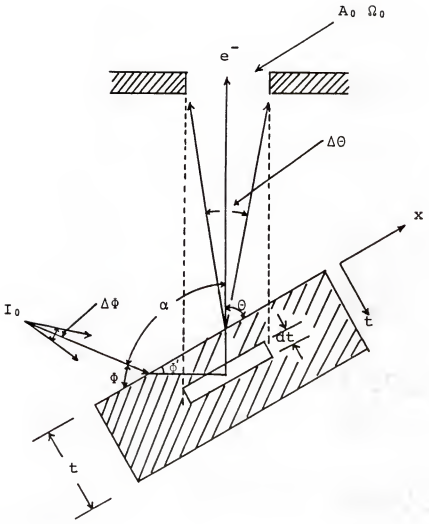

Figure 4.4 Schematic drawing of the idealized spectrometer geometry.

A_o will then go through the acceptance solid angle Ω_o of the spectrometer. Some assumptions were made:

. The sample surface is atomically flat and smooth.
. X-ray flux is very uniform.
. Electron mean free path is independent of θ.
. The acceptance solid angle for the electrons is constant.
. The attenuation of the electron is followed by an exponential decay along the path length.

With the above assumptions and the idealized spectrometer, the quantitative angular-resolved XPS can be established. The application of angular-resolved XPS for measuring the electron mean-free-path in polymeric materials was studied by Clark and Thomas (103). By depositing a known thickness of poly(p-xylylene) thin film onto a smooth Au substrate, they were able to determine the electron mean-free-path on the overlayer. The angular-resolved model was in good agreement with the experimental data with very little deviation. The development of angular-resolved XPS is also a very useful tool in biomaterials research such as biocompatibility and interaction between polymer and blood at the molecular level. In a recent paper, Wagener et al. (104) studied the surface structure of poly(oxyethylene)-Co-(pivalolactone) telechelomer. By using the angular-resolved XPS technique they found that the poly(oxyethylene) segment is enriched on the telechelomer surface. This is important

since the performance of the segmented polymer greatly depends on the surface composition. Miller and Peppas (105) reported the surface structure of poly(vinyl alcohol-Co-N-vinyl-2-pyrrolidone) and its interaction with water by angular-resolved XPS.

4.1.8 Electron Mean-Free-Path

Since the quantitative model of XPS is closly related to the electron mean-free-path, a brief background of this will be discussed here. It is known that XPS is a very surface-sensitive technique. This is due to the very short mean-free-path of electrons in the materials. Electron mean-free-path depends on the kinetic energy of the photoelectron and the materials considered. This is shown in Fig. 4.5., which indicates the mean-free-path varies from 3 Å to 50 Å with the lower value in the range of 50 ev. to 100 ev. of photoelectron kinetic energy (106).

There are two methods for researchers to estimate the electron mean-free-path either by experiment using an overlayer model or by mathematical prediction. It is, however, noted that various values were reported which show significant differences especially in organic polymers (107-109). This large variability may probably be attributed to the different materials used, different experimental techniques, and different theoretical approaches.

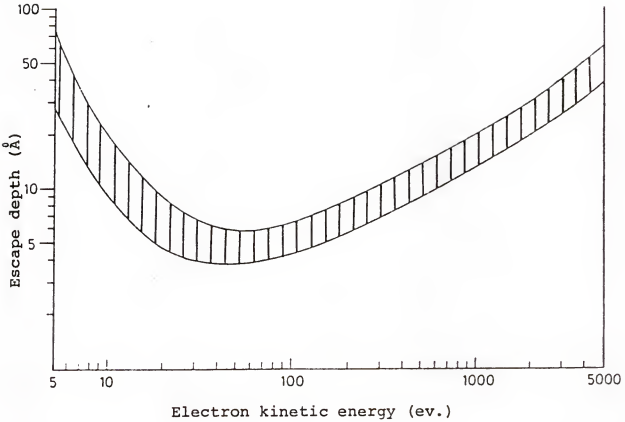

Figure 4.5 Universal curve of the electron escape depth as a function of the electron kinetic energy and materials (from reference 106)

Ashley (109) derived a mathematical equation for calculating the electron mean-free-path of organic polymers, which depends on molecular weight, density of materials, kinetic energy of photoelctron, and valence electron density. In later years (110) he and his coworker predicted electron mean-free-path using $\lambda = k (E)^p$ for different inorganic solids, where k and p are constants and depend on materials. Seah and Dench (111) also did an extensive compilation of various data by grouping them into element, inorganic compound, organic compound, and adsorbed gas. A general form of predicting the electron mean-free-path was reported. The electron mean-free-path used in this work is taken from references (109-111); a 1000 ev. electron has λ equal to 21 Å.

4.1.9 Scanning Electron Microscopy (SEM)

Scanning electron microscopy is a very useful instrument for studying the topography of organic or inorganic materials. The finely focused electron beam is swept over a localized area of the sample and a clear image of this sample surface can be visualized. By inspecting the image, the homogeneity of a sample, the dispersion of one phase to the base phase, and the bonding between two phases can be understood.

Because secondary electrons are produced by the primary electron beam, charging behavior on the sample surfacee is

always observed. One way to reduce or minimize the charging effect is to coat the sample surface with a thin film of conducting medium such as gold-palladium to build up a conduction path. Finally, the sample edge can be further coated with carbon paint which is directly connected to the sample holder to eliminate the charging effect.

4.2 Materials and Methods

4.2.1 Materials

Poly(vinyl butyral) resin (B-98) with hydroxyl content 19%, acetate content 1%, and butyral content 80% was obtained from Monsanto. OPE-3 polymer was synthesized as described in chapter 2, and 3. Al_2O_3 plates received from Coors INC. were cut into pieces with dimension of 1 cm x 1 cm. Labeling reagents 1-(4-fluorophenyl) piperazine and pentafluorophenyl hydrazine were purchased from Aldrich Chemical Company. Poly(vinylmethyl ketone) was obtained from Aldrich Chemical Company. Styrene-maleic anhydride (SMA) resins were obtained from ARCO Chemical Company. Acetone, methanol, reagent alcohol, hydrochloric acid, and ethyl ether were obtained from Fisher Scientific Company. All chemicals were used without further purification.

4.2.2 Sample Preparation

Al_2O_3 plates (1 cm x 1 cm) were Soxhlet extracted with acetone for 48 hours, ultrasonicated with ethyl alcohol, and finally rinsed with acetone and distilled water. Samples were then dried in a vacuum oven for 24 hours at 50°C. The clean samples were stored in a vacuum desiccator for further use.

Poly(vinylmethyl ketone) powders (1.8 g) were dissolved in 20 c.c. of acetone. The mixtures were then cast onto Mylar film with a thickness of 0.1 mm and dried in air at room temperature. The film was washed with pentane, ethanol, and distilled water. It was then dried in air and subsequently stored in the vacuum desiccator.

SMA 1000, 2000, 3000 resins were heated in a hot plate at approximately 160°C, 150°C, and 120°C, respectively. The films were sonicated in pentane, washed with absolute alcohol, distilled water, and then dried in air at room temperature.

4.2.3 Coating of Al_2O_3 and Heat-Treatments

Predried PVB and OPE-3 polymers (0.02 g) were dissolved in 100 c.c. of methanol and tetrahydrofuran, respectively. Al_2O_3 samples were then coated with 0.01 c.c. of the above solution with a micropipet. Samples were then dried in the vacuum oven at 50°C for 48 hours.

The coated Al_2O_3 samples were heated in a tube furnace (Lindberg Fisher) equipped with a temperature controller. Two heating rates (5°C/min, 1°C/min) and two gas streams (air, nitrogen) were applied in this thermal process. The flow rate of the stream was controlled at 100 c.c./min with a precision flowmeter. In a typical run, samples were heated from 30°C to 1150°C and cooled to room temperature, for subsequent XPS analysis or for derivatization reaction. Figure 4.6 shows the photographs of the tube furnace.

4.2.4 Derivatization Reactions

4.2.4.1 Reaction of Coated Al_2O_3 with Pentafluorophenyl Hydrazine

Samples of Al_2O_3, which had been thermally treated were inserted into the test-tube. Reagent ethyl alcohol (1 c.c.) with pentafluorophenyl hydrazine (0.03 g) dissolved in it was pipeted into the test-tube followed by addition of 1 drop of concentrated HCl. The test tube was sealed with a stopper. The reaction proceeded at room temperature for 30 minutes. For kinetics study, reaction times of 10 minutes and 6 hours were also applied. The sample was then washed with distilled water and absolute ethanol, and soxhlet extracted with ethyl ether for 24 hours. Finally samples were rinsed with absolute ethanol and ethyl ether three times (1 minute each), and dried in air at room temperature.

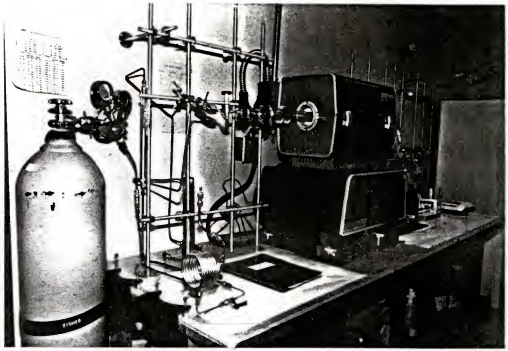

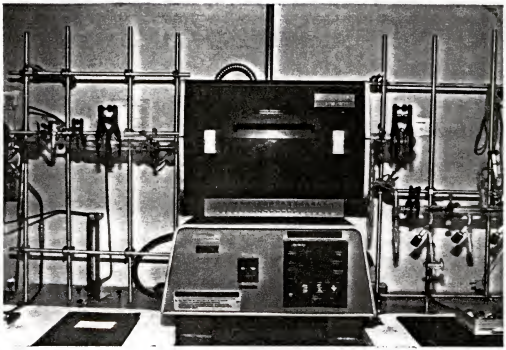

Figure 4.6 Photographs of the tube furnace for burn-out experiment.

4.2.4.2 Reaction of Coated Al_2O_3 with 1-(4-Fluorophenyl) Piperazine

A thermally treated sample was placed into a solution containing 1-(4-fluorophenyl) piperazine and methanol 2 c.c. and reacted for 30 minutes. The sample was washed with methanol, distilled water, absolute ethanol, and subsequently soxhlet extracted with ethyl ether for 40 hours. The sample was then air-dried at room temperature.

4.2.4.3 Reaction of Poly(vinylmethyl Ketone) with Pentafluorophenyl Hydrazine

Poly(vinylmethyl ketone) film with dimension 1 cm x 1 cm was inserted into a test-tube. Pentafluorophenyl hydrazine (0.03 g) dissolved in 1 c.c. of reagent alcohol was added to the test-tube. This was followed by the addition of one drop of concentrated HCl. The reaction was carried out at different reaction times: 30 seconds, 60 seconds, 5 minutes, 10 minutes, 30 minutes. The sample was then washed with reagent alcohol and ethyl ether and then air-dried in a vacuum desiccator.

4.2.4.4 Reaction of Styrene-Maleic Anhydride with 1-(4-Fluorophenyl) Piperazine

Styrene-maleic anhydride resins of 1 cm x 1 cm size were placed into a solution of 1-(4-fluorophenyl) piperazine and methanol, and reacted for 20 minutes at room temperature. the samples were then washed with methanol and

absolute alcohol three times and allowed to air-dried at room temperature.

4.2.5 The Apparatus of XPS

The XPS spectra were obtained with a Kratos, XSAM-800 spectrometer using the RT-11 operating system on a PDP 11/23 computer and Kratos DS-800 software. A dual anode which has a wedge shaped end coated with magnesium and aluminium on each side was used as the excitation source. The dual anode x-ray source can produce $AlK_{\alpha 1,2}$ and $MgK_{\alpha 1,2}$ x-rays at 1486.6 ev. and 1253.6 ev., respectively. However, only the magnesium source was used in this work. A 0.0002 inch thick piece of aluminium was used as the window material to prevent the white-radiation and scattered electrons from entering the sample-analysis chamber.

The photoelectrons emitted from the sample were selected by the electrostatic lens and the adjustable slit system of the hemispherical analyzer. The use of the electrostatic lens focuses the electrons toward the acceptance solid angle. The hemispherical analyzer is capable of operating in two modes: the fixed retarding ratio (FRR) and the fixed analyser transmission (FAT) modes. The use of the FRR mode results in the retardation of electron energy by a constant proportion of its kinetic energy while the FAT mode offers a constant transmission energy of the electrons. However, the former has greater sensitivity for

the high kinetic energy of electrons whereas the latter provides a greater sensitivity for the electrons with low kinetic energy. Additionally, quantitation is better defined in the FRR mode. In this work the analyzer was operated in the FRR mode.

The electrons passing the exit slit of the analyzer were directed to the detector which was operated in the pulse counting mode. The multiplied electron pulses were then fed into an amplifier unit where either a pulse counting (Δq) or a current ($\int$) mode could be used. In general, the pulse counting mode was applied in this work.

The vacuum system of this instrument consists of two turbomolecular pumps, two mechanical pumps, a titanium sublimation pump, and an ion pump. The 5 liters per second mechanical pump can pump the sample treatment chamber (STC) down to a pressure of 10^{-3} torr, at which time the 170 liters per second turbo pump is automatically turned on. The pressure of STC can be pumped down to 10^{-7} torr. The mechamical pump with 8 liters per second pumping speed can pump the sample analysis chamber (SAC) down to 10^{-3} torr. With the aid of 330 liters per second turbo pump the pressure can be further reduced to 10^{-8} torr in the sample analysis chamber. A photograph of the XSAM-800 is shown in Fig. 4.7.

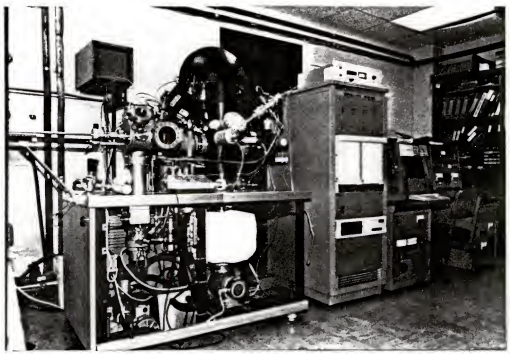

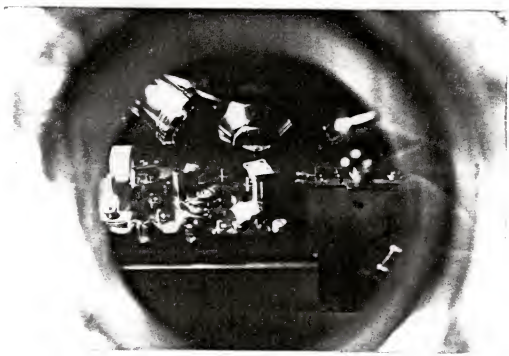

Figure 4.7 Photographs of the XSAM-800 instrument.

The work function of the spectrometer was calibrated by the dual x-ray source method using silver foil as a sample (112). Data aquisition and analysis were accomplished by using DS-800 software program developed by Kratos. For quantitative analysis the intensity of a photoelectron peak was measured and corrected with the photoionization cross-section, instrument transmission function, and escape depth function.

4.2.6 Thermogravimetric Analysis

Thermogravimetric analysis was carried out in a thermal analyzer, STA409, Netzsch Brothers, INC. A photograph of the system is shown in Fig. 4.8. The measurement can be done either under the normal pressure of a noncorrosive atmosphere or in a vacuum condition. The temperature range for operating is 25°C to 1600°C with a PtRh 10% - Pt thermocouple. The data were collected with a Hewlett-Packard 86B computer using the standard Netzsch software program. The heating rate was controlled at 5°C/min in air and in nitrogen.

4.2.7 Scanning Electron Microscopy (SEM) Study

Observation of the surface topography of the Al_2O_3 plate was accomplished by scanning electron microscopy (JEOL JSM-35C). Samples 1 cm x 1 cm in size were precoated with gold-palladium using a sputter coater (Technics, Alexandria,

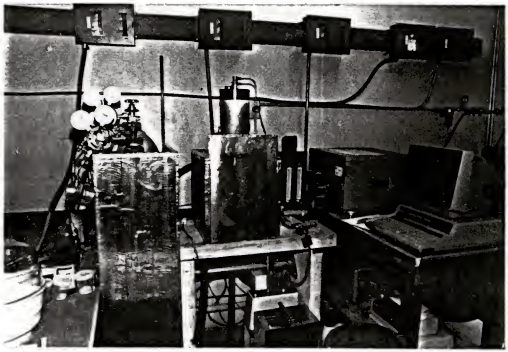

Figure 4.8 Photograph of the thermal analyzer.
(Netzsch Brothers, Inc.)

Virginia). A small amount of carbon paint was also coated on the edge of the sample so that a conducting path is formed.

4.3 Results and Discussions

4.3.1 XPS Spectrum of an Al_2O_3 Surface

Figure 4.9 shows a survey spectrum of an Al_2O_3 sample. There are several photoelectron lines and some minor peaks shown in this spectrum. The most intensive peak at 531 ev. is O_{1s} line while the peaks at 74 ev. and 119 ev. are assigned to Al_{2p} and Al_{2s} lines. It is interesting to note that some impurities are also shown in this spectrum, such as Ca, N, Sn, Si, C, and an AlK_α shadow. An expanded region of this spectrum is shown in Fig. 4.10. Some of these impurities may come from the milling process. In general, a small amount of impurities were added during the milling process so that a high density of sintering product can be achieved. The most common impurities are Mg, Ca, and Si. However, the Mg element was not found in this analysis. An assignment of binding energy for this elemental analysis is shown in Table 4.1.

4.3.2 Derivatization Reaction and Angular-Resolved XPS Studies

The objective of a derivatization reaction prior to XPS analysis is to label the specific functional groups of interest which are not distinguishable otherwise with a tag element. A high cross section for XPS measurement is useful.

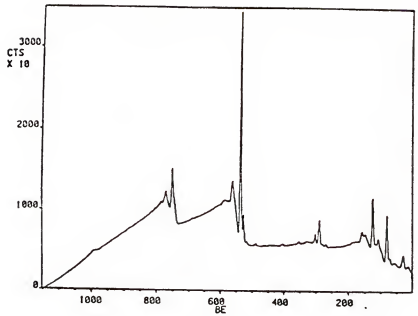

Figure 4.9

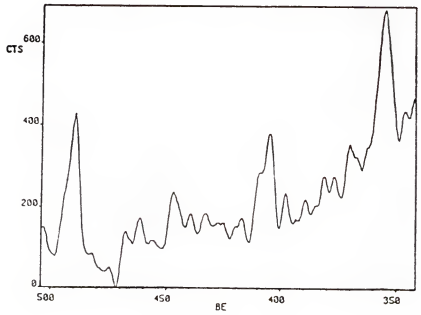

Figure 4.10

Figure 4.9 XPS survey spectrum of Al_2O_3.
Figure 4.10 Expanded spectrum of Figure 4.9.

TABLE 4.1

Elemental Analysis and Binding Energy Assignment for Al_2O_3 Plates

Elements	Atomic Concentration(%)	Binding Energy(ev.)
O_{2s}	57	23
O_{1s}		531
O_{Auger}		745
C_{1s}	7	285
Al_{2p}	33	74
Al_{2s}		119
Ca_{2p}	0.5	347
Ca_{2s}		439
N_{1s}	0.3	400
Sn_{3d5}	0.2	486
Si_{2p}	2	102
Si_{2s}		153

In the present work 1-(4-fluorophenyl) piperazine, and pentafluorophenyl hydrazine were used to react with anhydride groups and carbonyl groups, respectively. The chemical reactions are shown in Fig. 4.11. Batich (98) used morpholine as a labeling reagent for reaction with the acid anhydride groups on a polymer in order to identify the chemical structure as shown in the following equation:

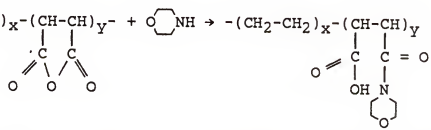

The ratio of x to y in the equation can be calculated by the atomic ratio of N to C. 1-(4-fluorophenyl) piperazine was chosen as the labeling reagent for reaction with anhydride groups because it contains a fluorine atom which has a better sensitivity than nitrogen in XPS analysis. Furthermore, the control sample showed a signal of nitrogen but did not show a signal of fluorine. Thus, it was decided to use F as the tag element for chemical derivatization. Pentafluorophenyl hydrazine was used as a labeling reagent for reaction with carbonyl functional groups by Everhart and Reilley (113). Their results indicated that pentafluorophenyl hydrazine can selectively react with carbonyl groups residing on the polyethylene film. Therefore, it was also used for chemical derivatization in this study. This

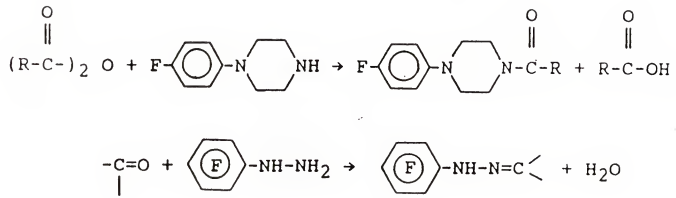

Figure 4.11 Chemical reaction of acid anhydride and carbonyl groups with labeling reagents.

chemical reagent contains five fluorine atoms in a molecule and can be used as a tag reagent.

4.3.2.1 Chemical Stability and Sensitivity of the Tag Element

In principle, the tag element used for chemical derivatization should have good sensitivity, i.e., a high photoelectric cross-section, and good stability under x-ray irradiation. Batich and Wendt discussed the requirements for chemical derivatization in detail (93). Everhart and Reilley (113) reported the decomposition of trifluoroacetic anhydride and mercuric trifluoroacetate which were used for chemical derivatiz ation of hydroxyl groups and unsaturated carbon double bond, respectively under XPS analysis. Decomposition of these two labeling reagents were found to be very significant in the DuPont 650 B spectrometer but not in the PHI 548 spectrometer. The photoelectric cross-section for N_{1s} and F_{1s} is 1.77 and 4.43, respectively (84). To measure x-ray stability, alumina samples reacted with 1-(4-fluorophenyl) piperazine and pentafluorophenyl hydrazine and analyzed for a period of time with the intensity of F_{1s} was recorded (see Figure 4.12). It is clear that both labeling elements show relative stability over the exposure time of analysis.

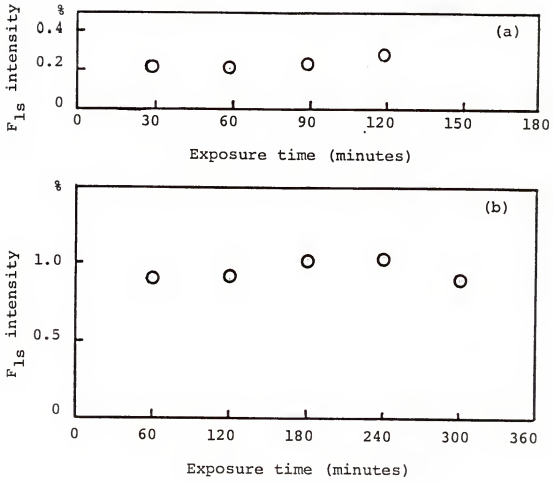

Figure 4.12 Stability of fluorine-containing labeling reagents exposed to x-ray for
(a) 1-(4-fluorophenyl) piperazine,
(b) pentafluorophenyl hydrazine.

4.3.2.2 Derivatization Reaction of Pentafluorophenyl Hydrazine and 1-(4-Fluorophenyl) Piperazine with Poly(vinylmethyl Ketone) and Styrene-Maleic Anhydride

Before labeling carbon residues on the Al_2O_3 substrate with pentafluorophenyl hydrazine and 1-(4-fluorophenyl) piperazine, the reaction was evaluated by derivatization and subsequent XPS analysis of poly(vinylmethyl ketone) and styrene-maleic anhydride. This is shown in the following equations:

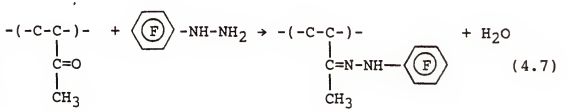

(4.7)

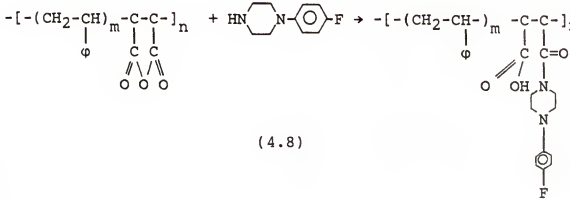

(4.8)

Figure 4.13 (a) shows the XPS spectrum of underivatized poly(vinylmethyl ketone) film. The principle peaks shown are C_{1s}, O_{1s}, O_{Auger}, and C_{Auger}. The small peak at binding energy 52 ev. is attributed to Al x-rays from the Al window in the anode and is termed a carbon 1s ghost peak. The observed mole fraction for carbon and oxygen is 0.82 and

0.18, respectively which is close to the calculated value 0.8 and 0.2. After derivatization with pentafluorophenyl hydrazine for 30 minutes at room temperature three new peaks were obtained as shown in Fig. 4.13 (b). The peaks at 400 ev., 599 ev., and 685 ev. are assigned to N_{1s}, F_{Auger}, and F_{1s}, respectively.

The reaction of styrene-maleic anhydride with 1-(4-fluorophenyl) piperazine is summarized in Table 4.2. Three different molecular weights of SMA resins were used. The acid number reported from the manufacturer did not correlate with the observed data of the F/O value. We are not able to explain this result at the present time; however it may be attributed to the degradation of unmodified copolymer sample because all the three samples were prepared by pressing in a hot plate near the melting temperature at 160°C, 150°C, 120°C for SMA 1000, SMA 2000, and SMA 3000, respectively. The products formed showed a light-yellow color which is different from the white color of the powder sample. SMA 1000 which has the highest melting range may degrade more significantly compared with SMA 3000. Another possible reason is that SMA 1000 could have a higher crystallinity than SMA 3000. The amounts of available reaction sites are less for SMA 1000 than SMA 3000.

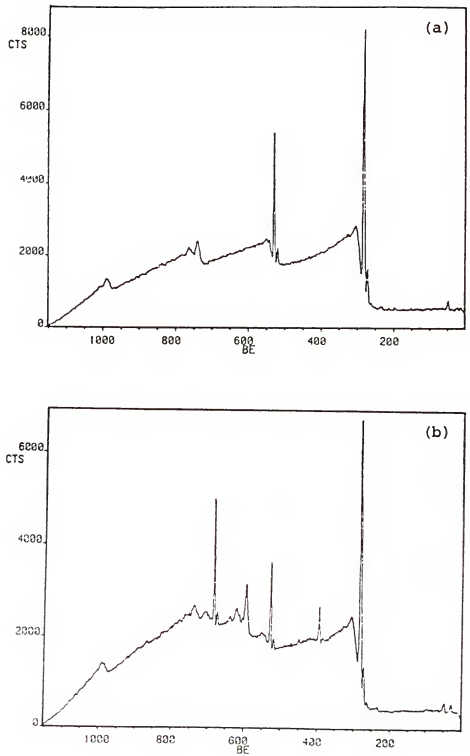

Figure 4.13 (a) XPS survey spectrum of underivatized poly(vinylmethyl ketone) film. (b) XPS survey spectrum of derivatized poly(vinylmethyl ketone) film.

TABLE 4.2

Summary of Chemical Derivatization of Styrene-Maleic Anhydride Reacted with 1-(4-Fluorophenyl) Piperazine

Peak Area Ratio

			Before Derivatization	After Derivatization		
Materials	$\bar{M}n$	Acid No.	O/C	O/C	F/O	N/O
SMA 1000	1600	480	0.166	0.202	0.023	0.040
SMA 2000	1700	350	0.118	0.141	0.044	0.079
SMA 3000	1900	275	0.105	0.119	0.119	0.206

4.3.2.3 Angular-Resolved XPS

As mentioned in the background section, angular resolved XPS is a very useful technique in studying the surface and interface properties of materials because the surface feature of the outermost few angstroms of the sample always plays an important role and shows very significant effects on the chemical, physical, and electrical properties of materials. By varying the electron take-off angle, the effective sampling depth of a sample can be reduced and shows much enhanced surface sensitivity. The effective sampling depth at high and low election take-off angles can be further illustrated in Fig. 4.14. The attenuation of photoelectron intensity at each angle (θ = 90°, 60°, 20°) was ploted as a function of analysis depth x. The sampling depth at which the two shaded areas are equal is the effective sampling depth. At the effective sampling depth 63% of the potoelectrons have been attenuated. The effective sampling depth ($\lambda \sin \theta$) for θ equal 20° and 90° is 0.34λ and λ , respectively. Furthermore, it is also worthy to note that 63% of the signal comes from the outermost three atomic layers at θ = 20° when the sampling depth is 0.34λ (assuming an atomic layer is 2.5 Å and the kinetic energy is 1000 ev.) Only 29% of the signal comes from the same layers at θ = 90°. Thus, Figure 4.14 highlights the concept of effective sampling depth and enhanced surface sensitivity at low electron take-off angle.

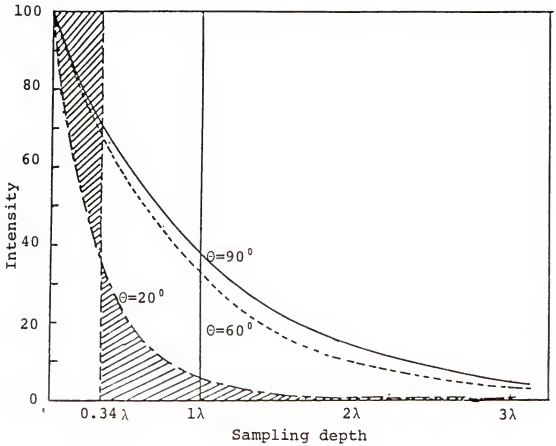

Figure 4.14 Photoelectron intensity of XPS as a function of sampling depth and electron take-off angle. (λ = electron mean-free-path)

Figure 4.15 and Figure 4.16 show the F_{1s} core level spectra of PVB and OPE-3 polymers which were pyrolyzed in a furnace in air from 30°C to 450°C at a heating rate of 1°C/min followed by nitrogen from 450°C to 1150°C at a heating rate of 1°C/min. Spectra were recorded at four different angles, θ = 90°, 60°, 40°, and 20°. The appearance of the F_{1s} photoelectron line indicates the derivatization reaction of pentafluorophenyl hydrazine with carbonyl groups of carbon residues from pyrolysis of polymer binders. A slightly decreasing intensity at 20° take-off angle may be due to the surface roughness effect resulting in the x-ray shading and electron shading. Surface roughness usually decreases the intensity of the photoelectron from the core level of surface layer. Shading effects in x-ray photoelectron spectroscopy were discussed by Ebel et al. (114). They concluded that the photoelectron count rate decreases at low electron take-off angle and becomes zero at θ equal to zero.

The intensity ratios of F/Al, F/O, and F/C are determined and are listed in Table 4.3. The F/Al and F/O ratios increase from high electron take-off angle (90°) to low electron take-off angle (20°) while the F/C ratio decreases from high electron take-off angle to low electron take-off angle. This clearly indicates that the distribution of carbonyl functional groups is not homogeneous in the surface and subsurface. Qualitatively, it is concluded that

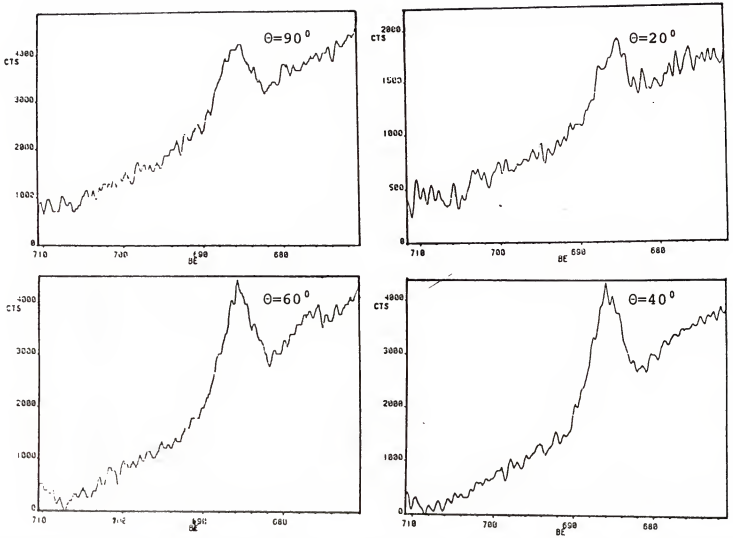

Figure 4.15 F_{1s} core level spectra for the derivatization of OPE-3 residues with pentafluorophenyl hydrazine at 4 angles.

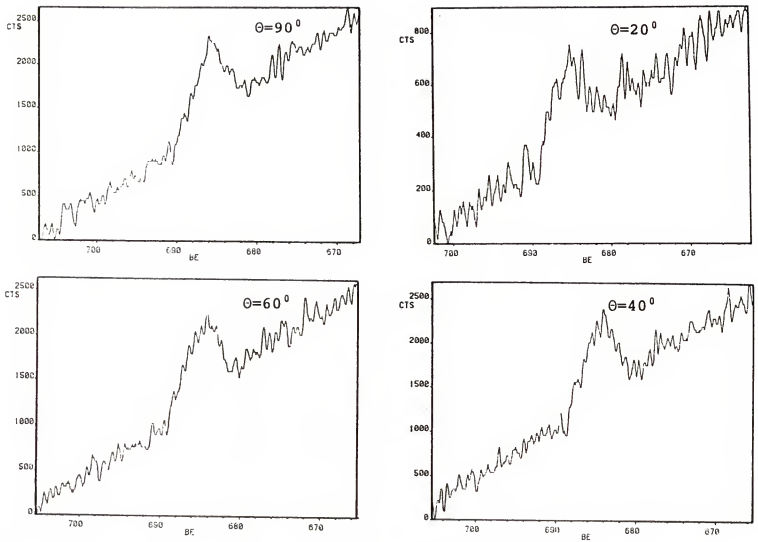

Figure 4.16 F_{1s} core level spectra for the derivatization of PVB residues with pentafluorophenyl hydrazine at 4 angles.

TABLE 4.3

Angular-Dependent Atomic Ratios of F/Al, F/C, and F/O for OPE-3 and PVB Reacted with PFPH

Sample	Take-off Angle	$\frac{F}{Al} \times 10^2$	$\frac{F}{C} \times 10^2$	$\frac{F}{O} \times 10^2$
OPE-3-(Air1, N1)-PFPH	90°	1.56	4.03	0.85
	60°	1.79	3.34	0.99
	40°	2.26	2.83	1.26
	20°	2.29	1.67	1.29
PVB-(Air1, N1)-PFPH	90°	1.47	4.33	0.80
	60°	2.00	2.68	1.16
	40°	2.18	2.40	1.20
	20°	3.06	2.58	1.61

a carbon-rich layer is present on the surface. The following symbols denote the process with which the samples were treated:

- OPE-3-(Air5, N1)-PFPH denotes that Al_2O_3 substrates were coated with OPE-3 polymers, pyrolyzed in a furnace using air from 30°C to 450°C at a heating rate of 5°C/min and then with nitrogen from 450°C to 1150°C at a heating rate 1°C/min. Samples were finally reacted with pentafluorophenyl hydrazine.
- PVB-(N5, N1)-FPP denotes that Al_2O_3 substrates were coated with PVB polymers, pyrolyzed in a furnace using nitrogen from 30°C to 500°C at a heating rate of 5°C/min and then with nitrogen from 500°C to 1150°C at a heating rate of 1°C/min. Samples were finally reacted with 1-(4-fluorophenyl) piperazine.

The result of OPE-3 and PVB treated with 1-(4-fluorophenyl) piperazine in nitrogen is tabulated in Table 4.4. A similar conclusion is also obtained, i.e., a carbon-rich layer is present on the sruface.

4.3.2.4 Reaction Kinetics of the Derivatization

The reaction kinetics of the derivatization were carried out at several reaction times for OPE-3 and PVB polymers at different heat treatments. Results are shown in Fig. 4.17 where the atomic concentration ratio F/Al is plotted vs. the reaction time in pentafluorophenyl

TABLE 4.4

Angular-Dependent Atomic Ratios of F/Al, F/C, and F/O for OPE-3 and PVB Reacted with FPP

Sample	Take-off Angle	$\frac{F}{Al} \times 10^3$	$\frac{F}{C} \times 10^2$	$\frac{F}{O} \times 10^3$
OPE-3-(N5, N1)-FPP	90°	7.63	1.00	4.58
	60°	9.28	0.88	5.75
	40°	13.22	0.96	8.38
	20°	17.61	0.83	11.11
PVB-(N5, N1)-FPP	90°	7.14	1.53	4.08
	40°	8.79	0.91	5.29
	20°	19.57	1.67	12.25

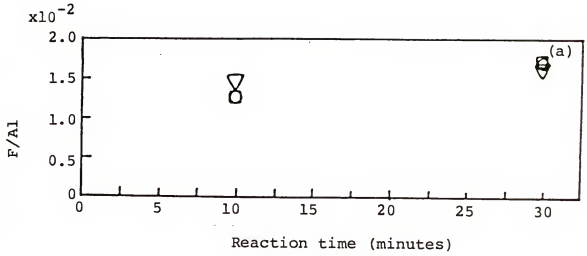

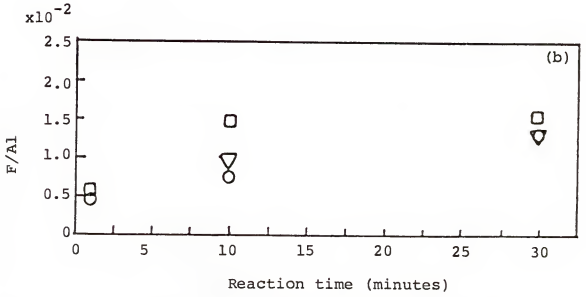

Figure 4.17 Kinetics of the derivatization reaction of residues of OPE-3 and PVB reacted with pentafluorophenyl hydrazine. (a)○:OPE-3-(Air5,N1)-PFPH,□:OPE-3-(N5,N1)-PFPH, ▽:OPE-3-(Air1,N1)-PFPH. (b)○:PVB-(Air5,N1)-PFPH,□:PVB-(N5, N1)-PFPH,▽:PVB-(Air1,N1)-PFPH.

hydrazine. For PVB polymer coated samples, slightly higher carbon residues are observed in a nitrogen-treated atmosphere but there is no significant difference in an air-treated atmosphere at a heating rate of 5°C/min and 1°C/min. For OPE-3 polymers three different heat-treatment processes show almost the same results.

4.3.3 Thickness Measurement of the Overlayer

One of the most important values, in the quantitative sense, of angular-dependent XPS study is the thickness measurement of an overlayer residing on a substrate as well as electron mean-free-path determination. This is achieved by application of the following equations (87):

For the overlayer, the intensity I_o of the photoelectrons from a core level of an overlayer with thickness d is

$$I_o(\theta) \propto 1 - \mathrm{Exp}(-d/\lambda_o \sin\theta) \qquad (4.9)$$

For the substrate, the intensity I_s of the signal from a core level of a substrate under an overlayer with thickness d is

$$I_s(\theta) \propto \mathrm{Exp}(-d/\lambda_s \sin\theta) \qquad (4.10)$$

The above equations can be combined to give:

$$\frac{I_o(\theta)}{I_s(\theta)} \propto (1 - \mathrm{Exp}(-d/\lambda_o \sin\theta))(\mathrm{Exp}(d/\lambda_s \sin\theta)) \qquad (4.11)$$

Where,

θ = photoelecton take-off angle.

λ_o = mean-free-path of a photoelectron in the overlayer.

λ_s = mean-free-path of a photoelectron in the substrate.

By measuring the intensity of $I_o(\theta)$ and $I_s(\theta)$ through the angular-resolved XPS and by knowing the value of λ_o and λ_s (109-111), the overlayer thickness can be obtained. Conversely, the electron mean-free-path can also be calculated if the overlayer thickness is precisely measured. It should be emphasized again that some assumptions were made as described previously in applying these equations. Figure 4.18 shows the results of XPS measurement of PVB-(N5, N1)-PFPH. The experimental data are in good agreement with the mathematical model predicted though the data point at low take-off angle shows some deviation. For the best fit of this attenuation model the reduced thickness (d/λ) was obtained by the linear regression and nonlinear least-square analyses. For the linear regression analysis (Fig. 4.18(b)) this was done by a semi-Ln plot of the intensity of Al vs. $1/\sin\theta$. The slope of the straight line is the value of d/λ. Such a plot is shown in Fig. 4.19. The correlation coefficient of this regression line is 0.99 which again indicates the consistency of experimental data and the theoretical model. The electron mean-free-path in the

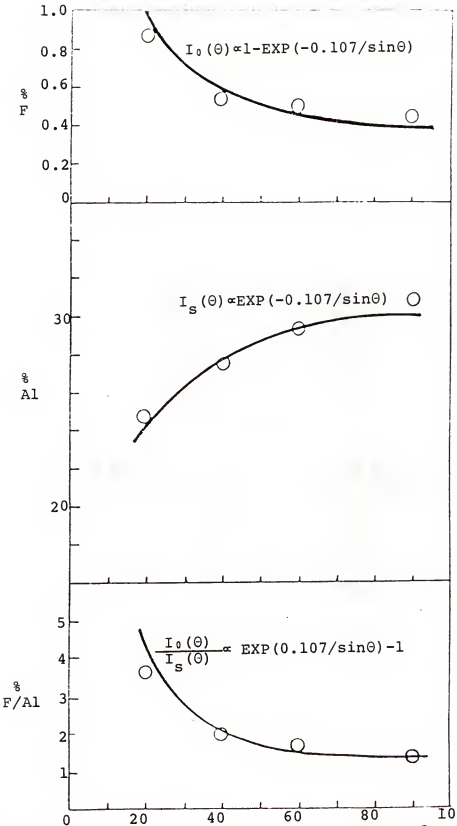

Figure 4.18 Intensity of angular-resolved XPS for PVB-(N5, N1)-PFPH showing enhanced surface sensitivity at low θ

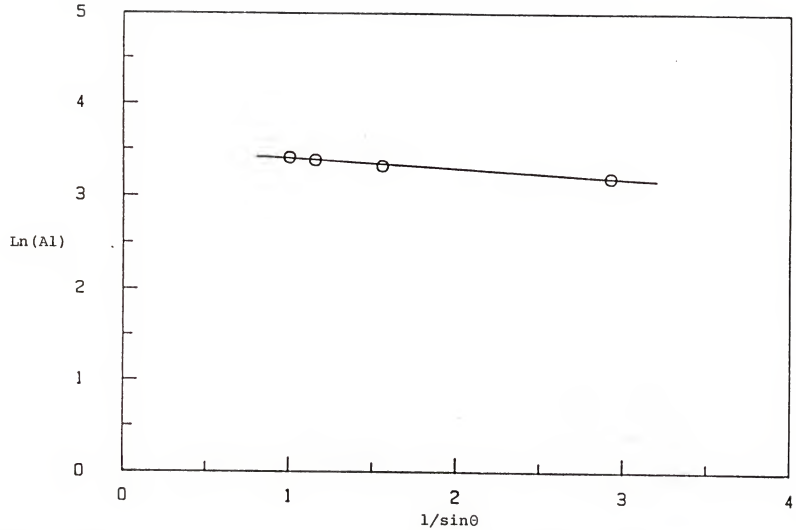

Figure 4.19 A linear regression plot of Ln(Al) vs. 1/sinθ for PVB-(N5,N1)-PFPH. The slope is equal to the reduced thickness of the overlayer.

substrate and in the overlayer was assumed to be the same during the analysis. The electron mean-free-path ususlly depends on the kinetic energy of the photoelectron as well as the materials. A densely-packed inorganic solid usually has a lower electron mean-free-path than a loosely-packed long-chain hydrocarbon. Ashley and Tung (110) reported the calculation of electron mean-free-path from inorganic materials using equation $\lambda = kE^p$, where k, p are constant depending on materials and E is the kinetic energy for electron. The electron mean-free-path for the organic materials reported varies in a wide range from the low values given by Clark et al. (107) to the higher values given by Cadman et al. (108). Ashley recently reported a theoretical model for calculation of the electron mean free path of organic materials (109). In this study the value of λ was calculated according to references (109-111) giving 21 Å (1000 ev.) The enhancement of surface sensitivity can be seen by the plot of the intensity ratio of F/Al vs. electron take-off angle. At low electron take-off angle, the intensity of a photoelectron line from a core level of the substrate decreases due to the increase of pentration length of an electron through the surface layer resulting in an increase of inelastic scattering while the intensity of a photoelectron line from a core level of the overlayer increases due to the increase of an effective sample area.

The result of OPE-3-(N5, N1)-PFPH is shown in Figure 4.20. The mathematical model fits the experimental data reasonably well with a reduced thickness of 0.172. A deviation was observed at low electron take-off angle 20°. Surface segregations of the carbonyl groups had also occurred at low electron take-off angle. A plot of semi-Ln intensity of Al vs. $1/\sin\theta$ is shown in Fig. 4.21. The data show a good fit by the regression line with a correlation coefficient being 0.99.

Table 4.5 summarizes the results of thickness measurement of overlayer by angular-resolved XPS method. It appears that the effective overlayer thickness is in the range of monolayers. Therefore, the angular-dependent XPS does give a true surface analysis. This overlayer thickness measurement will be further confirmed by an independent measurement as discussed in section 4.3.5. Furthermore, if the overlayer thickness can be determined by an alternative method other than angular-dependent XPS, the electron mean-free-path can be obtained.

4.3.4 Testing the Significance of Regression Analysis

It is important to assess the adequacy of the regression model. This can be achieved by testing the significance of regression through statistical analysis. By calculating the corrected sum of squares of independent and dependent variables, the corrected sum of cross products of

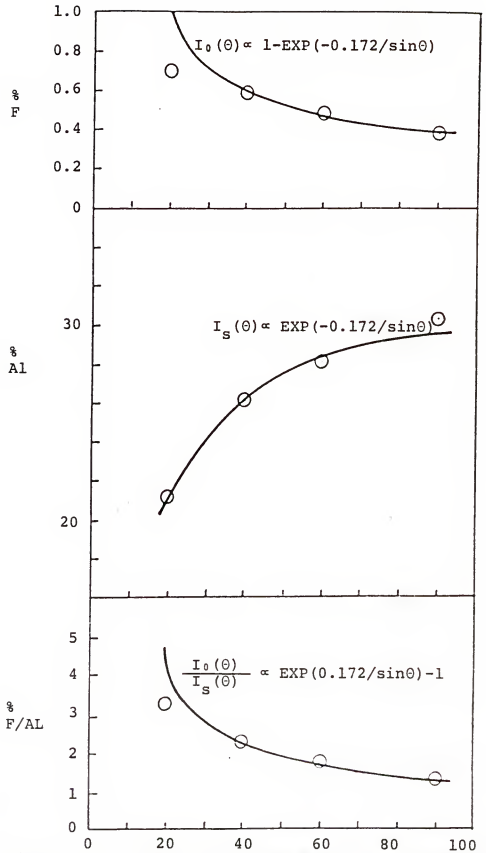

Figure 4.20 Intensity of angular-resolved XPS for OPE-3-(N5, N1)-PFPH showing enhanced surface sensitivity at low θ.

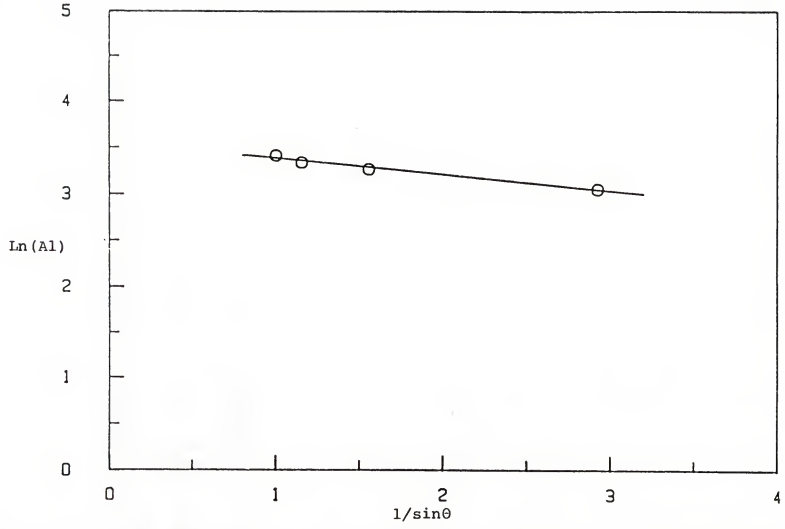

Figure 4.21 A linear regression plot of Ln(Al) vs. 1/sinθ for OPE-3-(N5,N1)-PFPH. The slope is equal to the reduced thickness of the overlayer.

TABLE 4.5

Overlayer Thickness Measurement by Angular-Resolved XPS Method

Polymer	Reaction[a]	Heat Treatment	Overlayer Thickness
OPE-3	PFPH	30°C → 500°C in N_2, 5°C/min	4 Å
		500°C → 1150°C in N_2, 1°C/min	
PVB	PFPH	30°C → 500°C in N_2, 5°C/min	3 Å
		500°C → 1150°C in N_2, 1°C/min	
OPE-3	PFPH	30°C → 450°C in Air, 1°C/min	2 Å
		450°C → 1150°C in N_2, 1°C/min	
PVB	PFPH	30°C → 450°C in Air, 1°C/min	2 Å
		450°C → 1150°C in N_2, 1°C/min	
OPE-3	PFPH	30°C → 450°C in Air, 5°C/min	3 Å
		450°C → 1150°C in N_2, 1°C/min	
PVB	PFPH	30°C → 450°C in Air, 5°C/min	2 Å
		450°C → 1150°C in N_2, 1°C/min	
OPE-3	FPP	30°C → 500°C in N_2, 5°C/min	3 Å
		500°C → 1150°C in N_2, 1°C/min	
PVB	FPP	30°C → 500°C in N_2, 5°C/min	2 Å
		500°C → 1150°C in N_2, 1°C/min	

[a] PFPH : Pentafluorophenyl hydrazine.
FPP : 1-(4-fluorophenyl) Piperazine.

independent and dependent variables, the error sum of squares, and the regression sum of squares, the significance of a regression line can be visualized. Table 4.6 and Table 4.7 show the results of this analysis. The tabulated values of $F_{0.05,\ 1,\ 2}$ is 18.51 (115). The calculated F value, i.e., F_0 is larger than the tabulated value. Thus, it is concluded that the angular-dependent XPS data are well fitted to the attenuation model.

4.3.5 Overlayer Thickness Measurement by C_{1s} and C_{kvv} Lines

The thickness of the overlayer has been measured by angular-dependent XPS method as discussed in section 4.3.3. It is useful to measure the thickness by an alternative and independent method to further confirm the data. This can be carried out by measuring the intensity ratio of the photoelectron line of C_{1s} and the Auger line of C_{kvv}.

Ebel et al. (116) first proposed this method for estimation of the overlayer thickness. The basic principle of this approach is to select two lines which have a very wide separation of kinetic energy resulting in a significant difference of electron mean-free-path. The lower kinetic energy electron has a shorter mean-free-path, while the higher kinetic energy electron posseses a longer mean-free-path. As a consequence, the in-depth information of these two photoelectrons will be different. The kinetic energy of C_{1s} is 970 ev. and the kinetic energy of C_{kvv}

TABLE 4.6

Testing the Significance of Regression for PVB-(N5,N1)-PFPH

Source of Variation	Sum of Square	Degree of Freedom	Mean Square	F_o
Regression	0.030	1	0.030	60
Error	0.001	2	0.0005	
Total	0.031	3		

TABLE 4.7

Testing the Significance of Regression for OPE-3-(N5, N1)-PFPH

Source of Variation	Sume of Square	Degree of Freedom	Mean Square	F_o
Regression	0.069	1	0.069	69.
Error	0.002	2	0.001	
Total	0.071	3		

Auger line is 260 ev. based on the MgK_{α} excitation. Thus, the energy difference between them is around 700 ev. leading to the in-depth information of C_{kvv} at only 40% of the C_{1s} based on the energy dependence of mean-free-path by $E^{0.7}$ (110, 111).

The following equation was applied:

$$r = p \left[\frac{1 - \mathrm{Exp}\left(\left(-\frac{x}{\sin\theta} \right) E_{C_{1s}}^{-0.7} \right)}{1 - \mathrm{Exp}\left(\left(-\frac{x}{\sin\theta} \right) E_{C_{kvv}}^{-0.7} \right)} \right] \qquad (4.12)$$

where,

E = kinetic energy in Kev.

x = reduced thickness of the overlayer.

θ = electron take-off angle.

p = constant.

r = intensity ratio of the measured two signals.

The constant p in the above equation needs to be evaluated before XPS analysis of the unknown sample. This was done by measuring the intensity ratio of the C_{1s} and C_{kvv} lines using a clean graphite as reference which was subjected to argon-ion etching before XPS measurement. The value obtained has an average 1.25. Therefore, by measuring the intensity ratios of C_{1s} and C_{kvv} for Al_2O_3 coated with PVB and OPE-3 the reduced thickness can be obtained by a computer iteration program using the above equation. The photoelectron mean-free-path 21 Å (1000 ev.) is then applied to calculate the thickness of the overlayer.

Table 4.8 summarizes the results. The calculated thickness is again around monolayers which correspond well with the value obtained by the angular-dependent XPS method. Both methods may indicate that the overlayer thickness with preheat treatment in N_2 shows a slightly higher value than preheat treatment in air. This is expected because oxygen in air can help degradation of the polymer. Thus, the incorporation of using angular-dependent XPS and C_{1s} - C_{kvv} methods offer a firm basis of the overlayer thickness measurement. Furthermore, the electron mean-free-path can also be measured in angular-dependent XPS if the thickness of the overlayer which can be obtained by the C_{1s} - C_{kvv} method is known. The average value obtained is 21 Å which is exactly the same as that used in the calculation of overlayer thickness.

It should be noted that the time required for doing angular-dependent XPS analysis is much longer than the C_{1s} -C_{kvv} method. This is the major advantage of the C_{1s} - C_{kvv} method. However, two electron lines with larger kinetic energy separation must be used when applying C_{1s} - C_{kvv} method ,while theoretically only one photoelectron line from the core level by angular-resolved XPS method can give the information of the overlayer thickness.

TABLE 4.8

Overlayer Thickness Measurement by C_{1s} - C_{KVV} Method

Polymer	Heat treatment	Overlayer Thickness
OPE-3	30°C → 500°C in N_2, 5°C/min 500°C → 1150°C in N_2, 1°C/min	4 Å
PVB	30°C → 500°C in N_2, 5°C/min 500°C → 1150°C in N_2, 1°C/min	3 Å
OPE-3	30°C → 450°C in Air, 1°C/min 450°C → 1150°C in N_2, 1°C/min	2 Å
PVB	30°C → 450°C in Air, 1°C/min 450°C → 1150°C in N_2, 1°C/min	3 Å
OPE-3	30°C → 450°C in Air, 5°C/min 450°C → 1150°C in N_2, 1°C/min	< 1 Å
PVB	30°C → 450°C in Air, 5°C/min 450°C → 1150°C in N_2, 1°C/min	< 1 Å

4.3.6 Model for the Surface Structure

It has been shown in Fig. 4.18 that the intensity of a photoelectron line from the overlayer increases with decreasing electron take-off angle, while the intensity of a photoelectron line from the substrate decreases with decreasing electron take-off angle. Consequently, the enhanced surface sensitivity was observed. However, a deviation between the experimental data and fitted line was observed at low electron take-off angle. The enhancement of the surface feature at low electron take-off angle is less pronounced. This effect can be attributed to the patchy overlayer and surface roughness as shown in Fig. 4.22. Fadley (117) discussed various factors which can result in a deviation of the experimental data to the flat model. The most important factors are non-uniform surface-layer, surface roughness, non-uniform x-ray flux, change of solid angle, and electron reflection.

If the substrate is not uniformly covered by the overlayer but with island-like overlayer, the intensity of the signal from the substrate will be attenuated less at low electron take-off angle leading to a less surface enhancement effect. Surface roughness can also act as a significant effect on the intensity measurement because the incident x-rays and the emitted photoelectrons may be shaded by adjacent raised areas. The electron take-off angle as well as the x-ray incidence angle will be different from the

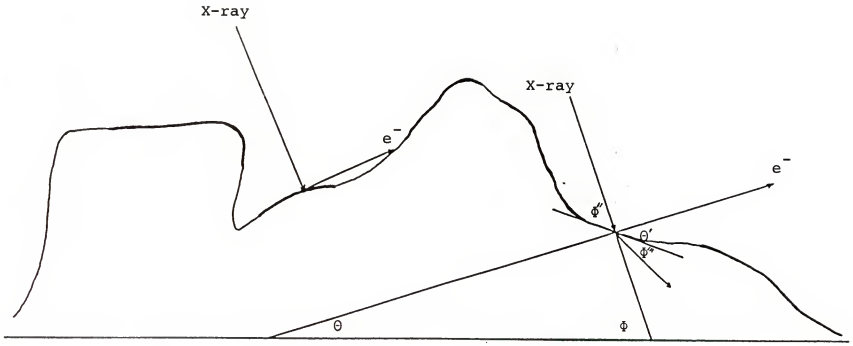

Figure 4.22 A surface model of Al_2O_3 substrate covered with a patchy overlayer to illustrate the effect of surface roughness on the angular-resolved XPS measurement.

angles predicted by the flat-surface model. The angles θ and φ shown in Fig. 4.22 are predicted electron take-off angle and x-ray incidence angle, while φ'', φ''', and θ' represent the true x-ray incidence angle, true x-ray refraction angle, and true electron take-off angle. This complicated surface feature in general results in a decreasing surface sensitivity. Only those photoelectrons which are not affected by shading (both x-ray and photoelectron) will contribute to the intensities of the signals. The effects of surface roughness on quantitative XPS analysis were also reported by Ebel and Wernisch (114).

The flux of incident x-ray usually is not uniform and shows a distribution on the surface. Therefore, the number of photoelectrons emitted will be different over the surface. The center flux of the x-ray beam is, in general, stronger than the flux at the edge. Because of this non-uniform flux, the intensities of the signals are also changed. The solid angle which defines the region that the emitted electrons can enter into the spectrometer for energy analysis also shows significant effects on the intensities of the signals. Solid angle will be gradually decreased and becomes zero leading to the decreasing of intensity when the sample area extends to a infinite size relative to the spectrometer. The final factor which can affect the intensity of the signal is electron reflection. Electrons emitted by x-ray may be reflected back to the bulk without

going to the analyzer due to the potential barrier at the surface. This will clearly decrease the photoelectron intensities of the signals. However, it only occurs significantly at angle of 10° to 15° which are smaller than encountered here.

All the above factors can contribute the deviation between the experimental data and fitted model at low electron take-off angle. However, this work substantiates the value of XPS, not only qualitative but quantitative determination, in study of the burn-out of binder/ceramics composite.

4.3.7 Scanning Electron Microscopy (SEM) Study

Scanning electron microscopy is a useful tool for observation of the surface topography. Fig. 4.23 and Fig. 4.24 show the micrographs of Al_2O_3 coated with PVB and OPE-3, respectively. The surface is very rough and shows an irregular shape which may lead to conclusions as discussed in the previous section. Agglomeration of the polymer on the surface was also observed. Compared to the micrograph of clean Al_2O_3 (uncoated), Fig. 4.25, it appears that the clean Al_2O_3 has clearer surface features than the samples coated with polymers follwed by a burn-out process.

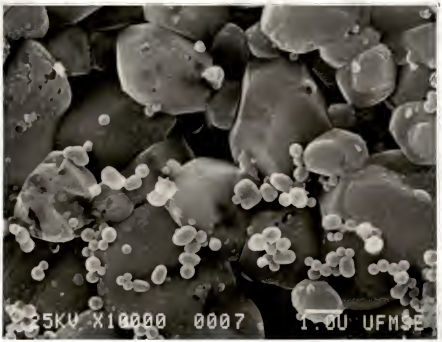

(a)

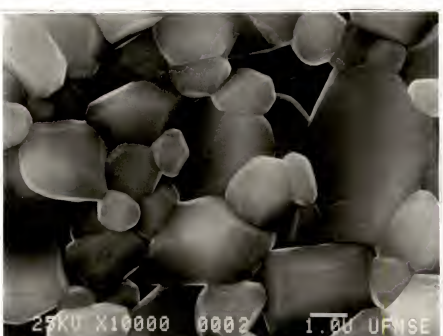

(b)

Figure 4.23 (a)Scanning electron micrograph of Al_2O_3 coated with PVB. (b)Scanning electron micrograph of Al_2O_3 coated with PVB followed by a burn-out process.

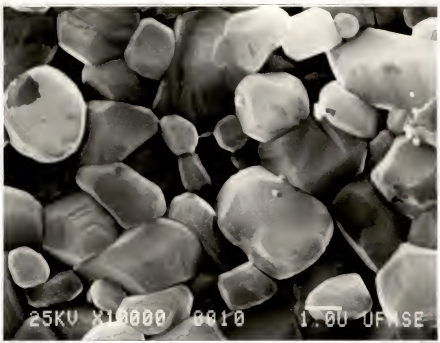

(a)

(b)

Figure 4.24 (a)Scanning electron micrograph of Al_2O_3 coated with OPE-3. (b)Scanning electron micrograph of Al_2O_3 coated with OPE-3 followed by a burn-out process.

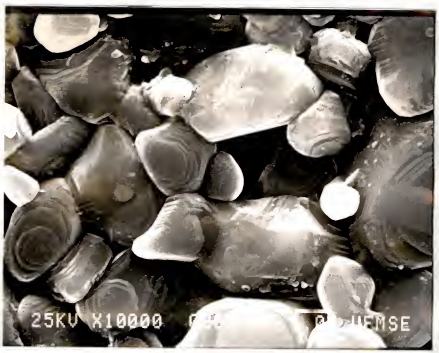

Figure 4.25 Scanning electron micrograph of untreated Al_2O_3.

4.3.8 Thermal Gravimetric Analysis

Thermal gravimetric analysis was used to monitor the dynamic weight loss of polymer film vs. temperature in air and in nitrogen. Figure 4.26 shows the degradation behavior of PVB both in air and nitrogen with thermal gravimetry (TG) and differential thermal gravimetry (DTG) plots. A distinct peak and two small peaks were observed on the DTG plot in air, while a sharp peak and a small shoulder were observed in nitrogen. Based on these available data it is suggested that the first weight loss peak is mainly associated with side-chain degradation, i.e., breakage of hydroxyl groups, butyral groups, and acetate groups. The second weight loss peak is due to breakage of carbon-carbon main chains. The second peak is small compared to the first peak. The final carbon residues left are around 2.8% and 1% for PVB burned in nitrogen and air, respectively. The burn-out study using TG and DTG for OPE-3 is also shown in Fig. 4.27. There are two weigh-loss peaks both in air and nitrogen. However, the peak area of the second peak of OPE-3 is much larger than that of PVB. This may be attributed to the introduction of COO groups into the main-chain. The degradation of main-chain through decarboxylation is easier than through carbon-carbon bond scission. The final carbon residues are approximately 3.0% and 1.2% for OPE-3 treated in nitrogen and air, respectively.

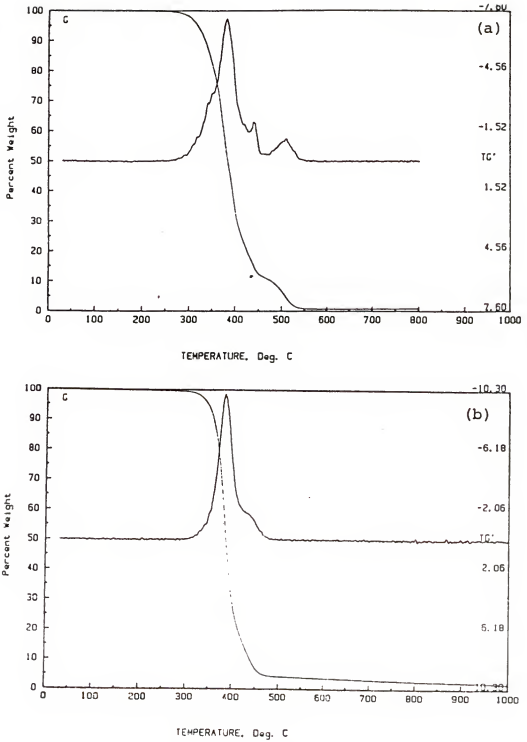

Figure 4.26 (a) Thermogravimetric analysis of PVB burned in air. (b) Thermogravimetric analysis of PVB burned in nitrogen.

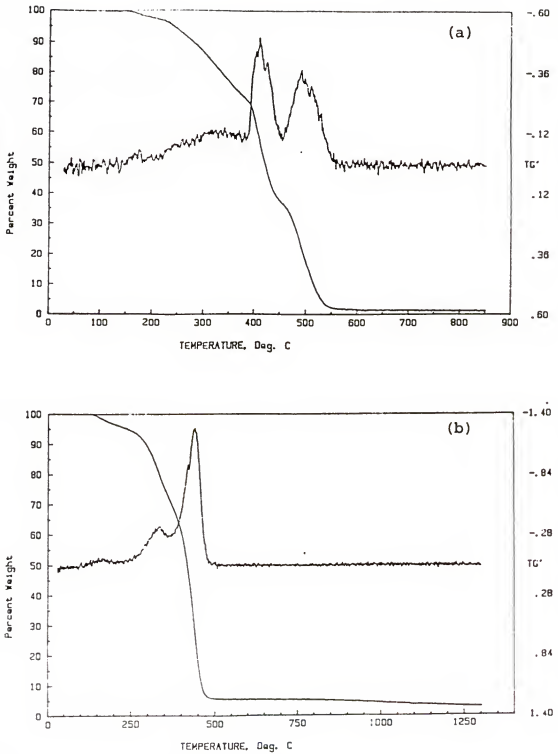

Figure 4.27 (a) Thermogravimetric analysis of OPE-3 burned in air. (b) Thermogravimetric analysis of OPE-3 burned in nitrogen.

There is little difference between the residues of PVB and OPE-3, and more detailed studies on the thermal behavior of these two polymers are required.

CHAPTER 5
SURFACE MODIFICATION OF POLYPROPYLENE FILM BY GAS-PHASE METHOD

5.1 Background

5.1.1 Surface Modification

The surface properties of polymeric materials from the application viewpoint, such as dyability, printability, adhesivity, and biocompatibility, are important factors to determine the usefulness of a polymeric material. However, the surface properties of commodity synthetic polymers are frequently chemical inertness, non-polar and this greatly decreases their application in the engineering as well as in the biomedical field. One way to improve their performance for specific use is to modify the surface either physically, or chemically.

Surface (or interface) can be defined as the outermost several angstroms of the solid region which is significantly different in structure and properties from the bulk due to different intermolecular forces. These surface-molecular properties, in terms of thermodynamic variables such as surface energy and surface entropy, can be readily modified through surface modification techniques and related to the

macroproperties as mentioned above (dyability, adhesivity, printability, and biocompatibility).

5.1.2 Methods for Surface Modification

Many processes have been developed to modify the polymer surfaces:

A. Wet chemical modification: by using strong acids such as chromic acid, sulfuric acid to oxidize the surface.

B. Physical modification: by dip-coating into the polymer solution.

C. Flame modification: by using mixture gas of oxygen and fuel to oxidize the surface.

D. Plasma modification: by using glow discharge either in reduced or atmospheric pressure with various gases.

E. Photochemical modification: by using U.V. source to graft a monomer onto the substrate.

F. Ionizing-radiation modification: by using Gamma radiation to graft a monomer onto the substrate.

The use of strong acid including chromic acid, sulfuric acid, phosphoric acid together with water and potassium dichromate for surface modification of synthetic polymers generally create a complex topography on the surface, which results in increasing wetability and bondability and may also produce some polar groups such as carboxylic acids or carbonyl compounds through the etching process (118). In addition, the degree of etching is not easy to control and

sometime causes extensive pitting which can change the bulk properties of the polymer and reduce the mechanical strength of the materials. Contamination of the surface during the treatment is also another disadvantage of this method.

Physical treatment of the polymer surface by dip-coating into a solution usually produces a relatively thick coating and may penetrate into the polymer substrate, which again can change bulk properties such as strength, elongation, and modulus. Another drawback of this process is the production of bubbles on the surface during dipping, which results in surface roughness.

Flame treatments of the polymer surface are already commercialized to improve wetability of the polymer film. However, the effects of such treatments sometimes are not well controlled.

As for plasma treatment of the polymer surface, a considerable amount of research has been done (119-121). The characteristic of plasma treatment is to graft/deposit a thin polymer film on the substrate matrix. However, the reaction mechanism is rather complicated as electrons, atoms, molecules, positive ions, and negative ions are all produced, which results in the nonspecific modification and sometimes depends on the reaction conditions such as power source, flow rate of starting materials, and vacuum pressure.

Surface modification by gamma-radiation has already been reported (122). Two methods can be applied by using either a pre-irradiation or a simultaneous irradiation technique. Although these two techniques offer some advantages such as clean and efficient surface modification, they also suffer some disadvantages, for example, the substrate polymers are susceptible to significant radiation damage, the grafting reaction occurs not only at the polymer surface, but may penetrate into the substrate polymer which can change the bulk property of the substrate; homopolymerization can inevitably take place in liquid monomer and thus decreases the efficiency of the monomer utilization. Due to the high possibility of damage to substrate polymers with gamma-radiation, the use of U.V. irradiation to initiate grafting of monomers has been investigated (123). Sensitizers such as benzophenone, benzoyl peroxide, and anthraquinone are usually required for the activation by U.V. These sensitizers are used to absorb the radiation energy to enhance the reaction. Thus, the substrate polymers must be specially prepared before irradiation by U. V. and the resulting grafted films may contain residual amounts of sensitizers.

The above mentioned methods all have their advantages and disadvantages. The choice of the method thus depends on the substrates, the monomers, and the properties required for the modified product. On the other hand, we used a

novel method to graft hydrophilic monomers onto a hydrophobic polypropylene film by gas phase deposition.

5.1.3 Flash Vacuum Thermolysis (FVT)

The general idea and reaction system in this study originated from FVT but with some modifications so that the gas-solid phase reaction can be initiated by activated peroxide.

In FVT, the sample is vaporized under high vacuum pressure below its decomposition temperature and then passed through a pyrolytic quartz tube with an inert carrier gas (flow system) or without a carrier gas (static system). The activated products then can be condensed in a cold trap for static analysis such as chromatographic or spectroscopic methods. Alternatively, the activated gas products can also be analyzed by dynamic method such as mass spectrometry. Because of the use of a high vacuum (10^{-3} to 10^{-4} torr) and a gas phase reaction, the intermolecular reactions between the reactive species are minimized and contamination from solvents or other species do not occur. This valuable method has been applied by chemists to study the reaction mechanism and to synthesize highly reactive compounds (124).

5.1.4 Gas Phase Grafting Method

Surface modification by the gas phase method has some advantages over the wet chemistry method, such as less contamination, more uniform deposition of monomers on the substrate, and more efficient use of the monomers.

Hayakawa et al. (125) studied the gamma and ultraviolet radiation graft copolymerization of maleimide by the vapor phase method. Both ethyl cellulose and polyethylene films were used as the substrates. The maleimide was grafted, using its sublimation vapor, onto the ethyl cellulose film, while the graft of maleimide onto the polyethylene film was not observed. Huglin and Smith reported the copolymerization of acrylic acid to nylon-6 film by gamma-irradiated vapor phase method (126). They found that the initial rate of grafting increased with dose within the range of 2 Mrad., and concluded that grafting proceeded from the surface and was free from diffusion control at the initial stage. Recently a more systematic study of vapor phase photo grafting of vinyl monomers on polymer films/plates has been performed by Y. Ogiwara et al. (123).

5.2 The Use of Polypropylene Film as a Substrate for Grafting Copolymerization

Polypropylene (PP) has a wide range of application in industry. However, this polymer is very hydrophobic, it is difficult to dye, it is difficult to print onto, and it is sensitive to photo-oxidation. For these reasons, PP was used

as the substrate in this study. In addition, there is a hydrogen atom attached to the tertiary carbon atom in the main-chain which can act as a source for degradation of the macromolecular chain. Therefore, an attempt was made to modify the surface of polypropylene film through grafting copolymerization of hydrophilic monomer to remove this unstable hydrogen atom and to increase its printability, dyability, photochemical stability, and mechanical properties.

X-ray Photoelectron Spectroscopy (XPS) or Electron Spectroscopy for Chemical Analysis (ESCA) and Fourier Transform Infrared-Attenuated Total Reflectance Spectroscopy (FTIR-ATR) were used to characterize the products.

5.3. Materials and Methods

5.3.1 Materials

Oriented polypropylene film with the trademark Bicor is a product of Mobil Oil Corporation. The thickness of the film is about 1.25 mils. Solvents such as acetone, methanol, reagent alcohol were purchased from Fisher Scientific Company. Azobisisobutyronitrile (AIBN) was obtained from Eastman Kodak Company. Tert-butyl peroxybenzoate was obtained from Aldrich Chemical Company. N-vinylpyrrolidone (from Kodak) and dimethylaminoethylmethacrylate (from Aldrich) were vacuum distilled before use.

5.3.2 Sample Preparation

Films of polypropylene were cut into 1 cm x 5 cm and were Soxhlet extracted with methanol for 24 hrs and then placed in acetone in an ultrasonification bath for 10 minutes to remove all the possible contaminants on the surface such as grease and dust. They were then rinsed with distilled water and dried under vacuum at 50°C for 24 hrs. The cleaned samples were stored in a vacuum desiccator for further use.

5.3.3 Apparatus

The apparatus for vapor-phase graft copolymerization is shown in Figure 5.1. Nitrogen gas was used as carrier gas which passed through the drying unit (Drierite) before entering the flow meter. The gas flow rate was regulated by a Manostat Instruments Model 36-541-045 flow meter. Monomer and initiator were evaporated in an oil bath equipped with a magnetic stirrer and a Variac. The reaction chamber with two inlets was immersed in an oil bath controlled by Thermomix 1460 immersion thermostat. The film strips were mounted on glass hooks attached to the cap of the reaction chamber. A thermometer was located at the center of the reaction chamber to indicate the reaction temperature. A liquid nitrogen trap and a McLeod gauge were connected to the rotary oil pump. All the joints were secured with high

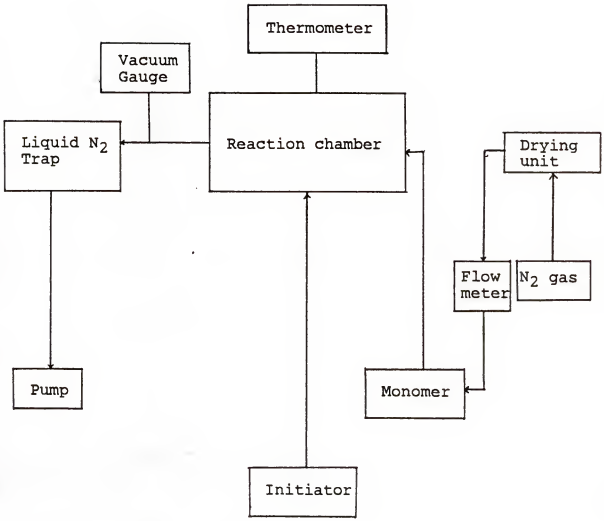

Figure 5.1 Schematic diagram for the vapor phase grafting.

vacuum grease and checked with a coil spark gun to ensure no leakage during the reaction.

5.3.4 Graft Copolymerization

The strip films 1 cm x 5 cm, were suspended inside the reaction vessel. The monomer and initiator were loaded into the Pyrex flask with the valves closed. The whole system was evacuated until the desired vacuum (0.05 - 0.1 mmHg) was reached. The valve of the initiator was then opened and the oil bath was kept at the desired temperature (60°C - 65°C). The valve to the monomer flask was opened and monomer was evaporated at temperature (55°C - 65°C) while the reaction chamber was heated simultaneously in the constant temperature bath (96°C).

After reaction was completed, samples were removed from the reaction vessel and extracted with acetone for 12 hours and then washed with methanol and distilled water three times to remove homopolymer.

5.3.5 FTIR-ATR

Fourier transform infrared-attenuated total reflectance (FTIR-ATR) was used to analyze the surface-modified PP film. All spectra were collected with a Nicolet 60 SX spectrometer coupled with computerized-software data manipulation system. Spectra were taken over the range of 4000-500 cm^{-1} with a resolution of 4 cm^{-1}, and a liquid nitrogen cooled mercury cadmium telluride (MCT) detector. A KRS-5 (Thalium-bromide-

iodide) crystal with dimensions 50 x 10 x 2 mm was held in a Harrick accessory, Harrick Scientific, Corp., Ossining, New York, at an entrance and exit angles of 45°. The KRS-5 prism was washed with acetone and absolute ethanol to remove contaminants.

The control and surface-modified PP films were placed in contact with KRS-5 crystal and IR beam was reflected through the reflecting crystal where absorption occurs at the sample/KRS-5 interface. The beam was properly aligned so that the maximum signal was obtained; the absorption spectrum was obtained by the sample spectrum relative to the background spectrum.

5.3.6 XPS

The experiment was done in a Kratos, XSAM-800 spectrometer. The details of the apparatus were described in Chapter 4, and will only be summarized here. A dual anode x-ray source with magnesium and aluminum excitation was used. However, in this experiment only the magnesium source producing $MgK_{\alpha 1,2}$ at energy 1253.6 ev. was used. The x-ray power was operated at 240 w, and the vacuum pressure in the analysis chamber was maintained at 2×10^{-7} torr. The hemispherical analyzer (127 mm) was operated in a fixed retardation ratio mode for a better sensitivity within the energy range analyzed. The spectrometer was interfaced to a PDP 11/23 computer with RT-11 operating system.

All spectra (narrow scans) were collected with a step size of 0.05 ev. 800 channels, and stored in a winchester hard disk. Due to the nonconductive characteristics of polymer film, a shift of the binding energy was observed. Thus, the C_{1s} peak of a hydrocarbon which was assigned a value of 285.0 ev. was used as a reference for chemical shift determination. Analysis of the data such as smoothing of spectra, background subtraction, curve fitting, and charge correction was accomplished using DS-800 software program, from Kratos. The area of photoelectron peak was measured by numerical integration after linear background subtraction. Atomic quantitative analysis was carried out by correcting measured areas for the Scofield cross-sections, instrument transmission function ($E^{-1.0}$), and escape depth ($E^{-0.75}$).

5.4 Results and Discussions

5.4.1 Grafting Copolymerization

The result of grafting hydrophilic monomers onto polypropylene film is shown in Table 5.1. Two kinds of initiators were used in this study, azobisisobutyronitrile (AIBN) and t-butyl peroxybenzoate. Two different monomers were also used, N-vinylpyrrolidone and dimethylaminoethyl-methacrylate. The use of azobisisobutyronitrile as an initiator showed no grafting while substantial grafting was observed with use of the t-butyl peroxybenzoate. This may be

TABLE 5.1

Reactants for Vapor-Phase Grafting Polymerization[a]

Initiator[b]	Monomer[c]	Result[d]
Azobisisobutyronitrile (AIBN)	N-vinylpyrrolidone (NVP)	-
Azobisisobutyronitrile (AIBN)	Dimethylaminoethyl-methacrylate (DAEM)	-
t-butyl peroxybenzoate (t-BPB)	Dimethylaminoethyl-methacrylate (DAEM)	+

a : Polypropylene as a substrate.

b : AIBN $(CH_3)_2 C(CN) - N = N - C(CN)(CH_3)_2$

t-BPB $\varphi - C(=O) - O - O - C(CH_3)_2 - CH_3$

c : NVP 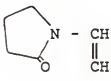

DAEM $H_2C = C(CH_3) - C(=O) - O - CH_2 - CH_2 - N(CH_3) - CH_3$

d : + Monomers were grafted on the substrate.
- Monomers were not grafted on the substrate.

attributed to the carbon radicals as shown in Fig. 5.2, which does not possess enough activity to abstract the hydrogen atom from the substrate in order to initiate the grafting copolymerization. These carbon radicals may recombine again as soon as they decompose. Bickel and Waters (127) reported that the decomposition of azobisisobutyronitrile in toluene yields 84% tetramethylsuccinodinitrile, 3.5% isobutyronitrile, and 9% 2,3,5 tricyano-2,3,5-trimethylhexane. Hammond et al. (128) also showed a 90% yield of the tetramethyl- succinonitrile in their experiment. On the other hand, t-butyl peroxybenzoate was decomposed to activated free radicals under thermal heat and abstracted the hydrogen atom from polypropylene resulting in an active center being created on the polymeric backbone.

The relative stability of free radicals can be evaluated by the hydrogen-bond dissociation energy of the parent compound (129) as shown in Table 5.2. From this Table, it can be seen that HO-H is the most stable compound because 498 kJ/mol bond dissociation energy is needed for breaking the O-H bond and the hydroxyl radical (HO·) is the least stable, i.e., the most reactive. On the other hand, R_3C-H bond is the least stable among these species since it needs only 381 kJ/mol bond dissociation energy. This implies that $R_3C\cdot$ radical is less reactive than OH· radical. By the

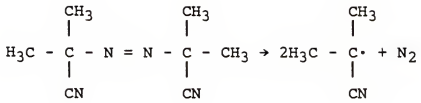

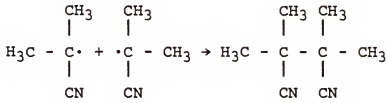

Figure 5.2 The decomposition and recombination of AIBN.

TABLE 5.2

The Hydrogen-Bond Dissociation Energy of Organic Compounds.[a]

Parent compound	Bond dissociation energy (KJ/mol)
HO - H	498
RCOO - H	469
ϕ - H	469
RO - H	439
CH_3 - H	435
RCH_2 - H	410
R_2CH - H	397
R_3C - H	381

a : See reference (129)

same token, we can predict that RO· radical and phenyl radical are more reactive than R_3C· radical.

Based on the above discussions, it is important to choose an initiator which has a very reactive free radical to abstract the hydrogen atom from the substrate material. Table 5.2 shows that the alkoxy and phenyl free radicals, which are the ones used in this study as initiators have a higher tendency for hydrogen abstraction reaction than the tertiary alkyl free radical which is probably produced from the polypropylene film.

5.4.2 Structure and Property Relationship of Initiators

The t-butyl peroxybenzoate decomposes by heat and breaks into two parts through cleavage of the oxygen-oxygen bond as shown in the following equation:

These two free radicals (acyloxy and alkoxy radicals) may subsequently decompose into other reactive species, such as

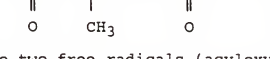

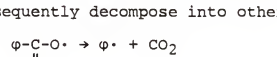

All the above free radicals are very reactive according to the bond dissociation energy in Table 5.2. The tertiary alkyl free radicals produced from the polypropylene substrate as shown in the following equation:

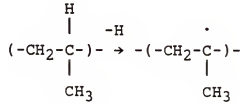

are less reactive than the phenyl, methyl, acyloxy, and alkoxy free radicals. From the thermodynamic viewpoint, the reactive species are unstable, i.e., it has a higher chemical potential which can act as a driving force for hydrogen abstraction in order to form a more stable compound, i.e., lowering its chemical potential.

5.4.3 Reaction Mechanism

Based on the above discussions, we propose the following overall reaction mechanism for grafting copolymerization by using a free radical initiator: For the initiation step, reactive species are produced by thermal decomposition,

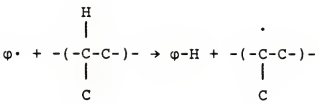

or

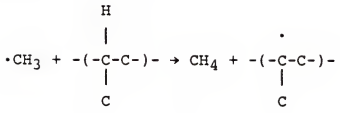

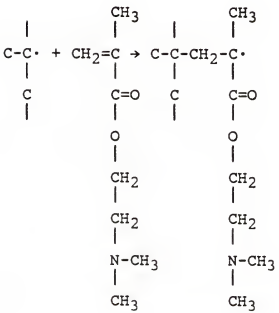

for the propagation step,

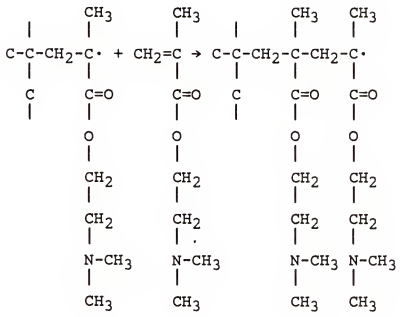

for the termination step,

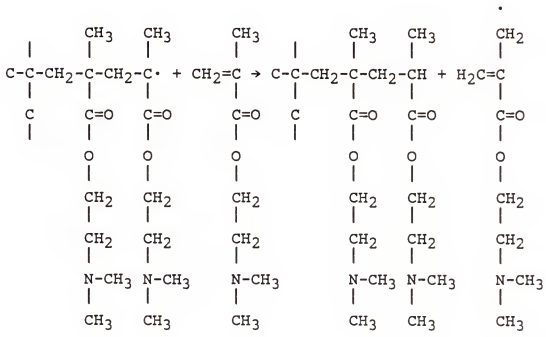

In the termination step, the allylic hydrogen is easier to abstract than other hydrogen atoms by the following order:

allylic > 3° > 2° > 1° > CH_4, vinylic

where,

3° = hydrogen atom is attached to a tertiary carbon,

2° = hydrogen atom is attached to a secondary carbon,

1° = hydrogen atom is attached to a primary carbon.

5.4.4 Wetability

Contact angle measurement is a convenient and effective method of analysis of the outer few angstroms of a sample. It can qualitatively monitor the change of the polarity of the surface functional groups. However, as mentioned previously, there are two factors which can affect the contact angle measurement; surface topography and surface functional groups. The results of the contact angle measurement are useful only if there is no significant change in the surface topography. In this way, we can attribute to the change in contact angle due to introduction of new functional groups onto the surface by chemical modification and not due to change in surface topography. The change in contact angle measurement following wet chemistry usually results from a change in surface roughness.

In this study, the contact angle is defined as the angle between the tangent to the probe liquid and the solid substrate measured through the liquid, and is determined on a Rame Hart NRL Contact Angle Goniometer. The Polypropylene film was mounted horizontally onto a glass slide using Scotch Tape. A microsyringe was used to drop the water onto the edge of the film and the contact angle was measured immediately. Contact angles of both sides of the drop were measured and the results are shown in Table 5.3. When the contact angles of unmodified and modified are compared, it can readily be seen that the surface energetics are changed which is attributed to the grafting of dimethylaminoethyl-methacrylate (DAEM).

5.4.5 XPS Spectrum of Unmodified Polypropylene Film

XPS is a very useful technique for studying surface and interface properties. It can provide information about elemental analysis,the chemical bonding state, and the functional groups that reside on the surface. Figure 5.3 shows the survey scan of an unmodified polypropylene film. The large peak at 285 ev. is assigned to C_{1S} photoelectron ($K_{\alpha 1,2}$) line. At the lower binding energy side of this main peak appears a small satellite peak which is due to x-ray $K_{\alpha,3}$ and $K_{\alpha,4}$ radiation. At the higher binding energy side of this main peak appears a very small peak of O_{1S} line at 531 ev. This is attributed to the photo-oxidation of the PP

TABLE 5.3

Contact Angle Measurement of the Modified PP Film

Sample	Right side	Left side
1[a]	95	93
2[b]	53	50
3[b]	54	53
4[b]	57	57

a : Control sample.

b : Samples were grafted with DAEM.

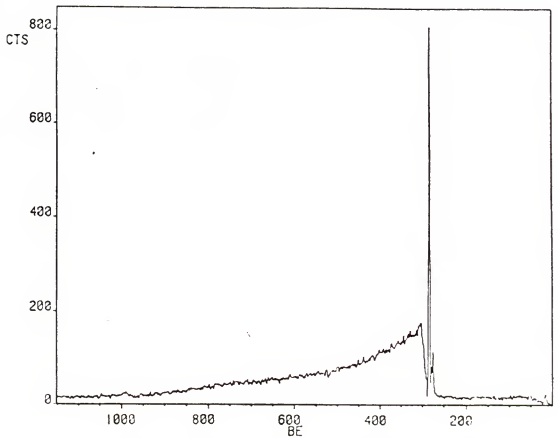

Figure 5.3 XPS survey spectrum of unmodified polypropylene film.

film, which may come from the environment or X-ray radiation. There are some minor peaks in the range of 0-60 ev. The peak at 17 ev. is due to C_{2s} line. The peak at 53 ev. is attributed to the C_{1s} ghost peak due to Al x-ray from the Al window in the anode.

5.4.6 Dimethylaminoethylmethacrylate Homopolymers

Clark and Thomas (130) studied a series of homopolymers, such as polyalkylacrylates, and polyalkylmethacrylates, by XPS. The model compound such as methanol, ethanol, ethyl acetate et al., was condensed directly onto a cooled gold substrate in the spectrometer, and the binding energy of each peak and intensity was determined. The absolute binding energy of the homopolymers was then assigned and the surface composition of each homopolymer was studied.

As far as we know, the binding energy of functional peaks of dimethylaminoethylmethacrylate (DAEM) and its surface composition have not been investigated by XPS. Therefore, it is necessary to study the binding energy of each functional peak and relative peak intensity in order to establish a firm basis for the interpretation of the grafting copolymer data. A survey scan (0-1150 ev.) of DAEM is shown in Fig. 5.4. As expected, three major photoelectron lines, i.e., C_{1s}, O_{1s}, and N_{1s} appear in the spectrum, and two small peaks centered at 102 ev. and 153 ev., which are

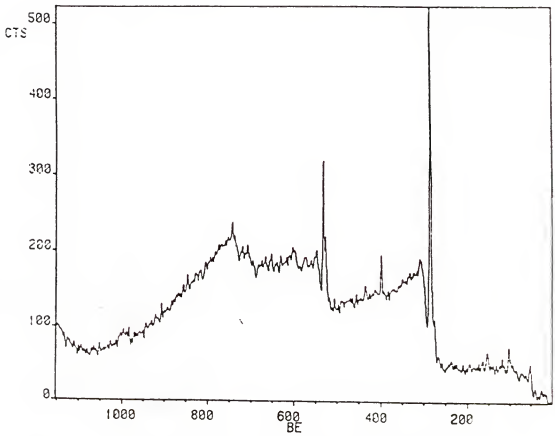

Figure 5.4 XPS survey spectrum of dimethylaminoethyl-methacrylate polymer.

attributed to Si_{2p} and Si_{2s} photoelectron lines coming from contaminants, were also shown in the spectrum. In general, there are two independent methods for establishing the polymer composition from the quantitative atomic concentration analysis.

The first method involves the measurement of the area of each photoelectron line which is then corrected with the quantitative factors. The atomic concentration of C, O, and N (not considering Si) of DAEM and their relative peak intensities are tabulated in Table 5.4. It is noted that the percentage of C is somewhat too high as a result of the contamination or uncovered polypropylene. However, the atomic ratio of O to N is 2.0 which is very close to its predicted value of 2.

5.4.7 Numerical Curve-Fitting Analysis

As mentioned before, one of the strengths of XPS is its ability to detect the binding energy shifts due to differences in the electronegativity of chemical species. However, sometimes it is difficult to determine the amount of binding energy shift due to the relatively small difference in electronegativity of the element with its environment. For example, it is impossible to distinguish the bonding energy of C-H, C-C, and C=C compounds because the width of the photoelectron lines are larger than the binding energy differences among them. This problem may be

TABLE 5.4

Atomic Concentrations and Peak Area Ratio for Dimethylaminoethylmethacrylate (DAEM)

Element	Experimental Concentration	Theoretical Concentration
C	78.7	72.7
O	14.3	18.2
N	7.0	9.1
O/N	2.0	2.0
C/O	5.5	4.0
C/N	11.2	8.0

overcome by curve-fitting analysis or chemical derivatization techniques. Only the curve-fitting technique will be discussed here.

The curve-fitting technique involves the computer iteration program which uses information on peak shapes (either Gaussian or Lorentizian), peak height, and peak full width at half maximum (FWHM). Application of this method requires knowledge of the chemistry of the system. The computer will then perform the iterations and compare the calculated value with experimental value until the calculated value matches the experimental one. Either the peak binding energy of the individual peak in an overlapped envelope follows the reference data if available or the peak assignment is done from the model compound from which is constructed a correlation chart between the peak position and specific functional groups. It is similar to the technique developed for NMR and IR spectroscopy. Information on the chemical shift of each functional group of polymers was collected by Clark and his colleague (131).

Thus, the second method for determining the surface composition of a polymer involves a detailed C_{1s} peak shape analysis. With the fine structure and relative intensity of each component, we are able to investigate the structure and bonding state of the compound. This is shown in Fig. 5.5. The experimental curve and computer calculated envelope are in agreement as shown in the upper Figure. The individual

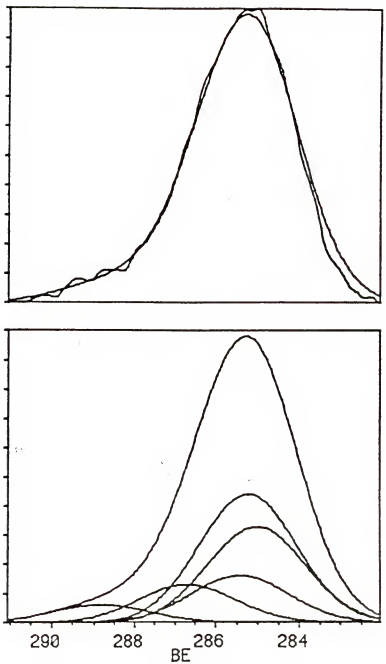

Figure 5.5 Curve-resolved components of C_{1s} spectrum of dimethylaminoethylmethacrylate polymer.

peak component and corresponding binding energy is also shown in the bottom Figure. The peak binding energy and corresponding chemical structure of C_{1s} is shown in Table 5.5. The peak energy centered at 285.0 ev. was assigned to the carbon atoms which are not directly bonded to oxygen or other elements having higher electronegativity than the carbon atom. Taking this as the energy reference, the chemical shift due to a different bonding state can be determined. Thus, for carbon singly bonded to one oxygen atom, the binding energy is 286.7 ev. (1.7 ev. higher than the hydrocarbon). For a carbon atom doubly bonded to oxygen and singly bonded to one oxygen, i.e. ester function group, the binding energy is 288.8 ev. (3.8 ev. higher than the hydrocarbon). These assignments are correlated to the data reported by Clark (130). Clark and Thomas (131) investigated the chemical shift of the functional groups for some homopolymers containing carbon, hydrogen, nitrogen, and oxygen. The carbon atom singly or triply bonded to a nitrogen atom (for pyridine and nitrile base polymers) was assigned approximately at energy 286 ev. Gerenser et al. (132) studied the molecular orientation of fluorosurfactant adsorbed on various substrates. In their report, the binding energy of C-N was graphically assigned to the same position as C-O and C-S functional groups. Batich and Donald (133) also studied the chemical shift of some nitroso compounds by XPS. The observed chemical shift of the nitrogen atom was

TABLE 5.5

Experimental Binding Energy and Corresponding Chemical Structure of C_{1s} Peak for DAEM

Component	a C - H	b C - N	c C - C - O	d C - O	e C - O
B. E.	285.0	285.2	285.4	286.7	288.8
ev. shift	0	0.2	0.4	1.7	3.8

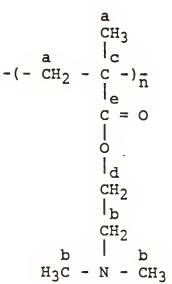

compared to the theoretical model. Recently, Munro (134) reported the effect of power and substrate temperature on chemical composition for RF plasma polymerization of acrylonitrile. He assigned a binding energy of 286.3 ev. for C≡N and C-O groups. Based on the above literature, the carbon atom singly bonded to a nitrogen was assigned at energy 285.2 ev.

5.4.8 Secondary Shift Effect

It is interesting to note that we have introduced a new binding energy at 285.4 ev. for a carbon atom not directly bonded to an oxygen atom. This carbon atom may be affected by the high electronegativity of the oxygen atom, known as secondary shift effect. The secondary shift effect of fluorine on a series of fluoro polymers has been demonstrated by Ginnard and Riggs (135). They reported that adjacent atom substitution produces binding energy changes about 10% as large as direct substitution depending on the electronegativity of the substituent atom. Recently, Pijpers and Donners (136) studied the surface composition of acrylate copolymer latex film. In addition to consideration of the primary shift effect, the secondary shift effect was also taken into account resulting in the experimental value close to the theoretical value.

In the systems studied, it is believed that the secondary shift effect on the carbon atom which is not

directly attached to the oxygen atom needs to be included in the calculation of binding energy. This chemical shift was estimated as having a value of 0.4 ev. relative to the reference energy 285 ev. The fit between the experimental curve and the computer iteration envelope suggests the appropriateness of this approach.

From the above discussion, the chemical structure of DAEM was evaluated by two independent methods, i.e., the intensity ratio of C, O, and N, and the resolved component peaks of C_{1s}. Both of these methods show the approximate atomic structure of the DAEM compound from the concentration of "tag" element of O and N.

5.4.9 Grafting of DAEM on Polypropylene Film

Based on the above fundamental methodology and discussions, the focus is now on the data of DAEM grafted on PP film. The results are shown in Fig. 5.6. As can be seen in the figure, the appearance of O_{1s} (532 ev.) and N_{1s} (400 ev.) peaks are very significant due to the grafting of DAEM onto PP substrate. It is important to note that the valence-band of O_{2s} was also shown at binding energy value 23 ev. The oxygen Auger peak was also shown in the Figure at 745 ev. Comparison of Fig. 5.3 and Fig. 5.6 concludes that DAEM was successfully grafted on PP substrate by the vapor phase method. The narrow scan of C_{1s}, and O_{1s}, and N_{1s}, are shown in Fig. 5.7, Fig. 5.8, and Fig. 5.9. C_{1s} with a

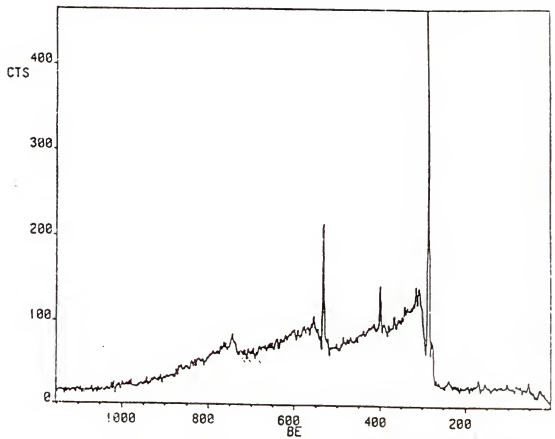

Figure 5.6 XPS survey spectrum of dimethylaminoethyl-methacrylate grafted onto polypropylene film.

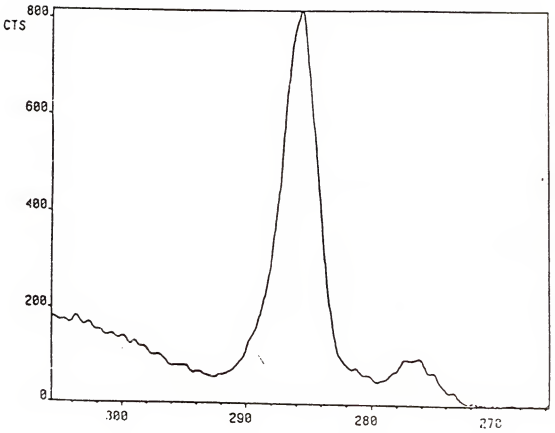

Figure 5.7 XPS C_{1s} spectrum of dimethylaminoethyl-methacrylate grafted onto polypropylene film.

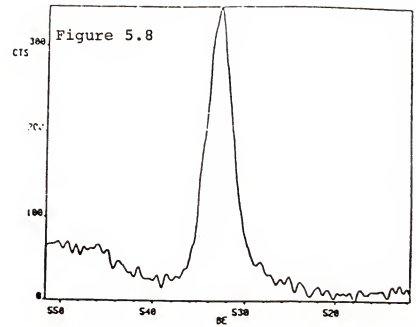

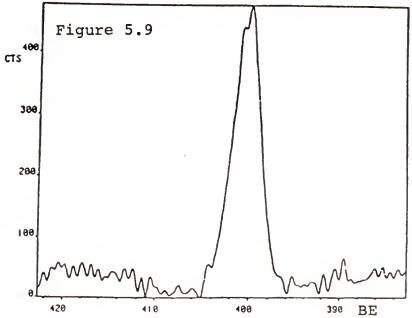

Figure 5.8 XPS O_{1s} spectrum of dimethylaminoethylmethacrylate grafted onto polypropylene film.
Figure 5.9 XPS N_{1s} spectrum of dimethylaminoethylmethacrylate grafted onto polypropylene film.

slight shoulder at a higher binding energy side was observed.

5.4.10 Angular-Dependent XPS (θ)

The basic principle of angular-dependent XPS has been described in detail in Chapter 4. Therefore, only the important points will be summarized here. Up to this point, all the data reported were analyzed at a 90° electron take-off angle. The electron take-off angle is defined as the angle between the surface and the emitted photoelectrons. This experimental arrangement will result in a maximum effective sampling depth. However, in some cases it is interesting to know the surface feature of the outermost several layers of angstroms, since the structure of this true-surface layer always plays an important role and shows significant effects on the physical, chemical, mechanical, and electrical properties of polymers. This can be achieved by varying the electron take-off angle so as to enhance surface sensitivity at low θ, i.e., decreasing the effective sampling depth. By the application of this method, surface thickness and surface homogeneity can sometimes be determined.

The sample was mounted on the sample holder with double-sided adhesive tape. The samples were then situated on a carrousel which could be loaded with ten samples at the same time. The sample was then rotated by a x-y-z

manipulator which can be operated in a 360° angle. Spectra were recorded at four different angles, 90°, 75°, 45°, and 20°.

Figure 5.10 compares the results of C_{1s} profiles and the corresponding resolved components at 90° and 20°. It is apparent that the C_{1s} peak at a 20° take-off angle has higher concentrations of C-N and C-O groups than a 90° take-off angle. This indicates that the distribution of functionalities such as C-O, COO, and C-N groups in the thin-grafted film are not homogeneous in the vertical depth, and implies the enhanced surface sensitivity at the low electron take-off angle. It is believed that oxygen and nitrogen atoms at the near surface are responsible for the formation of hydrogen bonding with water molecules. Consequently, surface energetics is changed from dewetting to wetting behavior. In other words, the bulk structure of this thin-grafted film is different from the surface structure. This is consistent with the contact angle data measurement which shows the contact angle decreases from 94° to 52° upon grafting the dimethylaminoethylmethacrylate.

5.4.11 Thickness Measurements of the Grafted DAEM Film on PP Substrate

We have discussed the surface feature enhancement, and surface homogeneity using experimental angular-resolved XPS data. Grafted thickness as well as electron mean-free-path information can also be obtained by this valuable technique.

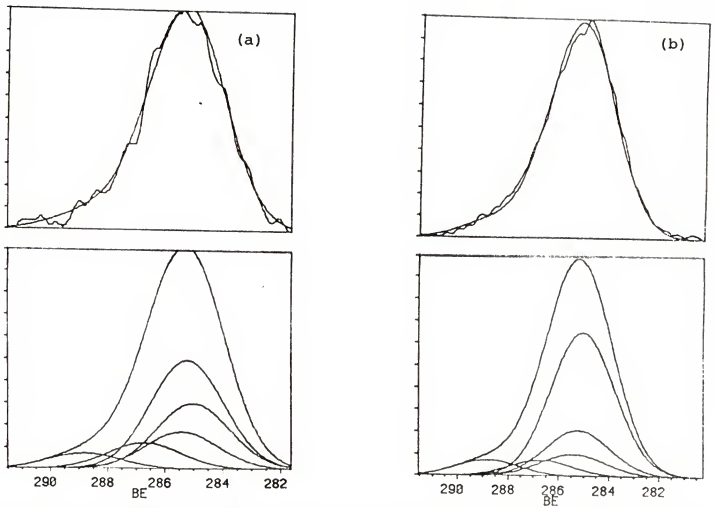

Figure 5.10 Comparison of curve-resolved data of C_{1s} at electron take-off angles (a) 20^0 and (b) 90^0

There are three methods which can be used for the calculation of film thickness, i.e., substrate-attenuation method, curve-resolved XPS, and overlayer-substrate angular-dependent XPS. The basic equation applied in the substrate-attenuation method is (87)

$$I = I_{\infty} \exp(-d/\lambda) \qquad (5.1)$$

where,

I = the intensity of a signal arising from the substrate under a surface overlayer of thickness d.

I_{∞} = the intensity observed for a substrate with infinite thickness.

λ = the mean-free-path of a photoemitted electron.

The physical meaning of the above equation is that the photoelectron peak arising from a component in the substrate will be attenuated under the presence of a thin overlayer by the factor $\exp(-d/\lambda)$.

I and I_{∞} value can be experimentally determined by the XPS data and λ value can be obtained in several references (109-111). Therefore, thickness of the overlayer can be calculated with the above equation. On the basis of XPS data and by taking the inelastic mean-free-path for C_{1s} electrons in polymeric materials (33Å), the calculated overlayer thickness is 26Å.

The overlayer thickness can be further estimated by angular-dependent XPS data. This procedure will be briefly

described here. Clark et al. (137) studied surface fluorination on polyethylene film. They used curve-resolved peaks of C_{1s} and calculated the relative area of hydrocarbon peak and fluorinated-carbon peaks. The equation used was:

$$\frac{A^F_{C_{1s}}}{A^P_{C_{1s}}} = (A^F_{\infty C_{1s}} / A^P_{\infty C_{1s}}) (e^{d/\lambda} - 1) \quad (5.2)$$

where,

A^F_{C1s} = sum of peak area of various C_{1s} environments of fluoropolymer film.

$A^P_{C_{1s}}$ = peak area of hydrocarbon of the fluoropolymer film.

$A^F_{\infty C_{1s}}$ = sum of peak area of various C_{1s} environments of the fluoropolymer film with infinitive thickness.

$A^P_{\infty C_{1s}}$ = peak area of hydrocarbon of polyethylene film with infinitive thickness.

An alternative form can be written as:

$$\text{Ln } (R_1/R_2 + 1) = d/(\lambda \sin\Theta) \quad (5.3)$$

For the present study,

R_1 = (sum of peak intensity of various C_{1s} environments shifted from hydrocarbon of the grafted PP film) / (peak intensity of hydrocarbon of C_{1s} of the grafted PP film)

R_2 = (sum of peak intensity of various C_{1s} environments of DAEM which were shifted from hydrocarbon) / (peak intensity of hydrocarbon of C_{1s} of PP film)

d = overlayer thickness

λ = electron mean-free-path of C_{1s}

Θ = photoelectron take-off angle

It is evident that a plot of Ln $(R_1/R_2 + 1)$ vs. $1/\sin\theta$ should give a straight line of slope d/λ. By applying the angular-resolved equation, a plot of Ln $(R_1/R_2 + 1)$ vs. $1/\sin\theta$ is shown in Fig. 5.11. A linear regression line with slope of 0.92 and correlation coefficient 0.98 is shown for take-off angle down to 45°. If we assume λ equals 33Å, then the calculated overlayer is 31Å.

The third method which can be applied for measuring the thickness of the overlayer is overlayer-substrate angular-dependent XPS. This can be done using equation (5.3). But now R_1 represents the ratio of a measured signal such as N in this study from the overlayer at each angle to the signal of N from the pure dimethylaminoethyl methacrylate and R_2 denotes the intensity ratio of the photoelectron line of hydrocarbon from the substrate at each angle to the photoelectron line of hydrocarbon of pure polypropylene film. By plotting the semi-log of the $(R_1/R_2 + 1)$ versus $(\sin\theta)^{-1}$, the thickness of the overlayer can also be calculated. The value obtained is 30 Å (assuming λ = 33 Å). It is interesting to note that the thickness of the overlayer obtained by three different methods is very close. However, it is noted that at low electron take-off angle (20°) the experimental data deviates significantly from the regression model. This suggests that non-uniform coverage of DAEM, surface roughness, and patchy-like DAEM may result in such deviation.

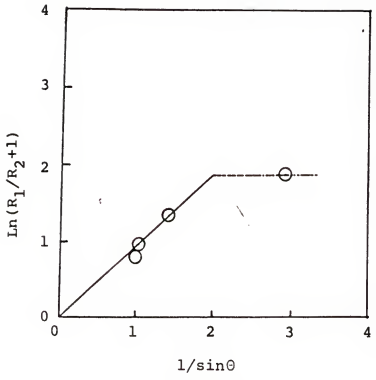

Figure 5.11 Angular-resolved XPS data for DAEM grafted onto PP film. Straight line shows the data fitted with a flat uniform overlayer model while the dashed line shows the deviation from this model at low electron take-off angle.

5.4.12 Overlayer Modeling

It should be noted that in applying the above equation, we assume that the surface overlayer is perfectly uniform and flat. Moulder et al. (138) proposed four possible models describing the surface overlayer. This is shown in Fig. 5.12. If the surface overlayer is flat and uniform, the experimental data can be fitted in the angular-dependent equation. However, four possible conditions can result in deviation of experimental data from the mathematical model. They are:

. surface contamination due to the hydrocarbon layer.
. non-uniform surface layer.
. patchy-like surface layer.
. surface roughness.

The driving force for surface contamination is to reduce surface free energy thermodynamically by adsorbing a thin layer of hydrocarbon. Because of the existence of some polar groups in the outermost several layers due to introduction of DAEM on PP substrate, surface free energy has been increased. Therefore, surface layer attempts to adsorb a thin layer of hydrocarbon in order to reduce its surface free energy. This hydrocarbon layer can cause attenuation of the photoelectron from the DAEM layer specially at low take-off angle and give a lower predicted value of thickness measurement. Non-uniform surface layer, patchy-like surface layer, and surface roughness also cause

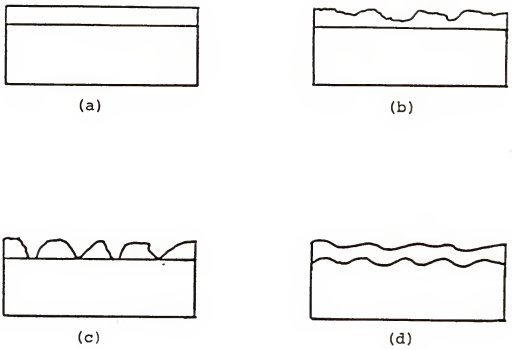

Figure 5.12 Four overlayer models for DAEM grafted onto polypropylene substrate.
(a) a flat uniform overlayer,
(b) non-uniform surface layer,
(c) patchy-like surface layer,
(d) non-uniform layer with rough substrate.

a lower predicted value of thickness measurement than the theoretical model. It will have little effect on the slope predicted at high photoelectron take-off angle because the sample depth is large while a significant effect occurs at low take-off angle due to the enhanced contribution of signals from the substrate.

5.4.13 FTIR-ATR Study

In addition to using XPS to characterize the surface-modified film, we also used Fourier Transform Infrared-Attenuated Total Reflection Spectroscopy (FTIR-ATR) to study the surface-modified PP film.

The ATR-IR technique has been applied to surface characterization of polymer film such as determination of molecular structure, orientation, and morphology. However, the development of FTIR spectrophotometry combined with ATR techniques has greatly expanded the potential use and reliability of infrared characterization of surface-modified polymers. Advantages such as high resolution, an increase of signal to noise ratio, and computerized data-manipulation have made this technique superior to the conventional grating IR method.

Figure 5.13 shows the spectrum of the unmodified PP film. The band around 2956 cm^{-1} is assigned to CH_3 group asymmetric stretching while the band around 2870 cm^{-1} is attributed to CH_3 group symmetric stretching. The peak at

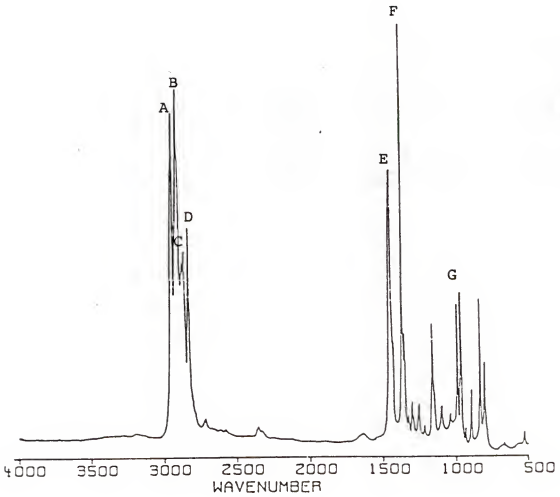

Figure 5.13 IR spectrum of unmodified polypropylene film.

2920 cm^{-1} represents the asymmetric stretching of CH_2 group and the peak at 2840 cm^{-1} is due to symmetric stretching of CH_2 group. The peak at 1455 cm^{-1} is attributed to symmetric bending of CH_3 group. The frequency below 1200 cm^{-1} is usually referred to as the fingerprint region which is due to CH_2 wagging, CH_2 rocking, CH_2 twisting, and sketal vibration. Table 5.6 summarizes these peak assignments.

Figure 5.14 depicts the IR spectrum of the modified PP film. When the spectra of unmodified and modified film are compared, it can readily be seen that some additional peaks appeared in the modified film. The new peak at 1727 cm^{-1} is assigned to the ester COO group. Another characteristic band for the COO group is also shown in 1260 cm^{-1}. However, these new bands can be seen more clearly by spectral subtraction method, i.e., a difference spectrum shown in Fig. 5.15 can be obtained by subtracting the spectrum of unmodified PP film in Fig. 5.13 from modified PP film in Fig. 5.14. The expanded spectra of Fig. 5.15 are shown in Figs. 5.16, and 5.17, respectively. The positive peaks at 1727 cm^{-1} and 1260 cm^{-1} are due to stretching of COO group and C-O-C group. As expected, two bands should appear for the functional group -COO-. The band at 1455 cm^{-1} and 1375 cm^{-1} are due to bending of the CH_3 group. The split bands around 1020 cm^{-1} and 1100 cm^{-1} in Fig. 5.17 are assigned to the C-N stretching. These broad bands are due to overlap with C-O-C band at 1050 cm^{-1}.

TABLE 5.6

Peak Assignments of IR Spectrum for the Unmodified PP Film

Peak	Frequency (cm^{-1})	Chemical structure
A	2956	Asymmetric stretching of CH_3
B	2920	Asymmetric stretching of CH_2
C	2870	Symmetric stretching of CH_3
D	2840	Symmetric stretching of CH_2
E	1455	Asymmetric bending of CH_3
F	1375	Symmetric bending of CH_3
G	1200 - 800	Sketal vibration

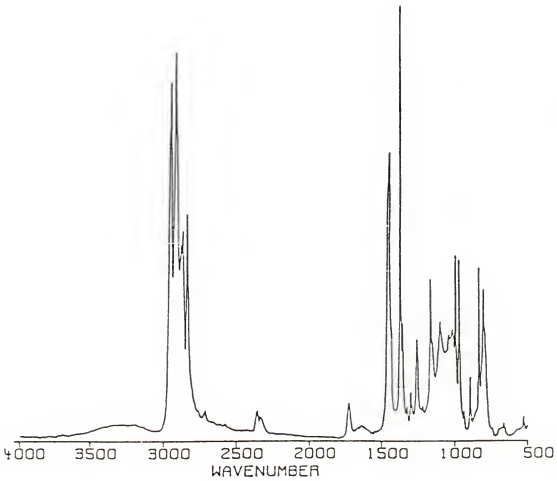

Figure 5.14 IR spectrum of modified polypropylene film.

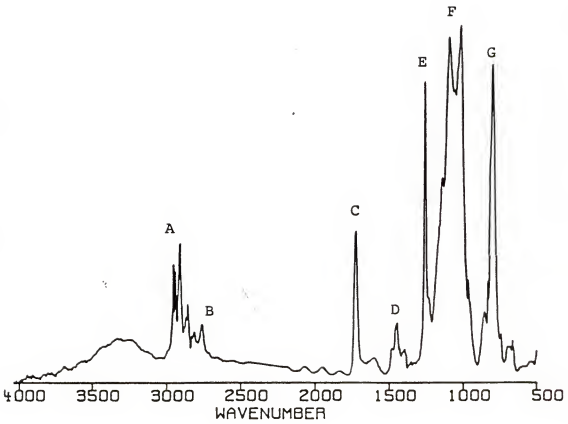

Figure 5.15 IR difference spectrum of modified and unmodified polypropylene film.

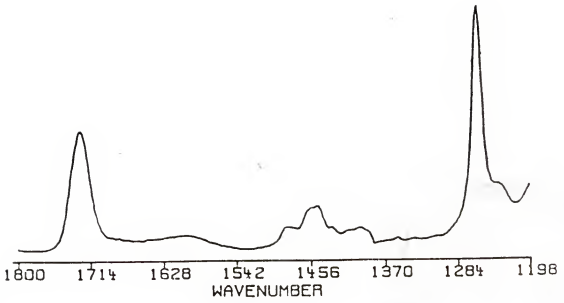

Figure 5.16 IR expanded difference spectrum of modified and unmodified PP film (1800 cm^{-1} - 1200 cm^{-1}).

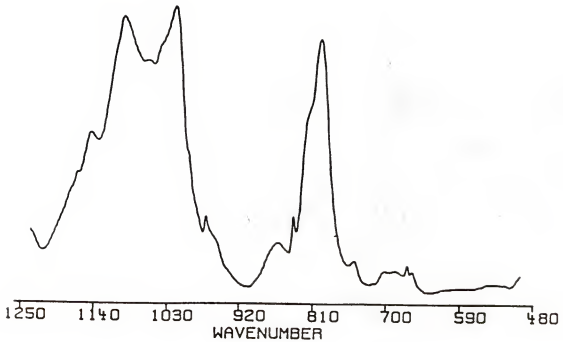

Figure 5.17 IR expanded difference spectrum of modified and unmodified PP film (1250 cm^{-1} - 500 cm^{-1}).

The peak at 800 cm^{-1} is attributed to the bending of CH group.

It is noteworthy that the grafting of DAEM on the substrate film results in the appearance of characteristic peaks of -COO and C-N groups. Result of the peak assignment of Fig. 5.15 is shown in Table 5.7.

The above difference spectrum demonstrates the applicability of the FTIR-ATR spectral subtraction method for surface analysis. This method is useful, especially for those bands which contain a small amount of component and are hidden under a large band of other components. However, this method is valid only when there is no interaction occurring among components, which might change the shape of the absorption bands. The assignments of the IR peaks are obtained from the literature (39, 40).

TABLE 5.7

Peak Assignments of IR Difference Spectrum for the Modified and Unmodified PP Film

Peak	Frequency (cm^{-1})	Chemical structure
A	2956 - 2840	Stretching of CH_3 and CH_2
B	2768	Stretching of N-CH_3
C	1727	Stretching of COO
D	1455 -1375	Bending of CH_3
E	1260	Stretching of C-O-C
F	1100 - 1020	Stretching of C-N
G	800	Bending of CH

CHAPTER 6
CONCLUSIONS AND RECOMMENDATIONS

6.1 Conclusions

The study covers two areas:

(1) synthesis of a functional polymer used as a binder in ceramic processing and measurement of some properties of the residues remaining after the burn-out process.

(2) modification of the surface of a hydrophobic polymer using a hydrophilic monomer through a peroxide initiation, gas-phase method.

The following conclusions can be drawn from the above experimental work:

A novel polymer which has ester groups on the main chain, hydroxyl groups and acetal groups on the side chain was synthesized. The formation of this functional polymer was confirmed by NMR and IR analysis. The method used in synthesizing the functional polymer was carried out at room temperature or under mild condition. This is different from the conventional method which is carried out at the high temperature. This method has advantages such as less energy consumption and less risk of degradation of the polymer that the conventional method (melt-polymerization) does not have.

Analysis of the functional groups of the carbon overlayer on the Al_2O_3 substrate by XPS derivatization technique was consistent with carbonyl and anhydride groups residing on the surface. The thickness of the carbon overlayer on the Al_2O_3 substrate was found, by angular-resolved XPS, to be a few monolayers. The thickness of this carbon overlayer was also calculated using an alternative C_{1s}- C_{kvv} method and showed good agreement with the data analyzed by the angular-resolved XPS. A mathematical expression based on the attenuation model was obtained by the linear and nonlinear least square fit of the experimental data. The fit between the mathematical model and the experimental data was further analyzed by the statistical method. Finally, a non-uniform overlayer and surface-roughness model could be used to describe the deviation between the mathematical model and the experimental data.

Dimethylaminoethylmethacrylate, a hydrophilic monomer, was successfully grafted on the polypropylene film through a peroxide initiation, gas-phase method. The grafting of the thin polymer layer was characterized by infrared and x-ray photoelectron spectroscopy. The change of surface energetics of the polypropylene film was further confirmed by the contact angle measurement. The thickness of the thin polymer layer was estimated by three different methods; and each estimated thickness is similar.

6.2 Recommendations

Based on the work in this study, several recommendations can be made. These are to use a high vacuum at the later stage of condensation reaction in order to enhance the degree of polymerization; to use the XPS derivatization technique to find out other functional groups formed during the burn-out experiment; and to use a very flat sample as a substrate to study, with angular-resolved XPS, the effect of surface roughness on the mathematical modeling.

APPENDIX
NOTATION, ABBREVIATION AND GREEK LETTERS

NOTATION

A : Peak area.

A_o : Effective aperture area.

C : Photoelectric cross section of a subshell of an atom.

E_B : Binding energy of an electron with respect to the Fermi level.

E_B' : Binding energy of an electron with respect to the vacuum level of a sample.

F_f : Fermi energy.

E_k : Kinetic energy of an electron with respect to the vacuum level of a spectrometer.

E_k' : Kinetic energy of an electron with respect to the vacuum level of a sample.

F : x-ray flux.

h : Plank's constant.

I : Photoelectron intensity.

$\bar{M}_n$: Number-average molecular weight.

$\bar{M}_w$: Weight-average molecular weight.

N : Atomic density.

S : Spectrometer function.

t : Thickness of a sample.

ABBREVIATION

AIBN : Azobisisobutyronitrile.

DAEM : Dimethylaminoethylmethacrylate.

DCC : dicyclohexylcarbodiimide.

DTA : Differential thermal analysis.

DTG : Derivative thermogravimetry.

FAT : Fixed analyzer transmission.

FPP : 1-(4-Fluorophenyl) piperazine.

FRR : Fixed retarding ratio.

FTIR : Fourier transform infrared.

GC : Gas chromatography.

MCT : Mercury cadmium telluride.

MLC : Multilayer ceramics.

MS : Mass spectroscopy.

NMR : Nuclear magnetic resonance.

NVP : N-vinylpyrrolidone.

PFPH : Pentafluorophenyl hydrazine.

PP : Polypropylene.

PVB : Poly(vinyl butyral).

SAC : Sample analysis chamber.

SEM : Scanning electron microscopy.

SMA : Styrene-maleic anhydride.

STC : Sample treatment chamber.

t-BPB : t-Butyl peroxybenzoate.

TVA : Thermal volatilisation analysis.

XPS : X-ray photoelectron spectroscopy.

GREEK LETTERS

θ : Photoelectron take-off angle.

φ : x-ray incidence angle.

φ' : x-ray refraction angle.

φ_c : Contact potential.

φ_s : work function of a sample.

φ_{sp} : work function of a spectrometer.

λ : Electron mean-free-path.

Ω_o : Solid angle of the spectrometer.

$[\eta]$: Intrinsic viscosity.

η_{sp} : Specific viscosity.

η_r : Relative viscosity.

ν : Frequency.

REFERENCES

1. W. S. Young, Multilayer Ceramic Technology, IBM Corporation, San Jose, California, 1986.

2. B. Schwartz, J. Phys. Chem. Solid, 45 (10), 1051 (1984).

3. J. E. Poetzinger and S. H. Risbud, J. De Phys., C4, 147 (1985).

4. J. M. Brownlow and T. S. Plaskett, U. S. Patent, 4, 474, 731, 1984.

5. H Hoppert, Chemical Abstract, 95, 63041w (1981).

6. Japan Kokai Patent, 74/21, 406, Feb. 25, 1974.

7. K. Kita, J. Fukuda, H. Ohmura, and T. Sakai, U. S. Patent, 4, 353, 958, 1982.

8. N. Ogata, K. Sanui, and A. Kato, J. Polym. Sci. Polym., 20, 227 (1982).

9. P. K. Kadaba, Synthesis, 4 (3), 167 (1974).

10. H. J. Liu, W. H. Chan, and S. P. Lee, Tetrahedron Lett., 4461 (1978).

11. F. Higashi, K. Kubota, M. Sekizuka, and M. Goto, J. Polym. Sci., Polym. Lett., 18, 385 (1980).

12. R. Nakao, K. Oka, and T. Fukumoto, Bull. Chem. Soc., Japan, 54, 1267 (1981).

13. S. Hashimoto, and I. Furukawa, Bull. Chem. Soc., Japan, 54, 2227 (1981).

14. S. Takimoto, J. Inanaga, T. Katsuki, and M. Yamaguchi, Bull. Chem. Soc., Japan, 54, 1470 (1981).

15. T. Garcia, A. Arrieta, and C. Palomo, Synthesis, 12 (9), 681 (1982).

16. E. Mohacsi, Synthesis, 12 (6), 453 (1982).

17. K. S. Keshavamurthy, Y. D. Vankar, and D. N. Dhar, Synthesis, 506 (1982).

18. S. Takimoto, N. Abe, Y. Kodera, and H. Ohta, Bull. Chem. Soc., Japan, 56, 639 (1983).

19. S. Yasuda, G. C. Wu, H. Tanaka, K. Sanui, and N. Ogata, J. Polym. Sci. Polym. Chem., 21, 2609 (1983).

20. O. Vogl, J. Macromol. Sci., Chem. Ed., A21 (8, 9), 1217 (1984).

21. W. Steglich and G. Höfle, Synthesis, 619 (1972).

22. S. Kim and S. Yang, Synthetic Communications, 11 (2), 121 (1981).

23. A. Hassner, L. R. Krepski, and V. Alexanian, Tetrahedron, 34, 2069 (1978).

24. A. Hassner and V. Alexanian, Tetrahedron Letters, 46, 4475 (1978).

25. E. R. Santee, Jr., V. D. Mochel, and M. Morton, J. Polym. Sci., B (11), 453 (1973).

26. Y. Tanaka, K. Hatada, Y. Terawaki, H. Okuda, and H. Sato, J. Polym. Sci., B (12), 305 (1974).

27. Q. T. Pham, R. Petiaud, M. F. Llauro, and H. Waton, Proton and Carbon NMR Spectra of Polymers, vol. 1, 2, 3, John Wiley & Sons Ltd., New York, 1983.

28. W. W. Simons and M. Zanger, The Satler Guide to the NMR Spectra of Polymers, Sadtler Research Laboratories, Inc., Philadelphia, 1973.

29. Q. T. Pham, Makromol. Chem., 182, 1167 (1981).

30. A. D. H. Clague, J. A. M. van Broekhoven, and L. P. Blaauw, Macromolecules, 7 (3), 348 (1974).

31. S. Bywater, Polym. Commun., 24, 203 (1983).

32. V. D. Mochel, J. Polym. Sci., A1 (10), 1009 (1972).

33. J. Furukawa, E. Kobayashi, T. Kawagoe, N. Katsuki, and M. Imanari, J. Polym. Sci., A1 (11), 239 (1973).

34. Y. Tanaka, H. Sato, M. Ogawa, K. Hatada, and Y. Terawaki, J. Polym. Sci., A1 (12),369 (1974).

35. F. Conti, A. Segre, P. Pini, and L. Porri, Polymer, 15, 5 (1974).

36. K. F. Elgert, G. Quack, and B. Stutzel, Polymer, 16, 154, (1975).

37. A. A. Berlin and N. G. Matvejeva, J. of Polym. Sci., Macromolecular Review, 15, 107 (1980).

38. N. Ogata and T. Ikari, J. Polym. Sci., A1 (11), 1939 (1973).

39. K. Nakanishi and P. H. Solomon, Infrared Absorption Spectroscopy., 2nd ed., Holden-Day Inc., San Francisco, 1977.

40. H. W. Siesler and K. Holland-Moritz, Infrared and Raman Spectroscopy of Polymers, Marcel Dekker Inc., New York, 1980.

41. M. Mugdan and D. P. Young, J. Chem. Soc., 2988 (1949).

42. D. Swern, Organic Peroxides, vol. II, Wiley Interscience, New York, 1971.

43. R. B. Woodward, U. S. Patent, 2, 687, 435 (1954).

44. R. Criegee, Ann. Chem., 522, 75 (1936).

45. R. T. Morrison and R. N. Boyd, Organic Chemistry, 3rd ed., Allyn and Bacon, Inc., Boston, 1973.

46. R. Stewart, Oxidation in Organic Chemistry, Part A, K. B. Wiberg, ed., Academic Press, New York, 1965.

47. J. E. Coleman, C. Ricciuti, and D. Swern, J. Am. Chem. Soc., 78, 5342 (1956).

48. S. Wolfe, C. F. Ingold, and R. U. Lemieux, J. Am. Chem. Soc., 103, 938 (1981).

49. R. H. Eastman and R. A. Quinn, J. Am. Chem. Soc., 82, 4249 (1960).

50. D. M. Walba, M. D. Wand, and M. C. Wilkes, J. Am. Chem. Soc., 101, 4396 (1979).

51. C. M. Starks, J. Am. Chem. Soc., 93, 195 (1971).

52. D. J. Sam and H. F. Simmons, J. Am. Chem. Soc., 94, 4024 (1972).

53. T. Okimoto and D. Swern, J. Am. Oil Chem. Soc., 54, 867 A (1977).

54. D. G. Lee and V. S. Chang, J. Org. Chem., 43, 1532 (1978).

55. T. Ogino and K. Mochizuki, Chemistry Letters, 443 (1979).

56. J. E. Taylor, D. Williams, K. Edwards, D. Otonnaa, and D. Samanich, Can. J. Chem., 62, 11 (1984).

57. T. Okimoto and D. Swern, J. Am. Oil Chem. Soc., 54, 862A (1977).

58. A. Brandstrom, Advanced in Physical organic Chemistry, vol. 15, V. Gold ed., Academic Press, London and New York, 1977.

59. N. A. Gibson and D. C. Weatherburn, Anal. Chim. Acta, 58 (149), 159 (1972).

60. D. G. Lee in Oxidation in organic Chemistry, Part D, W. S. Trahanovsky ed. Academic Press, New York, 1982.

61. W. O. Herrmann and W. Haehnel, Ger. Pat., 480, 866, 1924.

62. L. H. Rombach, U. S. Patent, 3, 153, 009, 1964.

63. A. Koshita, H. Sakata, H. Asahara, and N. Suyama, Chem. Abstr., 82, 86865 (1975).

64. R. G. Flowers and C. A. Winter, U. S. Patent, 3, 442, 834, 1969.

65. K. Burg and H. Schlaf, U. S. Patent, 3, 883, 450, 1975.

66. Y. Oshira, M. Miyasaka, Y. Shirota, and H. Mikawa, Chem. Abstr., 82, 86785m (1975).

67. K. D. Moller and W. G. Rothschild, Far-Infrared Spectroscopy, Wiley, New York, 1977.

68. J. L. Koenig, Applications of Fourier Transform Infrared to Polymers, in Analytical Applications of FT -IR to Molecular and Biological Systems, J. R. Durig, ed., Reidel Publishing Company, 1980.

69. L. I. Simandi and M. Jaky, J. Am. Chem. Soc., 98, 1995 (1976).

70. The Aldrich Library of NMR Spectra, C. J. Pouchert, ed., Aldrich Chemical Company, Milwaukee, 1983.

71. K. Imai, T. Shiomi, Y. Tezuka, and M. Miya, J. Polym. Sci., A1 (22), 841 (1984).

72. K. Imai, T. Shiomi, T. Tsuchida, C. Watanabe, and S. Nishioka, J. Polym. Sci., A1 (21), 305 (1983).

73. M. D. Bruch and J. K. Bonesteel, Macromolecules, 19 (6), 1622 (1986).

74. R. W. Billmeyer, Jr., Textbook of Polymer Science, 2nd ed., John Wiley and Sons, Inc., New York, 1971.

75. V. I. Grachev, I. B. Klimenko, L. V. Smirnov, and A. F. Gladkikh, Polym. Sci. USSR, A16, 367 (1974).

76. C. Vasile, E. M. Calugaru, and S. F. Bodonea, J. Polym. Sci. Polym. Chem., 19, 897 (1981).

77. J. W. Martin, B. Dickens, D. Waksman, D. P. Bentz, W. E. Byrd, E. Embree, and W. E. Roberts, J. Appl. Polym. Sci., 34, 377 (1987).

78. S. Zulfiqar, M. Zulfiqar, T. Kausar, and I. C. McNeill, Polym. Degrad. and Stability, 17, 327 (1987).

79. K. Otsuka, T. Usami, and M. Sekibata, Yogyo kyokaishi, 89, 6, 309 (1981).

80. K. Otsuka and S. Ogihara, Yogyo Kyokaishi, 92, 4, 210 (1984).

81. K. Otsuka and S. Ogihara, Yogyo Kyokaishi, 92, 11, 629 (1984).

82. K. Otsuka and S. Ogihara, Yogyo Kyokaishi, 93, 1, 28 (1985).

83. C. S. Fadley, in: Electron Spectroscopy, Theory, Techniques, and Applications, vol. 2, C. R. Brundle, A. D. Baker ed., Academic Press, New York, 1978.

84. J. H. Scofield, J. Electron Spectrosc., 8, 129 (1976).

85. A. E. Hughes and C. C. Phillips, Surf. Interface Anal., 4, 220 (1982).

86. J. D. Andrade, Surface and Interfacial Aspect of Biomedical Polymers, J. D. Andrade, ed., Chapter 5, Plenum Press, New York, 1985.

87. D. Briggs and M. P. Seah, Practical Surface Analysis by Auger and X-ray Photoelectron Spectroscopy, John Wiley & Sons, New York, 1983.

88. H. Chacin, C. D. Batich, and J. W. Williams, Abstracts from 14th Annual Symposium on Applied Vacuum Science and Technology, Florida Section, American Vacuum Society, 39 (1985).

89. C. D. Batich, and L. Ogbuji, J. Ultrastructural Research, 90, 1 (1985).

90. D. T. Clark in Structural Studies of Macromolecules by Spectroscopic Methods, K. J. Ivin, ed., John Wiley & Sons, New York, 1976.

91. W. M. Riggs and D. Dwight, J. Electron Spectrosc. Relat. Phenom., 5, 447 (1974).

92. D. Briggs, Polymer, 25, 1381 (1984).

93. C. D. Batich and R. C. Wendt, in Photon, Electron and Ion Probes of Polymer Structure and Properties, D. W. Dwight, T. J. Fabish, and H. R. Thomas, ed., ACS Symposium Series 162, American Chemical Society, 1981.

94. R. A. Dickie, J. S. Hammond, J. E. Devries, and J. W. Holubka, Anal. Chem., 54, 2045, (1982).

95. W. G. Collier, and T. P. Tougas, Anal. Chem., 59, (1987).

96. J. B. Johnson, and G. L. Funk, Anal. Chem., 27 (9), 1464 (1955).

97. F. E. Critchfield, Organic Functional Group Analysis, The MacMillan Comp. New York, 1963.

98. C. D. Batich, in Silanes, Surfaces and Interfaces Donald E. Leyden, ed., Gordon and Breach Science Publisher, New York, 1986.

99. L. J. Gerenser, J. F. Elman, M. G. Mason, and J. M. Pochan, Polymer, 26, 1163 (1985).

100. T. Ohmichi, H. Tamaki, and H. Kawasaki, in Physicochemical Aspects of Polymer Surface, K. L. Mittal, ed., vol. 2, Plenum Press, New York, 1983.

101. J. C. Eriksson, C. G. Golander, and A. Baszkin, J. Colloid Interface Sci, 100 (2), 381 (1984).

102. B. L. Henke, Phys. Rev., 6 (1), 94 (1972).

103. D.T. Clark and H. R. Thomas, J. Polym, Sci., Polym. Chem. Ed., 15, 2843 (1977).

104. K. B. Wagener, C. D. Batich, B. Kirsh, and S. Wanigatunga, Polymer Preprints, 27 (2), 1986.

105. D. R. Miller and N. A. Peppas, Macromolecules, 20, 1257 (1987).

106. Kratos, XSAM-800 Handbook, Analytical Instruments, New Jersey.

107. D. T. Clark and H. R. Thomas, J. Polym. Sci., Polym. Chem. Ed., 15, 2843 (1977).

108. P. Cadman, G. Gossedge, and J. D. Scott, J. Electron Spectrosc. Relat. Phenom., 13, 1 (1978).

109. J. C. Ashley, Inst. Electr. Electron. Eng., Trans. Nucl. Sci., NS-27, 1454 (1980).

110. J. C. Ashley and C. J. Tung, Surf. Interface Anal., 4 (2), 52 (1982).

111. M. P. Seah and W. A. Dench, Surf. Interface Anal., 1 (1), 2 (1979).

112. Kratos XSAM-800 Handbook, Analytical Instruments, New Jersey.

113. C. N. Reilley and D. S. Everhart, Anal. Chem., 53 (4), 665 (1981).

114. M. F. Ebel and J. Wernisch, Surf. Interface Anal., 3 (5), 191 (1981).

115. W. W. Hines and D. C. Montgomery, Probability and Statistics in Engineering and Management Science, 2nd ed., John Wiley and Sons, Inc., New York, 1980.

116. M. F. Ebel, M. Schmid, H. Ebel, and A. Vogel, J. Electron Spectros. Relat. Phenom., 34, 313 (1984).

117. C. S. Fadley, Progess in Solid State Chemistry, 11, 265 (1976).

118. S. Wu, Polymer Interface and Adhesion, Marcel Dekker, Inc., New York, 1982.

119. H. Yasuda, Plasma Polymerization, Academic Press, Inc., New York, 1985.

120. N. Inagaki, Y. Ohnishi, and K. S. Chen, J. of Applied Polymer Science, 28, 3629 (1983).

121. N. Inagaki, and H. Hirao, J. of Polym. Sci., A1 (24), 595 (1986).

122. B. N. Misra, and B. R. Rawat, J. of Polym. Sci., A1 (23), 307 (1985).

123. Y. Ogiwara, and H. Kubota, J. of Polym. Sci., Polym. Lett., 23, 15 (1985).

124. I. Hodgetts, S. J. Noyce, and R. C. Storr, Tetrahedron Letters, 25 (47), 5435 (1984).

125. K. Hayakawa, H. Yamakita, and K. Kawase, J. Polym. Sci., A1 (8), 1227 (1970).

126. M. B. Huglin, and J. Smith, Euro. Polym. J., 17, 389 (1981).

127. A. F. Bickel, and W. A. Waters, Rec. Trav. Chim., 69, 1490 (1950).

128. G. S. Hammond, J. N. Sen, and C. E. Boozer, J. Am. Chem. Soc., 77, 3244 (1955).

129. R. T. Sanderson, J. Am. Chem. Soc., 97, 1367 (1975).

130. D. T. Clark and H. R. Thomas, J. of Polym. Sci., A1 (14), 1671 (1976).

131. D. T. Clark and H. R. Thomas, J. Polym. Sci., A1 (16), 791 (1978).

132. L. J. Gerenser, J. M. Pochan, M. G. Mason, and J. F. Elman, Langmuir, 1, 305 (1985).

133. C. D. Batich and D. S. Donald, J. Am. Chem. Soc., 106 (10), 2758 (1984).

134. H. S. Munro, J. of Polym. Sci., A1 (23), 479 (1985).

135. C. R. Ginnard and W. M. Riggs, Anal. Chem., 44, 1310 (1972).

136. A. P. Pijpers and W. A. B. Donners, J. of Polym. Sci., A1 (23), 453 (1985).

137. D. T. Clark, W. J. Feast, W. K. R. Musgrave, and I. Ritchie, J. of Polym. Sci., A1 (13), 857 (1975).

138. J. F. Moulder, J. S. Hammond, and K. L. Smith, Appl. Surf. Sci., 25, 446 (1986).

BIOGRAPHICAL SKETCH

Yuan-Chang Lin was born on December 27, 1953, in Hsinchu, Taiwan, Republic of China (R. O. C.).

He received his B. S. degree in chemical engineering from National Central University (N. C. U.), Taiwan, R. O. C. in June 1977. He then joined the army as a second lieutenant to fulfill mandatory military service from August 1977 to May 1979.

After working at the National Central University as a teaching assistant in the Chemical Engineering Department from August 1979 to July 1981, he attended the University of Alabama, Tuscaloosa in August 1981. He was awarded a research assistantship in the reaction kinetics of oil shale and received the M. S. Ch. E. degree in June 1983.

In December 1983, he joined the Department of Materials Science and Engineering, University of Florida, Gainesville, where he studied surface and interface analysis with emphasis in XPS under the direction of Dr. Christopher D. Batich.

While pursuing the Ph. D. degree in materials science and engineering, he served as a graduate research assistant. He is a member of the American Chemical Society in the

division of organic chemistry, the division of materials science and engineering, and the division of polymer chemistry.

I certify that I have read this study and that in my opinion it conforms to acceptable standards of scholarly presentation and is fully adequate, in scope and quality, as a dissertation for the degree of Doctor of Philosophy.

C. D. Batich, Chairman
Associate Professor of Materials Science and Engineering

I certify that I have read this study and that in my opinion it conforms to acceptable standards of scholarly presentation and is fully adequate, in scope and quality, as a dissertation for the degree of Doctor of Philosophy.

D. E. Clark
Professor of Materials Science and Engineering

I certify that I have read this study and that in my opinion it conforms to acceptable standards of scholarly presentation and is fully adequate, in scope and quality, as a dissertation for the degree of Doctor of Philosophy.

R. T. DeHoff
Professor of Materials Science and Engineering

I certify that I have read this study and that in my opinion it conforms to acceptable standards of scholarly presentation and is fully adequate, in scope and quality, as a dissertation for the degree of Doctor of Philosophy.

J. W. Williams
Assistant professor of Materials Science and Engineering

I certify that I have read this study and that in my opinion it conforms to acceptable standards of scholarly presentation and is fully adequate, in scope and quality, as a dissertation for the degree of Doctor of Philosophy.

K. B. Wagener
Associate Professor of Chemistry

This dissertation was submitted to the Graduate Faculty of the College of Engineering and to the Graduate School and was accepted as partial fulfillment of the requirements for the degree of Doctor of Philosophy.

December 1987

Herbert A. Beier
Dean, College of Engineering

Dean, Graduate School